PANNON EGYETEM

Fe- és Cu-tartalmú szintetikus 1-aminociklopropán-1-karbonsav oxidáz modellek

PhD értekezés

Készítette:
Papné Góger Szabina
okleveles vegyészmérnök

Témavezető:
Dr. Kaizer József
egyetemi tanár, az MTA doktora

Kémiai és Környezettudományi Doktori Iskola

Szerves Kémia Intézeti Tanszék
Veszprém
2017

UNIVERSITY OF PANNONIA

Synthetic Fe- and Cu-containing 1-aminocyclopropane-1-carboxylic acid oxidase models

PhD dissertation

Szabina Papné Góger
chemical engineer

Supervisor:
Dr. József Kaizer
professor

Doctoral School of Chemistry and Environmental Sciences

Departement of Organic Chemistry
Veszprém
2017

Fe- és Cu-tartalmú szintetikus 1-aminociklopropán-1-karbonsav oxidáz modellek

Értekezés doktori (PhD) fokozat elnyerése érdekében

Írta:
Papné Góger Szabina

Készült a Pannon Egyetem Kémiai és Környezettudományi Doktori Iskolája/
(programja/alprogramja) keretében

Témavezető: Dr. Kaizer József ....
(aláírás)

Elfogadásra javaslom (igen / nem)

A jelölt a doktori szigorlaton ....%-ot ért el,

Az értekezést bírálóként elfogadásra javaslom:

Bíráló neve: …....................... …................... igen /nem

………………………….
(aláírás)

Bíráló neve: …....................... …................... igen /nem

………………………….
(aláírás)

A jelölt az értekezés nyilvános vitáján ….............%-ot ért el.

Veszprém/Keszthely,   ………………………….

a Bíráló Bizottság elnöke

A doktori (PhD) oklevél minősítése…................................

………………………….
Az EDHT elnöke

KIVONAT

A legegyszerűbb növényi hormon, az etilén bioszintézisének utolsó lépését kételektronos oxidációban az 1-aminociklopropán-1-karbonsav oxidáz (ACCO) enzim katalizálja. A reakció melléktermékeként CO_2, HCN és H_2O keletkezik. Az enzim aktív centrumában vasat tartalmaz, amelyet két hisztidinből származó N és egy aszparaginsavból koordinálódó O, továbbá alapállapotban három vízmolekula vesz körül. Az említett „2 His 1 Asp”-nak jelölt csoport sajátságos jellemzője ennek az enzimcsaládnak.

Fe- és Cu-tartalmú komplexek előállításán, jellemzésén és aktivitásának vizsgálatán keresztül olyan funkcionális modellekhez jutottunk, amelyek az enzimatikus útnak megfelelő terméket szolgáltatták. A reakciókat számos ciklikus, illetve aciklikus aminosav valamint aminofoszfonát esetében végeztük különböző oxidálószerek jelenlétében. Részletes reakciókinetikai vizsgálatok eredményei alapján javaslatot tettünk a lehetséges mechanizmusra.

ZUSAMMENFASSUNG

Das einfachste Phytohormon, Ethylene wurde von 1-aminocyclopropane-1-carboxylicacid Oxidas (ACCO) in einer zweielectronischen Oxidation - die neben Hauptprodukt CO_2, HCN und H_2O produziert - hergestellt. Das Enzym beinhaltet ein einzig Eisen Ion im Zentrum und gehört zu der Superfamilie „2 His 1 Asp" denn zentraler Metal ist von 2 N Atom von Histidin, 1 O Atom von Aspartat und drei Wassermolekülen im Ausgangspunkt der enzimatischen Reaktion umgegeben. Das Ziel der Doktorarbeit war die Untersuchung dieser besonders merkwürdigen Reaktion.

Ausserhalb Fe, Komplexe mit der Inhalt von Cu wurden synthetisiert, ihre Struktur mit verschiedenen spektroskopischen Methoden (UV-Vis, IR, EPR, X-Ray) bestätigt und untersucht in der Reaktion von zahlreichen Aminoaciden in der Anwesenheit von verschiedenen Oxidanten. Modelle zeigten sich gute funktionelle Mimics für ACCO denn alle produzierten korrespondierenden Karboniele oder Ethylene von anwendeten Substrat abhängig. Mechanismen wurden studiert (GC, UV-Vis) und mögliche Lösung auf Basis der Ergebnisse wurde vorgeschlagen.

ABSTRACT

Ethylene, the simplest plant hormone, is synthesized by 1-aminocyclopropane-1-carboxylicacid oxydase (ACCO) in a two-electron oxidation process giving CO_2, HCN and H_2O besides the main product. The enzyme – having a single ferrous ion in the active site – belongs to the superfamily called „2 His 1 Asp", since the central metal ion is surrounded by two nitrogen atoms from histidine and an oxygen belonging to a carboxylate group from aspartate, plus three H_2O molecules in the resting state.

Beyond the synthesis and characterization of Fe-, Cu-containing complexes, the reactions of numerous cyclic and acyclic amino acids as well as amino phosphonates were studied in the presence of various oxidants. Models appeared to be good functional mimics for ACCO giving the corresponding products. In this work, the results of kinetic studies are described and plausible mechanisms are proposed.

ACKNOWLEDGEMENT

TABLE OF CONTENTS

ABBREVIATIONS

ACCO	1-aminocyclopropane-1-carboxylic acid oxidase
AA	amino acid
TauD	taurine dioxygenase
MMO	methane monooxygenase
His	histidine
α-KGDO	α-ketoglutarate dependent oxygenase
NDO	naphtalene dioxygenase
DIC	dicamba O-demethylase
CARDO	carbazole 1,9-dioxygenase
TH	thymine hydroxylase
P4H	prolyl-4-hydroxylase
CAS	clavaminate synthase
BH_4	tetrahydrobiopterin
PheH	phenylalanine hydroxylase
Tyr	tyrosine
SOR	sulfur oxygenase reductase
IPNS	isopenicillin synthase
ACV	δ-(L-α-aminoadipoyl)-L-cysteinyl-D-valine
IPN	isopenicillin
CAO	copper amine oxidase
ACCH	1-aminocyclopropane-1-carboxylic acid
BDE	bond dissociation energy
k_{cat}	rate constant of product formation
K_M	*Michaelis-Menten* constant
DMF	*N,N*-dimethylformamide
ENDOR	electron nuclear double resonance
AIBH	2-aminoisobutyric acid
ALAH	alanine
GLY	glycine

Asc	ascorbate
DHAsc	dehydroascorbate
PHM	α-hydroxylating monoxygenase
PAL	α-amidating lyase
N4Py	*N,N*-bis(2-pyridilmethyl)-*N*-bis-(2-pyridilmethyl)amine
TPA	tris(2-pyridilmethyl)amine
Bn-TPEN	*N*-benzyl-*N,N',N'*-tris(2pyridilmethyl)-1,2-diaminoethane
TMC	1,4,8,11-tetramethyl-1,4,8,11-tetraaza-cycloteradecane
MCD	magnetic circular dichroism
ACBCH	1-aminocyclobutane carboxylic acid
ACPCH	1-aminocyclopentane carboxylic acid
ACHCH	1-aminocyclohexane carboxylic acid
NORH	norvaline
HPTP	*N,N,N',N'*–tetrakis(2-pyridylmethyl)-1,3-diamino-2-propanol
HXTA	*N,N'*-(2-hydroxy-5-methyl-1,3-xylylene)bis(*N*-carboxymethylglycine)
TACN	triazacyclononane
DMF	*N,N*-dimethylformamide
RDS	rate determining step
ET-PT	electron transfer-proton transfer
SIE	solvent isotop effect
SALEN	*N,N*-bis(salicilidene)ethylene diamin
PhIO	iodosobenzene
TBHP	*tert*-butyl hydroperoxide
MCPBA	*meta*-chloro perbenzoic acid
PMS	peroxo monosulfate
CV	cyclic voltammetry
AMEPH	(1-amino-1-methyl)ethylphosphonic acid
TON	turnover number
TOF	turnover frequency
TBAP	tetrabutylammonium perchlorate
SOD	superoxide dismutase

1. INTRODUCTION

Our growing population and changing environment raise several questions to be solved. Clean water and nutritious food are crucial for our well-being. The way we are able to acquire and/or maintain them varies from time to time. Nowadays, it is called biotechnology, although humankind is using this label without having particular information about the phenomenon or describing it in detail. A part of „biotechnology" is the application of enzymes. Their industrial (food processing, leather and textile industry) and every-day usage (washing and dishwashing agents, digestive supplements) is now quite common.

Bioinorganic chemistry – a relatively new field of research – struggles to find alternative solutions, since the usage of enzymes might have some difficulties and/or hindrances. Creating model reactions by using simple transition metal complexes for these biologically active species is an option for substituting them, or gaining information about their nature in an indirect way.

The current dissertation focuses on the enzyme 1-aminocyclopropane-1-carboxylic acid oxidase (ACCO), which is responsible for the regulation of ripening processes in fruits and vegetables, by means of producing the growth hormone ethylene. In this work, Fe- and Cu-containing complexes were synthesized, characterized and investigated as potential synthetic models of ACCO.

2. LITERATURE OVERVIEW

2.1 Enzymes

How to make a reaction work without harmful side-products? How to get a catalyst with a turnover number of 7.4×10^5 min^{-1} per active site? [1] How to make it work without applying extreme conditions, *i.e.,* at neutral pH under 100 °C and atmospheric pressure? [2] Nature knows the answer: enzymes. They keep life and its processes going as fast, efficient and simple as possible. This astonishing group of molecules consists of six classes depending on the type of the catalyzed reaction (Scheme 1).
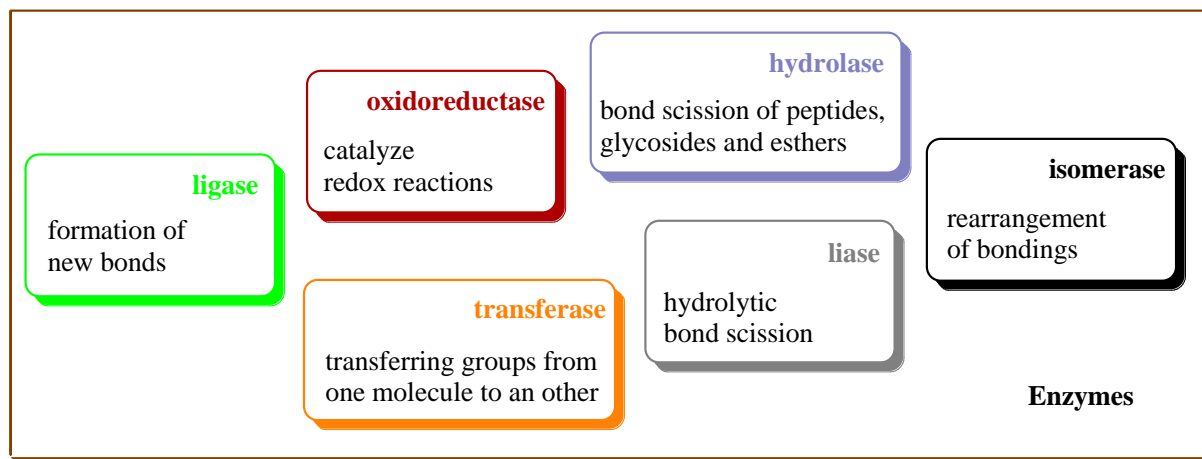
Scheme 1. Classification of enzymes

The history of enzymology is considerably long; however, the majority of information obtained is the result of the past decades. Modern separation (chromatography, electrophoresis, ultracentrifugation), analytical (NMR, X-ray diffraction, EXAFS, etc.) and computational methods made possible to gain better insight into the nature of these remarkable species. [2]

The estimated size of a typical period in sequence length is approximately 152 amino acids for prokaryotic and 123 amino acids for eukaryotic enzymes [3] and weight range from 1.2×10^4 to 5×10^5 Dalton. [4]

The specificity of enzymes is directed by van der Waals, electrostatic, hydrophobic interactions and H-bonding. Some of them catalyze only one reaction of a single molecule, although most of them are able to carry out reactions with different

substrates. The part of an enzyme actually participating in a chemical reaction is called the binding site or the active centre. The building unit amino acids are arranged in a receptive manner and shape towards eligible substrates (Scheme 2). [2]
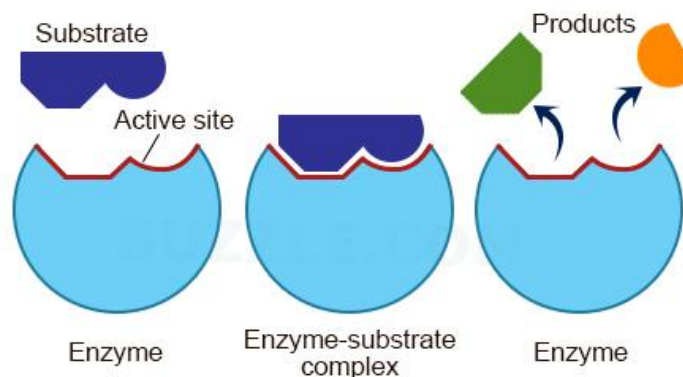

Scheme 2. Generalized activity of the binding site of an enzyme

Beyond the proper chemical and geometrical layout of the active site, enzymes often require co-factors for performing reactions. Without these they become inactive (Equation 1).

$$\text{apoenzyme (inactive)} + \text{cof-actor} = \text{holoenzyme (active)} \tag{1}$$
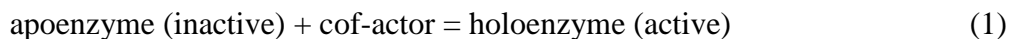
Co-factors can be organic molecules (co-enzymes, co-substrates or prosthetic groups) or metal ions. For example, the oxygenase enzymes use predominantly Cu [5], Fe [6] or Mn [7], and incorporate one or two oxygen atoms of O_2 into the substrate (S) (Equations 2-4). The different types are named mono- and dioxygenases.

$$S + O_2 + 2e^- + 2H^+ = SO + H_2O \tag{2}$$

$$S + O_2 = SO_2 \tag{3}$$

$$S + S' + O_2 = SO + S'O \tag{4}$$
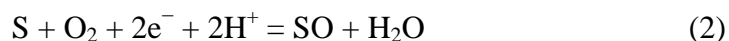
In oxidases, O_2 is not incorporated into the substrate, instead, it acts as electron acceptor in the course of the oxidative transformation of the target molecule (Equation 5).

$$SH_2 + O_2 = S + H_2O_2 \tag{5}$$

The reaction between a ground state organic compound (singlet state – no unpaired electron) and molecular oxygen (triplet state - two unpaired electrons) is a spin-forbidden process [8]. Yet, triplet dioxygen participates in biochemical reactions. The key is usually the presence of a redox active transition metal, bound in enzymes. Mainly Fe and Cu ions are responsible for the activation of dioxygen. They are able to overcome the barrier enforced by the spin mismatch. The evolved metal-oxo species are already efficient enough to activate the corresponding substrates (Scheme 3). [9]
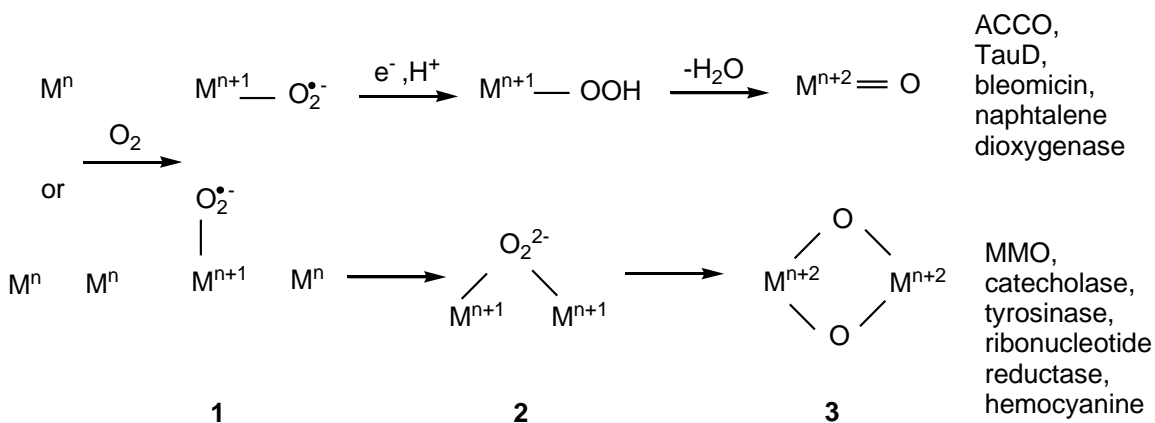

Scheme 3. Activation of dioxygen by metal ions bound in metalloenzymes

The nature of metal ions, coordinated ligands, geometric and electronic effects, additional co-factors and their influence on the structure, stability and reactivity of the occuring intermediate oxo (**3**) and peroxo species (**2**) have been in the focus of several studies. Synthetic model complexes might help as well to gain more information about the individual steps and reactive species of the enzymatic reactions.

2.1.1 Biological activation of dioxygen by Fe-containing enzymes

Enzymes responsible for dioxygen activation having Fe in the active site can be divided to heme and non-heme type enzymes. The former consist of a ferrous ion bound in the middle of a porphyrin ring. An extensively studied and widely known member is cytochrome P450. [10] Non-heme Fe enzymes make a diverse group of dioxygen activating metalloproteins. The group can be divided to mono- and dinuclear enzymes catalyzing a wide range of reactions. Although the active sites of these enzymes are more complicated to study than those of the heme enzymes, due to the lack of intense spectral features, X-ray diffraction offers a tool to obtain structural information. According to the growing crystallographic data about mononuclear iron enzymes, a common motif for a superfamily of this group is the Fe centre surrounded by one Aspartate and two Histidine residues. This set of ligands is often cited as "2-His-1-carboxylate facial triad". [11-13] The remaining three places are commonly occupied by solvent molecules, which are weakly bound and easily displaceable. This structural flexibility is believed to be the main reason for the diverse reactivity of the enzyme group. Notwithstanding their different functions, there are some mechanistic features typical for all members of this family of enzymes (Scheme 4). [12]
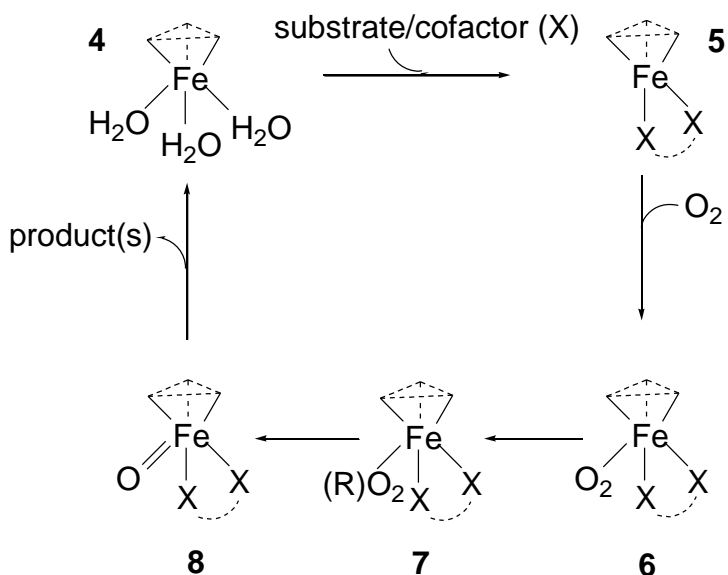

Scheme 4. General mechanism suggested for the reactions catalyzed by enzymes containing the "2-His-1-carboxylate" metal binding site

These are the six-coordinate resting state **4** and subsequent binding of substrate and/or cofactor **5** giving a five-coordinate metal centre with an enhanced affinity towards dioxygen **6** and the formation of a high valent oxo intermediate as active oxidant **8**. It takes a proton from the substrate by homolytic scission giving substrate radical as a result. [14, 15] Fe^{IV}-oxo species has been detected and described by freeze-quench Mössbauer-spectroscopy for TauD [16] and P4H [14]. The TauD results were supported by resonance Raman spectroscopy [17] and EXAFS data [18].

The superfamily having "2-His-1-carboxylate facial triad" can be divided further to five groups: extradiol cleaving catechol dioxygenase, Rieske oxygenase, α-ketoglutarate dependent enzymes (α-KGDO), pterin dependent hydroxylases and miscellaneous enzymes.

Bacteria can decompose aromatic substances by oxidative ring cleavage, which is catalyzed mainly by extradiol cleaving catechol dioxygenases. Besides catechol, they are able to transform analogs like gentisate, salicylate, hydroquinone and 2-aminophenol. The ring cleavage occurs next to the –OH group as shown in Scheme 5. [19]
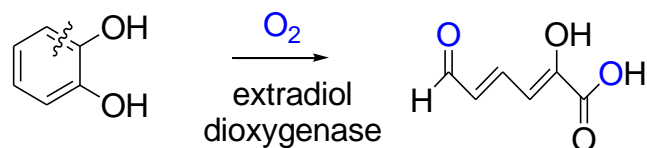
**Scheme 5.** Ring cleavage of extradiol dioxygenases

Rieske oxygenases are responsible for the *cis* dihydroxilation of aromatic compounds, which is the first step in the biodegradation of aromatic substances. Reactions performed by some members (NDO, DIC, CARDO) are shown in Scheme 6. [11]
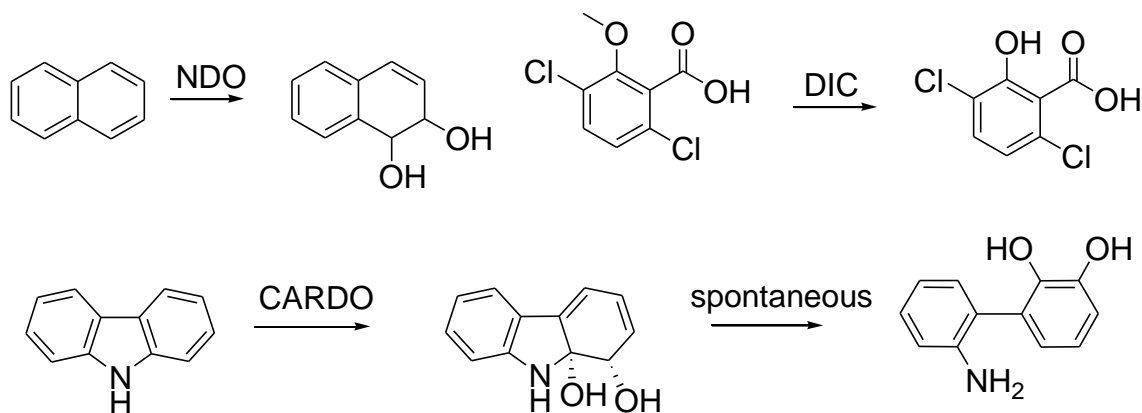
**Scheme 6.** Reactions performed by Rieske oxygenases

Manifold oxidative transformations are catalyzed by α-KGDO. Reactions like ring expansion, desaturation, ring closure and hydroxylation belong here. Perhaps it is the largest group within the "2-His-1-Carboxylate facial triad" superfamily. The usage of α-ketoglutarate as co-substrate is a general feature for α-KGDO and some major mechanistic steps [20] they share as well. (Scheme 7)
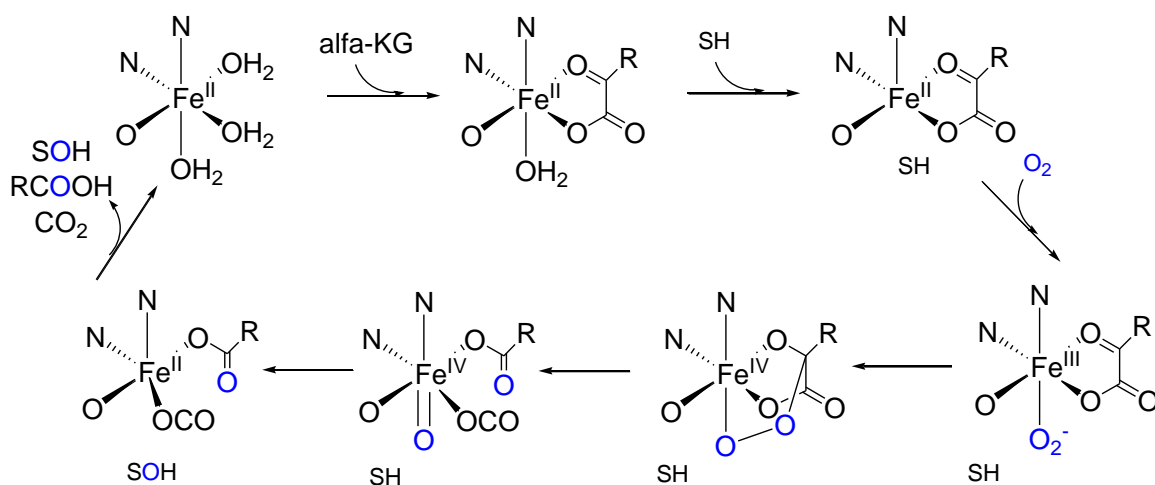
Scheme 7. General mechanism of α-KGDO enzymes

Enzymes like TauD: responsible for the oxidative transformation of taurine [21], TH: have role in the metabolism of nucleic acids [22], P4H: stereospecific hydroxylation

of proline [23] or CAS: hydroxylation, ring closure and desaturation in the synthesis of clavulinic acid [24] belong here. (Scheme 8)
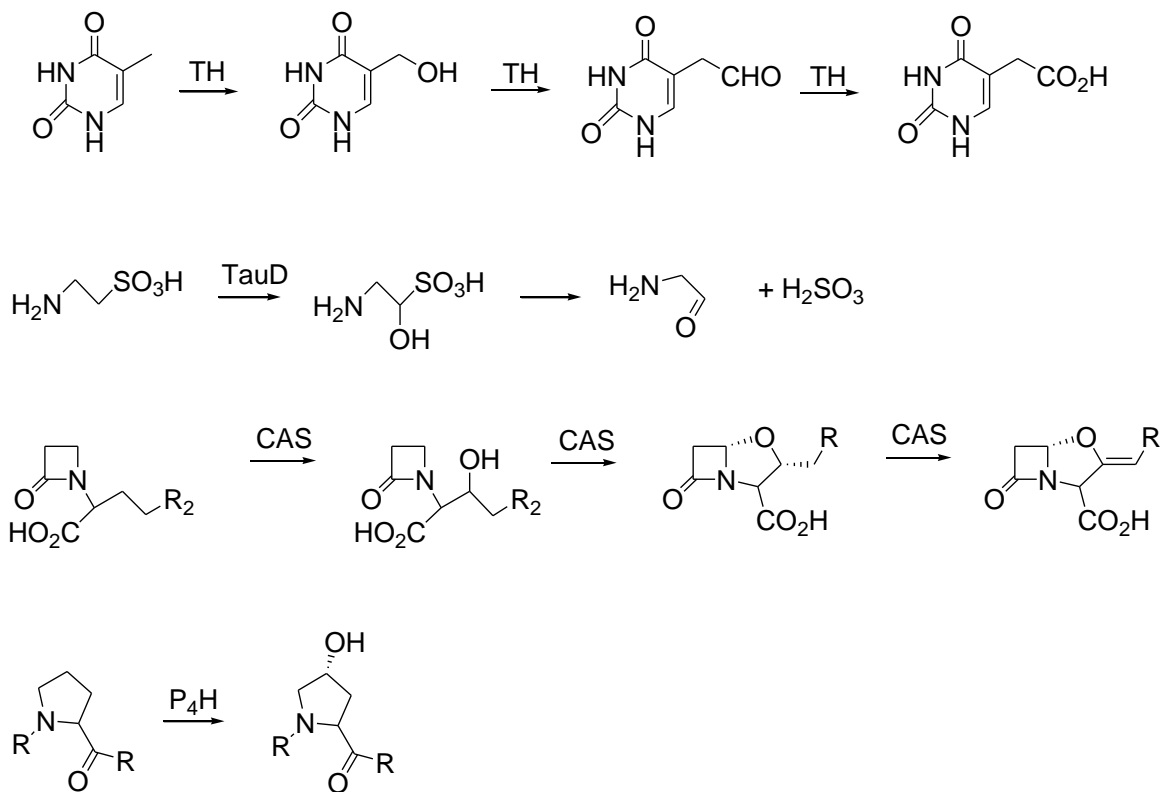

Scheme 8. Reactions catalyzed by α-KGDO enzymes

Pterin dependent hydroxylases make a smaller group. The members use BH_4 as co-factor. These enzymes catalyze the regioselective monohydroxylation of amino acids parallel with the oxidation of the co-factor and are essential for mammalian physiology, although PheH is present in prokaryotes, too. The latter catalyzes the transformation of phenylalanine to Tyr (Scheme 9). [20]
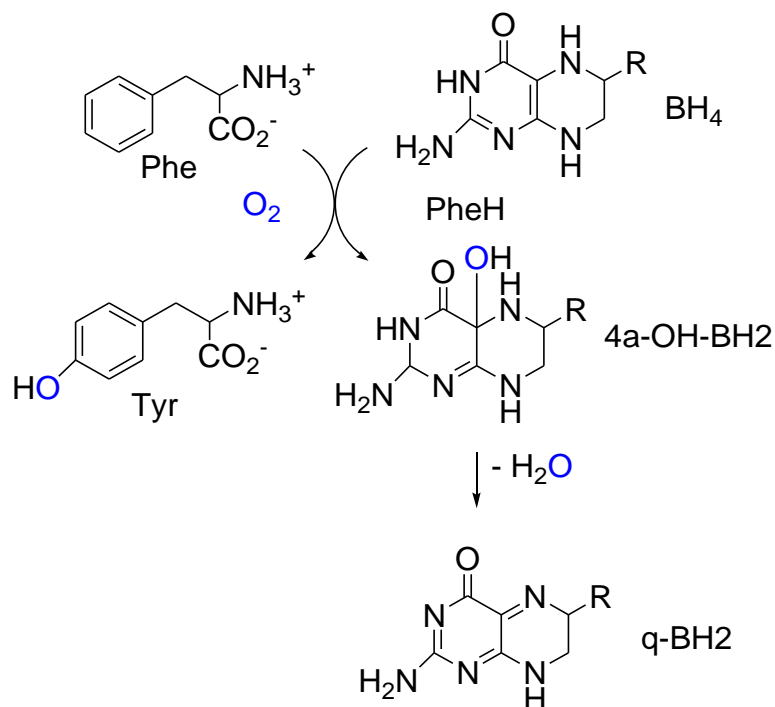
Scheme 9. Reactions performed by phenylalanine hydroxylase (PheH)

The last group is categorized as miscellaneous, since enzymes belonging to this group take part in quite diverse reactions. The recently discovered ones are classified here, not fitting into any other group. SOR, for instance, is crucial for performing the disproportionation of elemental sulfur (Equation 6). [25]

$$4\ [S] + O_2 + 4\ H_2O \longrightarrow 2\ HSO_3^- + 2\ HS^- + 4\ H^+ \tag{6}$$
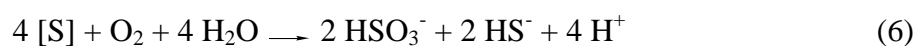
IPNS performs the double oxidative ring closure of the tripeptide ACV to IPN (Scheme 10), the precursor of penicillins and cephalosporins. [26]
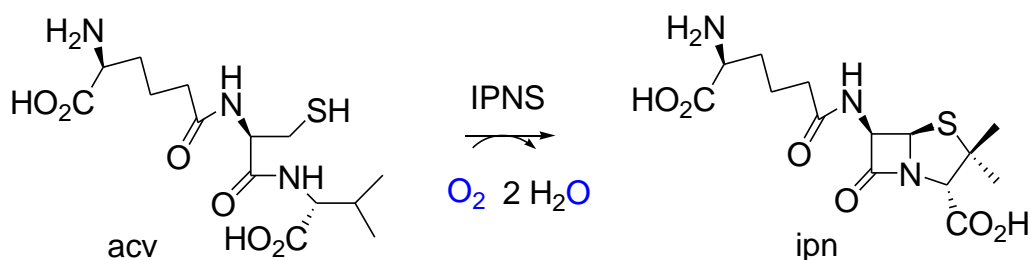

Scheme 10. Reaction catalyzed by IPNS

The enzyme 1-aminocyclopropane-1-carboxylic acid oxidase (ACCO) – responsible for ethylene production in plants – belongs to this group as well. Since current research was related to ACCO, in the followings, more attention is devoted to the introduction of this family of enzymes.

2.1.2. Cu-containing enzymes and the way of dioxygen activation

Copper ion plays significant role in metabolic processes. The functions are as follows: the transport of oxygen, the action of peptide hormones, SOD activity and the enzymatic activation of dioxygen with subsequent substrate oxidation. The active site of the metalloenzymes can be mono- or coupled multinuclear, yet nuclearity has no correlation with the type of reaction catalyzed. Due to the high redox potential of Cu^{III}/Cu^{II} pair the one electron shuttle supported by biological copper takes places via the Cu^{II}/Cu^{I} redox system. The reaction of reduced Cu^{I} centre with dioxygen resulting in intermediate species or adducts able to perform actions on the substrate is the key step in the chemical process performed by this group of enzymes. Notwithstanding this common feature, different mechanisms are carried out depending on the structure of the active site and the type of the reaction. By the function, three main classes can be distinguished among copper-containing enzymes such as mono-, dioxygenases and oxidases. [27]

The level of the neurotransmitter hormones dopamine and norepinephrine is controlled by the enzyme dopamine-β-monooxygenase according to Scheme 11. [28] This process requires four electrons overall, from which two come from the substrate, while the other two are donated by ascorbic acid. EPR spectra indicate a "type 2" cupric ion in the active site.
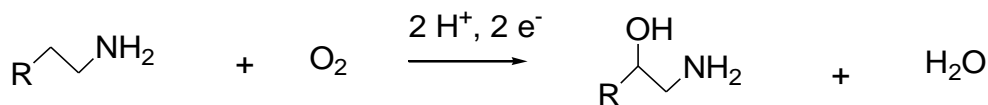

Scheme 11. Action of dopamine-β-monooxygenase

Particulate MMO catalyzes the oxidation of methane giving methanol as product. On the contrary to soluble MMO, particulate MMO is membrane-bound and contains a single Cu ion in the active site. [29]

The cleavage of the *O*-heterocycle of flavonoids is catalyzed by quercetin 2,3-dioxygenase (Scheme 12) resulting in more easily degradable carboxylic acid ester derivatives. The mononuclear copper centre is a homodimer as revealed from X-ray and EPR data (Scheme 13). [30]
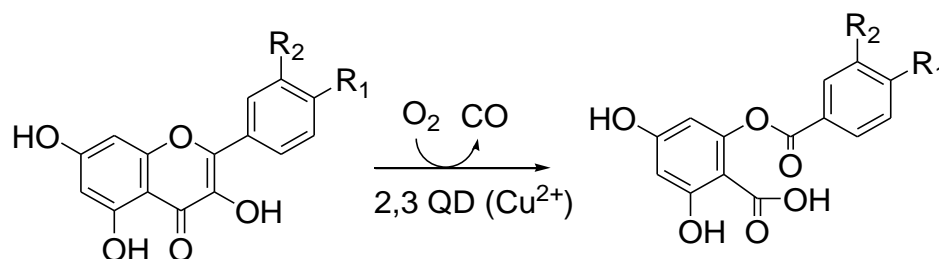

Scheme 12. Reaction catalyzed by quercetin 2,3-dioxygenase
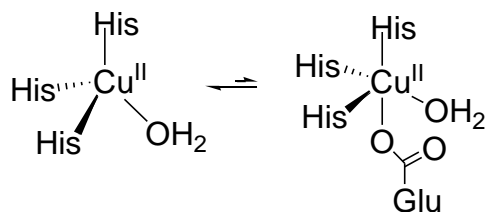
Scheme 13. Structure of active centre of quercetin 2,3-dioxygenase

The regulation of biogenic amine (like dopamine or histamine) level in eukaryotes is controlled through the oxidative metabolism of CAO (Scheme 14). The same process allows the growth of microorganisms on primary amines as a N source in prokaryotes. [31]

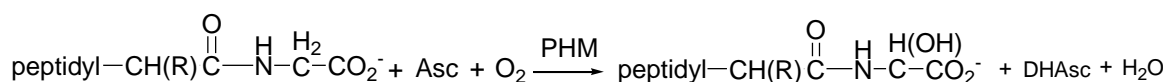$$R-NH_3^+ + O_2 + H_2O \longrightarrow R-CHO + H_2O_2 + NH_4^+$$
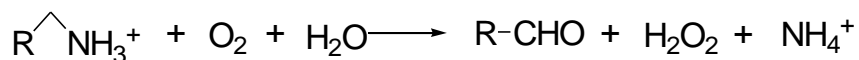
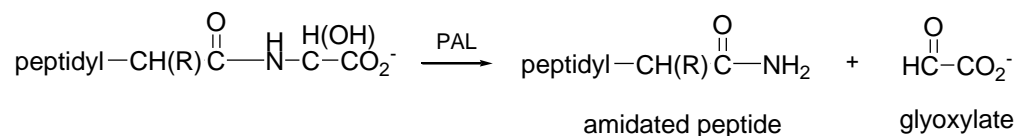**Scheme 14.** General reaction performed by CAO

Fungal enzyme, galactose oxidase performs a two-electron oxidation transforming a wide range of alcohols to aldehydes with the concomitant reduction of oxygen to hydrogen peroxide. The active site is five-coordinate with a distorted square pyramidal geometry and an interesting covalent linkage between sulfur (coming from Cys) to Tyr. [31]

At least half of the known peptide hormones (like oxytocin, thyrotropin or calcitonin) are modified by peptydilglycine α-amidating process. The general procedure – as shown below in Scheme 15 – takes place in two steps. The activity of the purified enzyme is dependent on copper, molecular oxygen and a reducing cofactor. The presence of evolved α–amid moiety is essential for the biological activity for many peptides. The supposed key role of amidation is the prevention of ionization of the CO_2H-terminus and an easier binding to sufficient receptors. [32, 33]

Step 1

$$\text{peptidyl}-CH(R)\overset{O}{\overset{||}{C}}-\overset{H}{\overset{|}{N}}-\overset{H_2}{\overset{|}{C}}-CO_2^- + Asc + O_2 \xrightarrow{PHM} \text{peptidyl}-CH(R)\overset{O}{\overset{||}{C}}-\overset{H}{\overset{|}{N}}-\overset{H(OH)}{\overset{|}{C}}-CO_2^- + DHAsc + H_2O$$

Step 2

$$\text{peptidyl}-CH(R)\overset{O}{\overset{||}{C}}-\overset{H}{\overset{|}{N}}-\overset{H(OH)}{\overset{|}{C}}-CO_2^- \xrightarrow{PAL} \text{peptidyl}-CH(R)\overset{O}{\overset{||}{C}}-NH_2 + \overset{O}{\overset{||}{HC}}-CO_2^-$$

amidated peptide glyoxylate

Scheme 15. Modification of peptide hormones by peptydilglycine α-amidating enzyme

2.1.3. 1-Aminocyclopropane-1-carboxylic acid oxidase

The unique gaseous phytohormone ethylene is involved in the regulation of the lifecycles of plants. It is produced rapidly in dividing and growing cells. Beyond growth, ethylene affects shapes, ripening and senescence. It is actually present in almost all kinds of stress, which affect plants. [34] In the biosynthesis of ethylene (Scheme 16) methionine **9** is first converted to S-adenosyl-L-methionine **10** by SAM synthase, then 1-

aminocyclopropane-1-carboxylic acid (ACCH) **11** is formed by ACC synthase, which can be oxidized to ethylene by ACCO. [35]
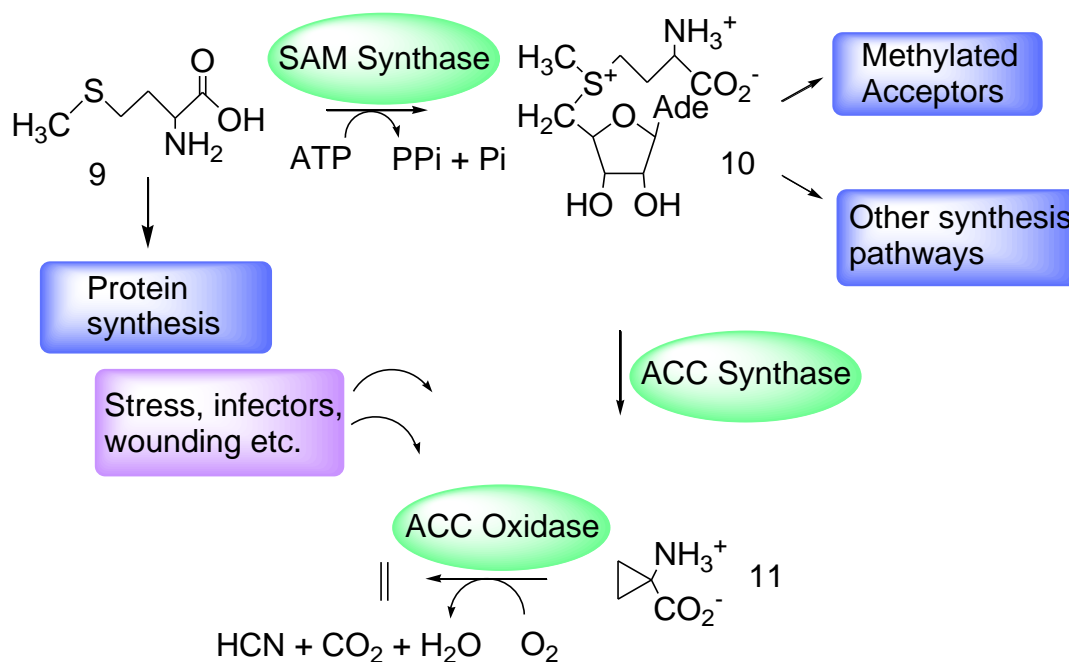
Scheme 16. Main steps of ethylene biosynthesis

Numerous investigations were carried out focusing on the nature of ACCO including *in vivo* tests and genetic probes. [36-41] Results show some unique features for this peculiar reaction. One of them is the usage of ascorbate as co-substrate – in contrast with α-KGDO, which shows sequence homology to ACCO – and the bidentate coordination mode of substrate supported by ENDOR studies. [42, 43] Another interesting feature is the role of CO_2 or HCO_3^-. *In vivo* tests unveiled it as an essential factor for ethylene production. ACCO showed no activity in the absence of CO_2 while at higher CO_2 concentration shift at pH optimum (from 7.0 to 6.5) appeared. [36, 44-46]

Klinman and coworkers studied the action of the enzyme in the reaction of different cyclic (N-MeACCH, ACC-NH₂, ACC-OMe) and acyclic (AIB, D-ALA, GLY) analogues. They found that cyclic substrates form ethylene while products are formed by decarboxylation giving corresponding carbonyls in the case of acyclic substrates. [47]

Regarding calculated K_M, k_{cat} and BDE values (Table 1) for all examined amino acids they excluded substrate activation as the rate determining step.

Table 1. Results of kinetic measurements in the reaction of ACCO [47]

(BDE: bond dissociation energy)

Substrate	k_{cat} (s^{-1})	K_M (10^{-6} M)	BDE (kJ/mol)
ACCH	36.4±1.4	0.099±0.018	407.79
N-MeACCH	12.2±0.5	0.107±0.021	382.67
ACC-NH$_2$	11.3±0.6	0.214±0.047	364.67
ACC-OMe	27.3±1.7	2.76±0.55	407.38
AIBH	22.1±1.6	0.92±0.29	418.68
D-ALA	29.8±0.9	4.42±0.49	413.66
GLY	9.5±0.6	1.0±0.4	414.49

The proposed enzymatic mechanism is shown in Scheme 17. The starting step is the addition of substrate and dioxygen in the presence of co-substrate to the coordination sphere **12**. The evolved Fe^{III}-superoxo adduct abstracts a proton from ascorbate and a high-valent iron-oxo species **14** is formed, which is responsible for the activation of substrate by taking a proton and forming a substrate radical **15**. In higher ascorbate concentration, a competitive inhibition takes place producing H$_2$O and the starting Fe^{II} complex. [47] A high-spin iron-oxo species was described in studies of related TauD. [15, 48]
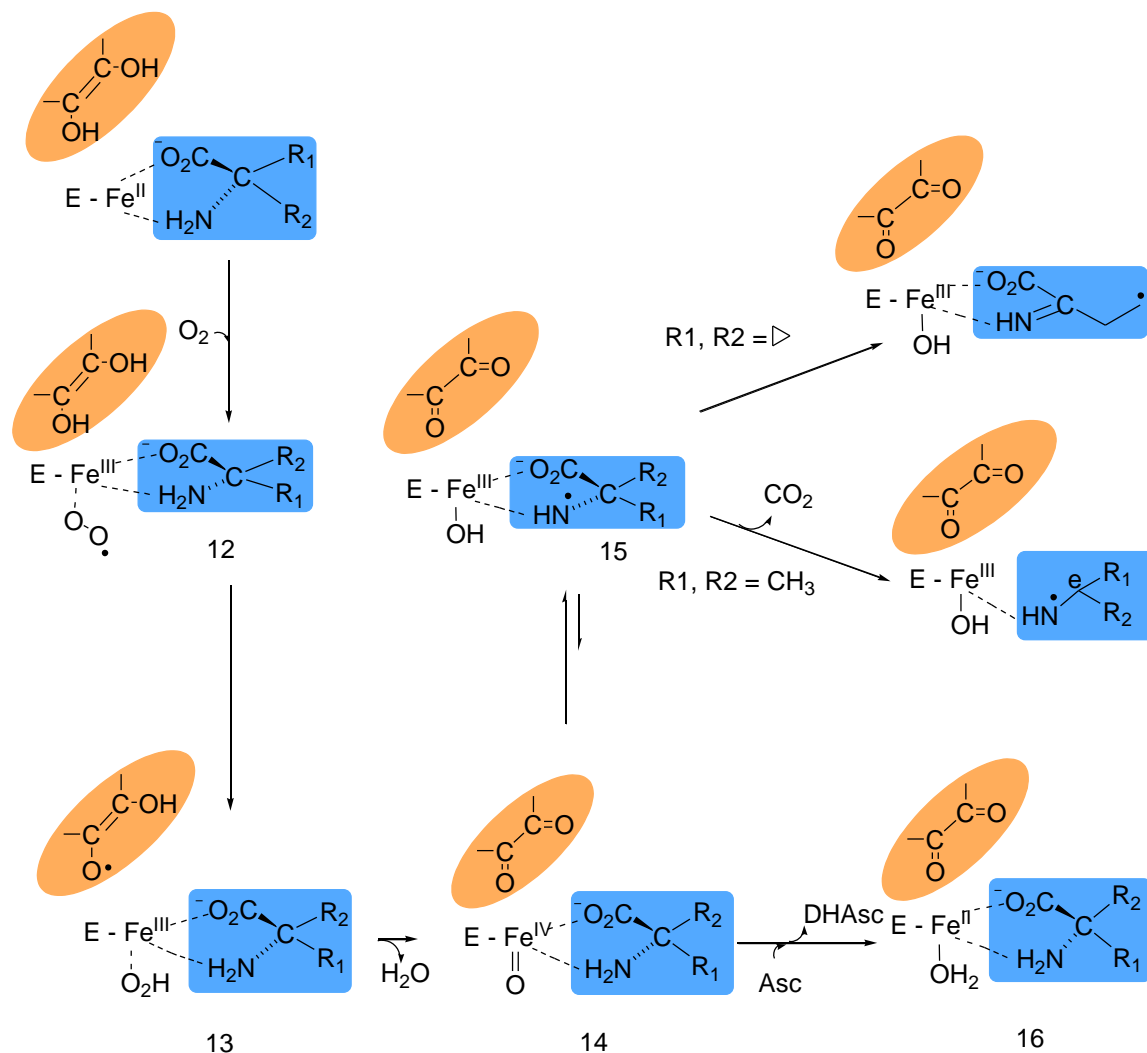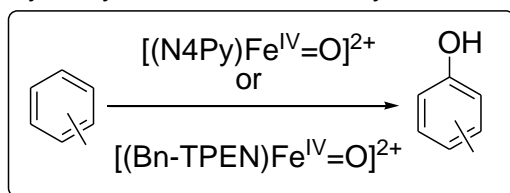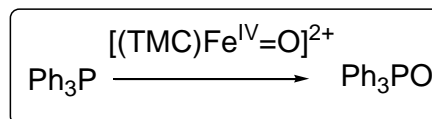
Scheme 17. Steps of the enzymatic reaction suggested by Klinman and colleagues

To elicit the nature of this key component numerous investigations were carried out. Synthetic model complexes of non-heme iron enzymes were investigated. Iron(IV)-oxo intermediates were observed and described extensively by X-ray crystallography, EXAFS, ESI-MS, Mössbauer and UV-Vis spectroscopy. [49-57] Complexes appeared to be active in P-oxidation, epoxidation, hydroxylation reactions and in the oxygenation of sulfides to sulfoxides. Some examples and applied ligands are presented in Scheme 18.
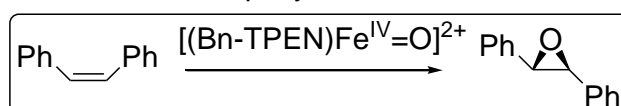
hydroxylation of aromatic hydrocarbons

$$[(N4Py)Fe^{IV}=O]^{2+}$$
or
$$[(Bn\text{-}TPEN)Fe^{IV}=O]^{2+}$$

P-oxydation

$$[(TMC)Fe^{IV}=O]^{2+}$$

$Ph_3P \longrightarrow Ph_3PO$

hydroxylation of aliphatic hydrocarbons

$$[(N4Py)Fe^{IV}=O]^{2+}$$
or
$$[(Bn\text{-}TPEN)Fe^{IV}=O]^{2+}$$

epoxydation

$$[(TPA)Fe^{IV}=O]^{2+}$$

epoxydation

$Ph \diagdown \diagup Ph$ $\quad [(Bn\text{-}TPEN)Fe^{IV}=O]^{2+} \quad$ Ph, Ph
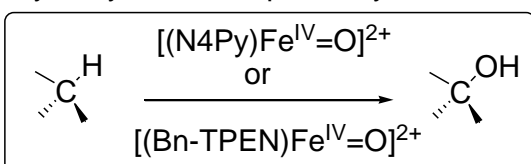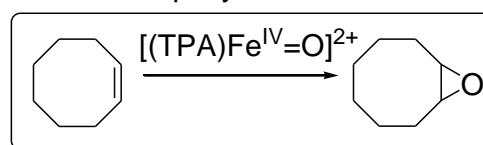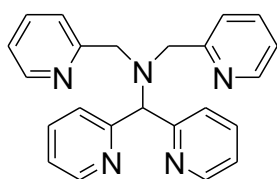
N4Py
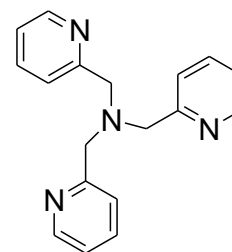
TPA
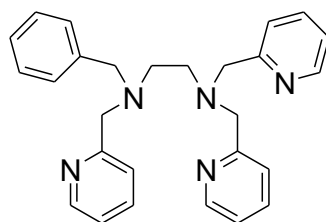
Bn-TPEN
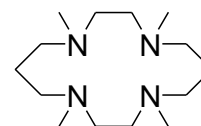
TMC

Scheme 18. Ligands applied in iron(IV)-oxo complexes (lower part)
and their reactions (upper part)

    X-ray measurements revealed information about the structure of ACCO. The crystal structure (Scheme 19) obtained from *Petunia hybrida* shows an active site

consisting of two histidine and one aspartate residues with a single ferrous ion in the centre. [58] MCD studies support that the central metal is six-coordinate in the resting state. [59] The remaining three places are occupied by H_2O molecules, which can be replaced by the substrate or dioxygen. The binding mode of ACC is bidentate, while O_2 binds as a monodentate ligand to the metal ion. Coordination of ACC takes place first followed by O_2; however, the order in attachment of ascorbate is yet pending as unveiled from "steady-state" kinetic measurements. [60]
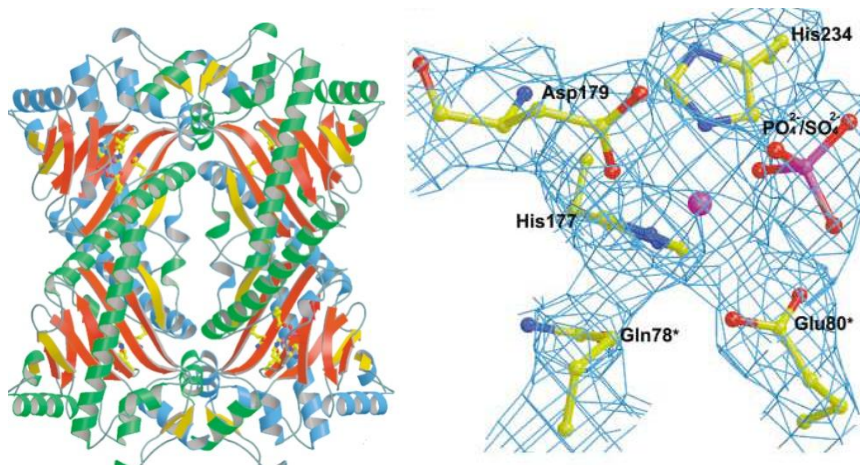
**Scheme 19**. Crystal structure of ACCO

Detailed mechanistic investigations presumed the formation of an amine radical cation as key intermediate in substrate activation. Two possible ways were suggested, as shown in Scheme 20. In **Path A** carbon-centered radical **18** is formed first by a ring-opening step followed by proton abstraction giving carbon-centered radical **20** and products in the last step.
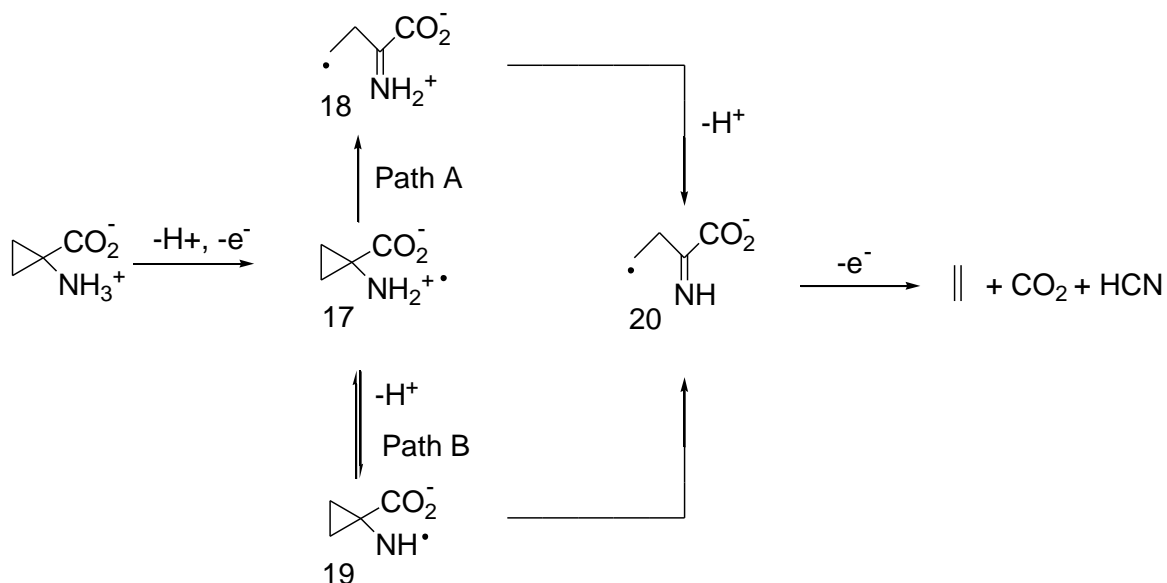
Scheme 20. Possible steps of substrate activation by ACC

Theoretical calculations are more supportive of **Path A** than **Path B** on the basis of the calculated stability and reactivity of the intermediate amine radical **17**.

Pirrung and colleagues investigated extensively the reaction of ACCO by using different cyclic (ACCH, ACBCH, *N*-hydroxy-ACCH, *N*-hydroxy-ACBCH) and acyclic (AIBH, *N*-hydroxy-AIBH) substrates and proposed the mechanism shown below (Scheme 21). [61] Hydroxy-rebinding (**Path D**) was excluded since *N*-hydroxy derivatives were rather inhibitors in the reactions. Direct ring opening was found to be the favorable route (**Path E**) for cyclic substrates and decarboxylation (**Path C**) was described as the possible way for product formation. Later, their suggestions were supported by quantum chemical calculations. [62]
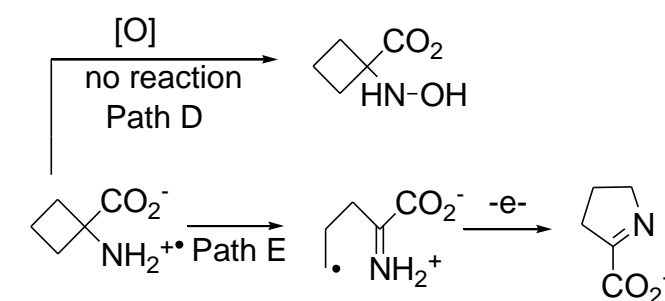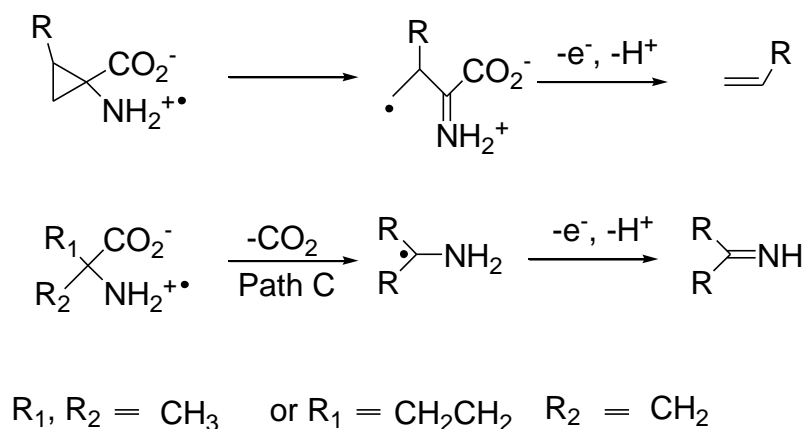
Scheme 21. Proposed mechanism for the oxidation of cyclic and acyclic substrates by ACCO

2.1.3.1. Model studies

Mimicking and altering the action of living organisms are at the focus of interest ever since our civilization evolved. Understanding elemental steps of biochemical reactions might give us the opportunity to control them to some extent. However, there might be hindrances, especially regarding complex systems. It is the case in connection with enzymes as well. Their purification, handling and investigation have many difficulties besides the high costs. The design of enzyme-like molecules offers a number of possibilities to get information about the steps of their parent reactions and the way they work. They offer a tool for easier management and analysis. One way for creating enzyme models is the synthesis of transition metal complexes, which can act as structural and/or functional analogous of native enzyme. The target reaction of the current project is the action of the enzyme ACCO, which has a limited number of models so far.

Nishida's group studied the reaction of ACC in the presence of H_2O_2 using binuclear Fe(III)-complexes. They detected ethylene as product in the reaction of $[Fe_2(HPTB)(OH)(NO_3)_2]^{2+}$ and $[Fe_2(HPTP)(OH)(NO_3)_2]^{2+}$ and ACC; however, an excess of H_2O_2 was necessary.[63] They synthesized and investigated other binuclear transition metal complexes, too (Ni(II), Fe(III), V(III), Co(II), Mn(III)), with HXTA as ligand, but only found Co(II) and Mn(III) containing ones to be active. [64] Ligands are shown in Scheme 22.

HHPTP: R = py
HHPTB: R = bzm

HXTA
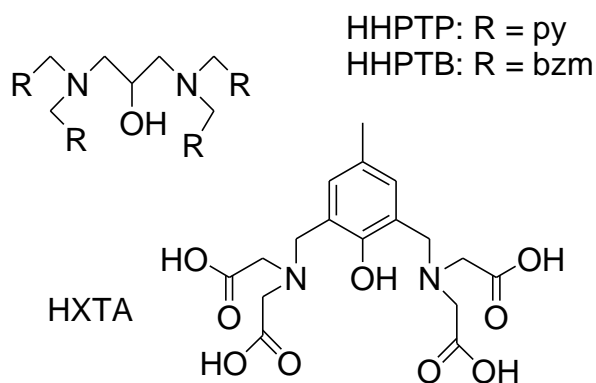
Scheme 22. Ligands used by Nishida and co-workers

Cu(II)-ACC containing systems were investigated by Simaan and co-workers with ligands demonstrated in Scheme 23. [65, 66] They performed reactions in H_2O and CH_3OH with H_2O_2, and found all complexes active giving ethylene as product. They were able to obtain information about the structure of their complexes by using X-ray crystallography and EPR measurements. A brown intermediate was observed during the reaction, which was assumed to be the active oxidizing intermediate, and identified as a Cu(I)-O_2H species.

2,2'-bipyridine

2-picolylamine

1,10-phenanthroline
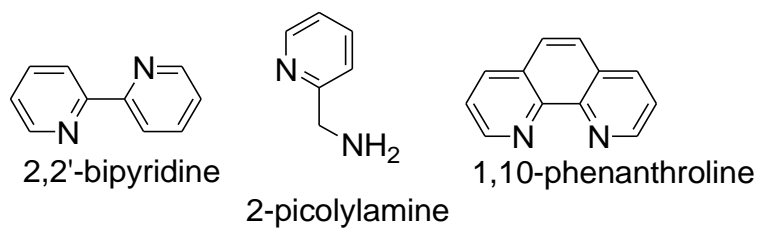
Scheme 23. Ligands applied by Simaan and co-workers

This group also investigated an ACC-containing μ-oxo-diiron(III) complex: $[(TACN)Fe_2(\mu\text{-}o)(\mu\text{-}ACCH)_2](ClO_4)_4.2H_2O$. Ethylene was formed in the reaction of the complex with H_2O_2. Upon addition a large amount of base, decomposition and loss of activity were observed. The maximum conversion (16%) was achieved with 2-3 equivalents of NaOH. [67]

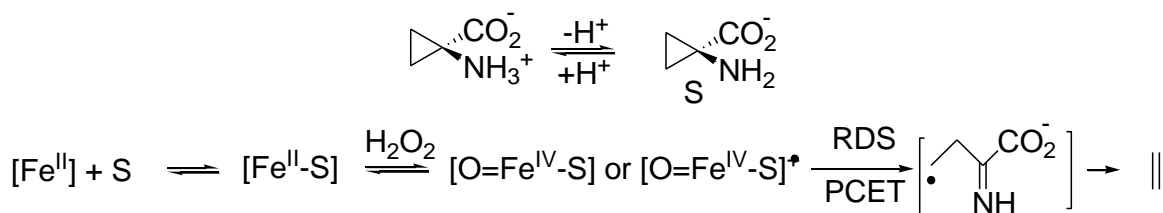Tolman's group described $Cu(I)$-$OOC(O)R$ and derived $[Cu^{II}\text{-}O^{-\bullet} \longleftrightarrow Cu^{III}\text{=}O^{2-}]^+$ as possible active intermediates in the reaction of α-ketocarboxylates also supported by computational studies. [68]

A SALEN-ligated Fe complex was synthesized, characterized and assigned as active catalyst in the reaction of amino acids using H_2O_2 in the presence of base by Baráth et al. [69] They optimized conditions regarding concentrations and solvent. Alternative substrates (AIBH, ALAH) were used besides ACCH. Reactions are summarized in Scheme 24. Ethylene was detected in the reaction of ACC, while the formation of the corresponding carbonyls was observed in the two other cases.

AIBH: $R_1 = R_2 = CH_3$
ALAH: $R_1 = H, R_2 = CH_3$
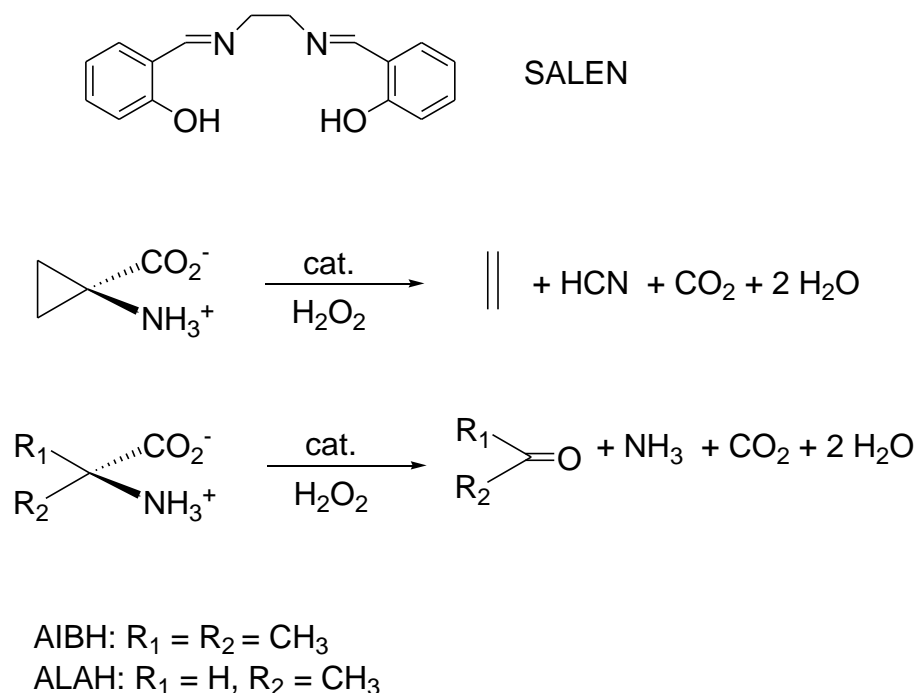
Scheme 24. Reactions catalyzed by $[Fe^{III}(SALEN)]Cl$ in the presence of H_2O_2 and base in DMF/H_2O

21

The proposed mechanism is shown in Scheme 25. They described it with a fast pre-equilibrium in the first step between the substrate and the catalyst relying on kinetic measurements (*Michaelis-Menten* type kinetics). They suggested Fe^{IV}-oxo intermediates being responsible for the activation of substrate based on UV-Vis results, and described rate determining step (RDS) with ET-PT process, since the determined SIE values were below 4.

$$[Fe^{II}] + S \rightleftharpoons [Fe^{II}\text{-}S] \xrightarrow{H_2O_2} [O=Fe^{IV}\text{-}S] \text{ or } [O=Fe^{IV}\text{-}S]^{\bullet} \xrightarrow[PCET]{RDS}$$

Scheme 25. Suggested mechanism for the reactions catalyzed by [Fe^{III}(SALEN)]Cl in presence of H_2O_2 and base in DMF/H_2O

2.2. Degradation of amino acids

Amino acids are probably best known as the monomeric units of proteins. Besides this, they take part in several metabolic steps, and serve as basic nutrients for animals. [2]

During the treatment of water and wastewater, amino acids might give harmful substances as the result of chlorination. Dichloroacetonitrile and chloral were determined as major side-products during the chlorination of aspartic acid, tyrosine and tryptophan. [70, 71] The oxidation of amino acids – beyond the enzymatic way – can be performed by reactive oxygen species [72, 73], or as metal-catalyzed oxidation process. [74, 75]

Noorhasan and co-workers studied the oxidation of glycine and glycylglycine with $Fe^{VI}O_4^{2-}$, and detected acetate, CO_2, NH_3 and N_2 as products. [76] Another group investigated the reaction of valine, leucine and alanine besides that of glycine in alkaline medium with chloramine and *β*-cyclodextrin as catalyst. They detected aldehydes as products. [77] Degradation of other L-amino acids was also investigated in acidic medium by different groups. For instance, Ru^{III}chloride was described as efficient catalyst in the reaction of glycine, valine, alanine and leucine giving aldehydes, NH_3 and CO_2 as products using sodium *N*-chloro-*p*-toluenesulfonamide. [78] However, sodium *N*-chloro-*p*-toluenesulfonamide is able to perform the reaction alone as well. [79]

22

3. THE AIMS OF THE WORK

The purpose of my research was to gain information about the action of ACCO through synthetic model complexes, which were available only in limited number this far. Accordingly, the following objectives were set:

- Synthesis and characterization of Fe- and Cu-containing model complexes.

- Application of the synthesized complexes as possible catalysts in the oxidation of various cyclic and acyclic amino acids.

- Eliciting the nature of possible reactive intermediates.

- To describe the kinetics of the reactions.

4. RESULTS AND DISCUSSION

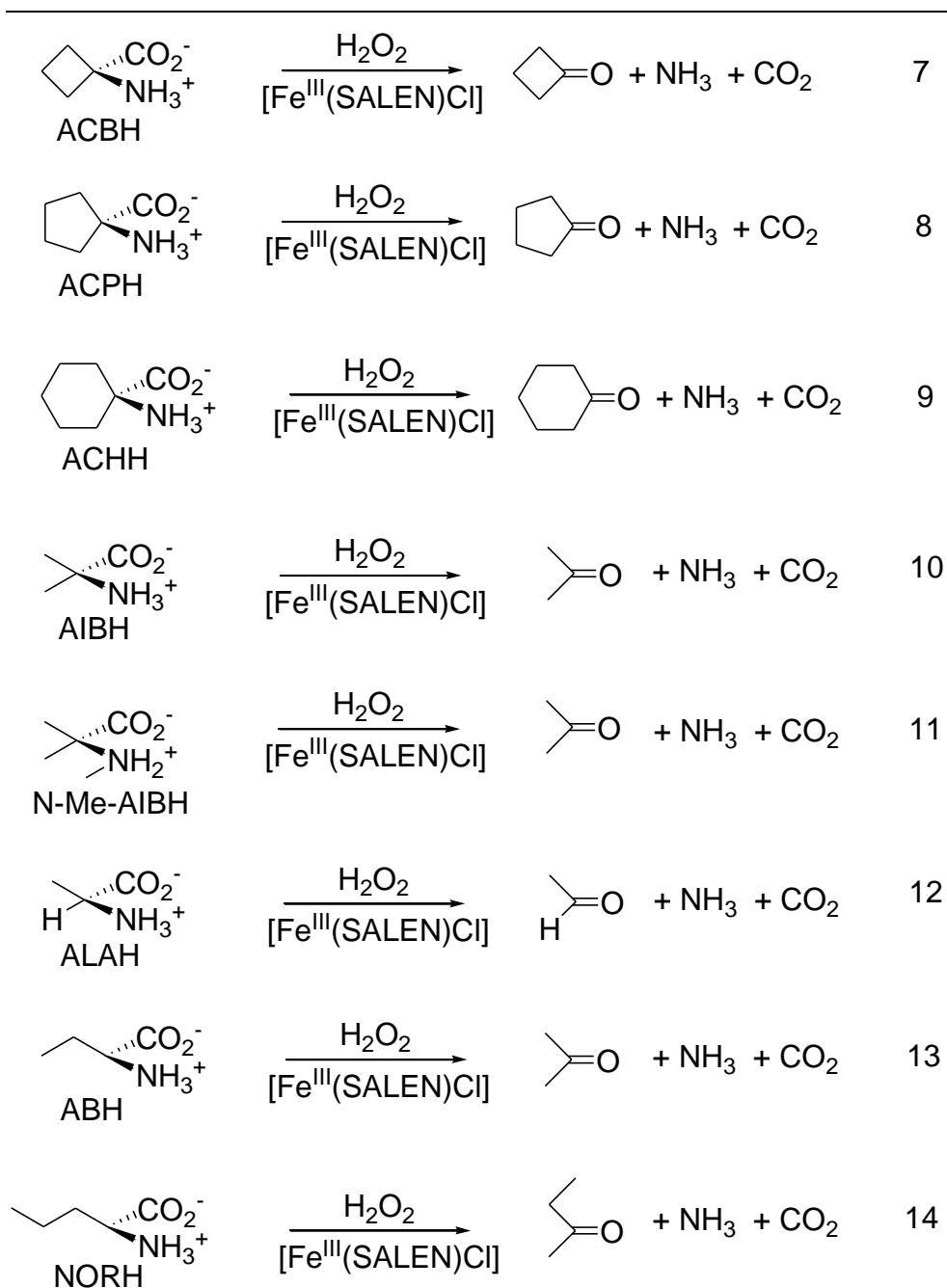## 4.1 Investigation of [Fe^{III}(SALEN)Cl] as catalyst in the oxidation of amino acids

Schiff bases − like the applied SALEN − are commonly used in catalysis. They are able to stabilize different transition metals (Ni, Co, Cu, Zn, Ti, Fe, Ru, Al, Cr) in various oxidation states giving the tool to control a number of catalytic reactions like polymerization, epoxidation, *Diels-Alder* synthesis or *Claisen* rearrangement. [80-82] Schiff bases are moderate electron donors with a chelating structure, and their synthesis is easy and cheap, in addition. The term SALEN was originally used only for tetradentate Schiff bases derived from ethylenediamine. Now it is referred to the *N,N,O,O* tetradentate bis-Schiff base ligands. The members of this group with the remaining open axial sites are quite similar to porphyrins but much easier to prepare. The applied complex [Fe^{III}(SALEN)Cl] was synthesized following a literature method. [83]

The oxidation of ACCH and AIBH were investigated using [Fe^{III}(SALEN)Cl] as catalyst. Reactions were performed in a vial closed with a rubber septum in a solvent mixture of DMF/H_2O (3 : 1) at 35 °C. An induction period was observed in the oxidation of amino acids, which can be reduced with the addition of a certain amount of base. [70] The phenomenon is most likely due to the increased reactivity of amino acids in their anionic form. Molar ratios were [Fe^{III}(SALEN)Cl] : [AA] : [NH_4OH] : oxidant 1 : 5000 : 5000 : 5000, respectively. H_2O_2, PhIO, TBHP, MCPBA and PMS were applied as oxidizing agents. Samples were taken from the head-space of the vial, and injected to a gas chromatograph as is going to be described in Section 5. Reactions were selective giving ethylene or acetone as products. Calculated TOF values are collected in Table 2. The highest values were obtained for H_2O_2, in general.

**Table 2.** Comparison of product formation in the oxidation of amino acids (ACCH, AIBH) in DMF/H_2O (3 : 1) at 35 °C. $[S]_0 = 3.6 \times 10^{-2}$ M, $[Fe^{III}(SALEN)Cl]_0 = 7.2 \times 10^{-6}$ M, $[H_2O_2]_0 = 3.6 \times 10^{-2}$ M, $[NH_4OH]_0 = 3.6 \times 10^{-2}$ M.

		H_2O_2	PhIO	TBHP	MCPBA	PMS
ACCH	TOF (catalyzed) [1/h]	565±56	310±22	3±0.2	734±65	578±6
	TOF (uncatalyzed) [1/h]	1±0.1	190±14	-	522±41	353±3
AIBH	TOF (catalyzed) [1/h]	9273±349	27±3	61±5	1328±36	1508±48
	TOF (uncatalyzed) [1/h]	460±59	7±1	33±2	288±19	378±23

Since ACCO is able to perform reaction with a number of amino acids [47], further analogues were chosen for kinetic studies. For particular data see Table A1 – A10. Different cyclic and acyclic amino acids were investigated as alternative substrates. [Fe^{III}(SALEN)Cl] appeared to be active catalyst in all cases examined. Interestingly, no base was nessecary in the reaction of cyclic substrates. Corresponding carbonyls (cyclobutanone, cyclopentanone, cyclohexanone, acetone, acetaldehyde and ethyl-methyl-ketone) were formed according to equations (7-14) below. Reactions were selective with one exception. For ACBCH two other peaks appeared on the chromatogram in addition to cyclobutanone. Products were identified as Δ^1-pyrroline-2-carboxylic acid (dehydroproline) and *n*-butyronitrile. These compounds can be formed through ring opening and decarboxylation pathways (Scheme 21). [61]
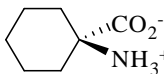
$$\overset{\text{ACBH}}{\underset{\text{NH}_3^+}{\text{⬭}}\text{CO}_2^-} \xrightarrow[\text{[Fe}^{\text{III}}\text{(SALEN)Cl]}]{\text{H}_2\text{O}_2} \quad \text{⬭=O} + \text{NH}_3 + \text{CO}_2 \qquad 7$$

$$\overset{\text{ACPH}}{\underset{\text{NH}_3^+}{\text{⬠}}\text{CO}_2^-} \xrightarrow[\text{[Fe}^{\text{III}}\text{(SALEN)Cl]}]{\text{H}_2\text{O}_2} \quad \text{⬠=O} + \text{NH}_3 + \text{CO}_2 \qquad 8$$

$$\overset{\text{ACHH}}{\underset{\text{NH}_3^+}{\text{⬡}}\text{CO}_2^-} \xrightarrow[\text{[Fe}^{\text{III}}\text{(SALEN)Cl]}]{\text{H}_2\text{O}_2} \quad \text{⬡=O} + \text{NH}_3 + \text{CO}_2 \qquad 9$$

$$\overset{\text{AIBH}}{\underset{\text{NH}_3^+}{\text{⋊}}\text{CO}_2^-} \xrightarrow[\text{[Fe}^{\text{III}}\text{(SALEN)Cl]}]{\text{H}_2\text{O}_2} \quad \text{⋊=O} + \text{NH}_3 + \text{CO}_2 \qquad 10$$

$$\overset{\text{N-Me-AIBH}}{\underset{\text{NH}_2^+}{\text{⋊}}\text{CO}_2^-} \xrightarrow[\text{[Fe}^{\text{III}}\text{(SALEN)Cl]}]{\text{H}_2\text{O}_2} \quad \text{⋊=O} + \text{NH}_3 + \text{CO}_2 \qquad 11$$

$$\overset{\text{ALAH}}{\underset{\text{NH}_3^+}{\text{H⋊}}\text{CO}_2^-} \xrightarrow[\text{[Fe}^{\text{III}}\text{(SALEN)Cl]}]{\text{H}_2\text{O}_2} \quad \text{H⋊=O} + \text{NH}_3 + \text{CO}_2 \qquad 12$$

$$\overset{\text{ABH}}{\underset{\text{NH}_3^+}{\text{⋀}}\text{CO}_2^-} \xrightarrow[\text{[Fe}^{\text{III}}\text{(SALEN)Cl]}]{\text{H}_2\text{O}_2} \quad \text{⋊=O} + \text{NH}_3 + \text{CO}_2 \qquad 13$$

$$\overset{\text{NORH}}{\underset{\text{NH}_3^+}{\text{⋀⋀}}\text{CO}_2^-} \xrightarrow[\text{[Fe}^{\text{III}}\text{(SALEN)Cl]}]{\text{H}_2\text{O}_2} \quad \text{⋋=O} + \text{NH}_3 + \text{CO}_2 \qquad 14$$
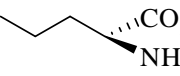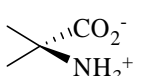
The calculated conversion and TOF values for each amino acid are summarized in Figure 1.
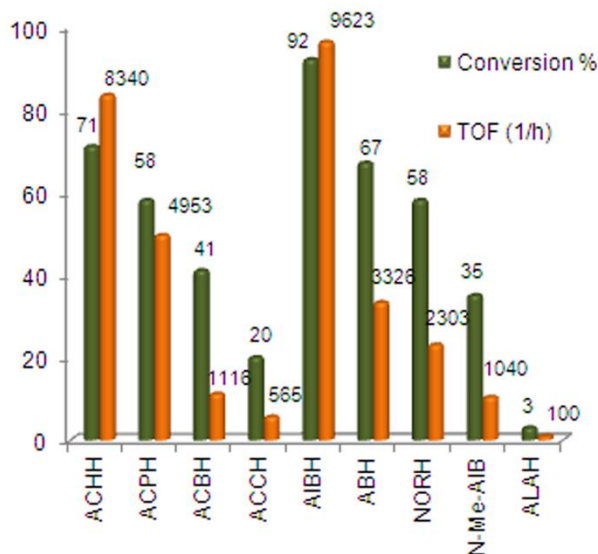
Figure 1. Conversion and TOF values for amino acid oxidations (substrate (reaction time in minutes)): ACCH (100), ACBCH (110), ACPCH (35), ACHCH (25), AIBH (25), ABH (60), NORH (60), N-Me-AIB (100), ALAH (120)) in DMF/H_2O (3 : 1) at 35 °C. $[S]_0 = 3.6 \times 10^{-2}$ M, $[Fe^{III}(SALEN)Cl]_0 = 7.2 \times 10^{-6}$ M, $[H_2O_2]_0 = 3.6 \times 10^{-2}$ M, $[NH_4OH]_0 = 3.6 \times 10^{-2}$ M.

Reactions were also performed in DMF/D_2O solvent mixture. Determined SIE values are collected in Table 3. Data suggest the presence of solvent isotop effect. The calculated SIE values are considerably low (between 1.2 and 2.5), similarly to the enzymatic ones [83], which indicates a PT-ET mechanism regarding the rate determining step. According to studies, SIE values are relatively low for PT-ET reactions [49, 84], and the oxidation of O-H and N-H bonds is more likely to occur in a stepwise mechanism. [85]

Table 3. Steady state kinetic parameters for [Fe^{III}(SALEN)Cl]-catalyzed amino acid oxidation

	K_M (10^{-3} M)	k_{cat} (s^{-1})	k_{cat}/K_M (M^{-1}s^{-1})	V_{max} (10^{-5} Ms^{-1})	SIE
cyclopropyl-CH(CO$_2^-$)(NH$_3^+$)	17.03 ± 2.50	0.10 ± 0.01	5.45	0.07 ± 0.01	1.38
cyclobutyl-CH(CO$_2^-$)(NH$_3^+$)	13.59 ± 0.05	0.41 ± 0.01	30.27	0.29 ± 0.01	2.50
cyclopentyl-CH(CO$_2^-$)(NH$_3^+$)	21.29 ± 2.03	2.35 ± 0.16	110.51	1.70 ± 0.12	1.33
cyclohexyl-CH(CO$_2^-$)(NH$_3^+$)	23.78 ± 3.13	3.04 ± 0.28	127.85	2.19 ± 0.20	1.80
H-CH(CO$_2^-$)(NH$_3^+$) (CH$_3$)	15.99 ± 3.46	0.06 ± 0.01	3.69	0.05 ± 0.01	2.10
n-propyl-CH(CO$_2^-$)(NH$_3^+$)	20.52 ± 4.24	1.57 ± 0.24	76.41	1.13 ± 0.18	2.13
isobutyl-CH(CO$_2^-$)(NH$_3^+$)	14.86 ± 1.74	2.07 ± 0.17	139.36	1.49 ± 0.12	2.47
tert-butyl-CH(CO$_2^-$)(NH$_3^+$)	12.92 ± 1.09	4.13 ± 0.28	319.68	2.98 ± 0.20	1.24

Detailed kinetic measurements were carried out with all amino acids under pseudo first order conditions to determine rate constant. Figure 2 shows the measured initial rate values vs. different substrate concentration for ACCH. Similar saturation curve was obtained in all other cases. Results indicate *Michaelis-Menten* type kinetics, which is typical for enzymatic reactions. Data suggest the binding of substrate to the catalyst in a fast pre-equilibrium step.
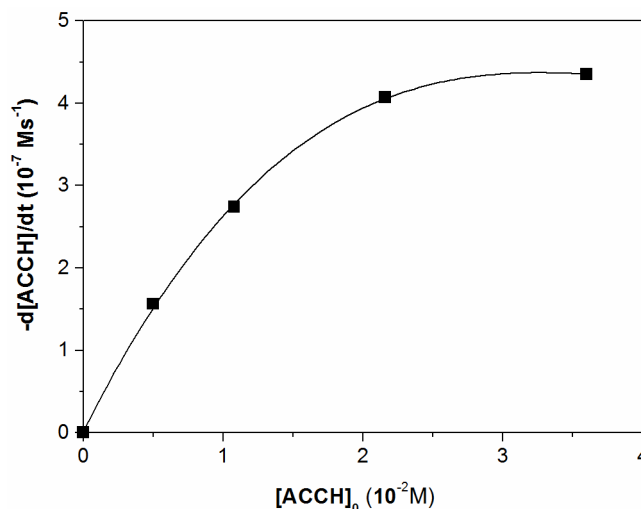
Figure 2. Correlation between substrate concentration and the rate of the reaction for the reaction of ACCH in DMF/H$_2$O (3 : 1) at 35 °C. [Fe^{III}(SALEN)Cl]$_0$ = 7.2×10^{-6} M, [H$_2$O$_2$]$_0$ = 3.6×10^{-2} M, [NH$_4$OH]$_0$ = 3.6×10^{-2} M.

If the reciprocal of the initial rate of the reaction is plotted vs. the reciprocal of substrate concentration (*Lineweaver-Burk* plot, shown for ACCH in Figure 3) kinetic parameters can be determined. Data are summarized in Table 3.
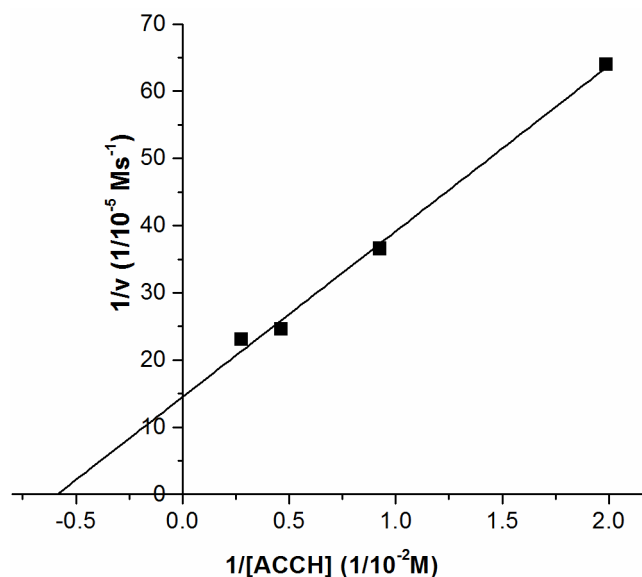

Figure 3. *Lineweaver-Burk* plot for ACCH. Correlation between substrate concentration and the rate of the reaction. [Fe^{III}(SALEN)Cl]$_0$ = 7.2×10^{-6} M, [H$_2$O$_2$]$_0$ = 3.6×10^{-2} M, [NH$_4$OH]$_0$ = 3.6×10^{-2} M, DMF/H$_2$O (3 : 1) at 35 °C.

In order to determine the reaction rate for the oxidant, experiments were carried out with different initial H_2O_2 concentrations for cyclic and acyclic substrates as well. Results (Figure 4-6) unveiled first order dependence for H_2O_2 concentration. Catalyst remained active even on the addition of significant excess of H_2O_2. Proportion of the products formed in the reaction of ACBCH are presented in Figure 7.
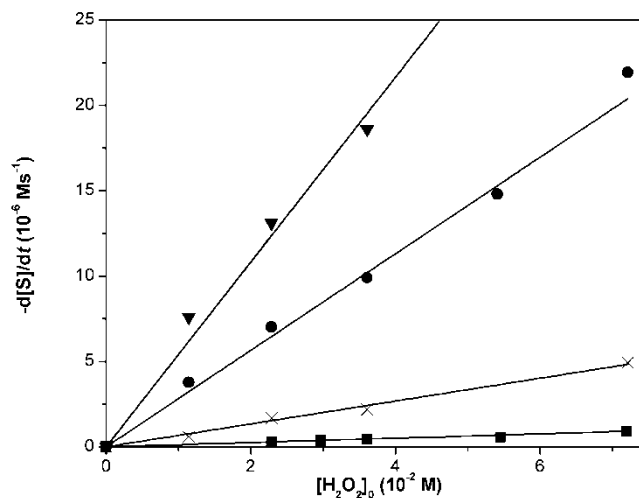
Figure 4. Hydrogen peroxide dependence of amino acid oxidation reactions in DMF/H_2O (3 : 1) at 35 °C for cyclic substrates. $[S]_0 = 3.6 \times 10^{-2}$ M, $[Fe^{III}(SALEN)Cl]_0 = 7.2 \times 10^{-6}$ M, $[NH_4OH]_0 = 3.6 \times 10^{-2}$ M. ■ ACCH, × ACBCH, ● ACPCH, ▼ ACHCH
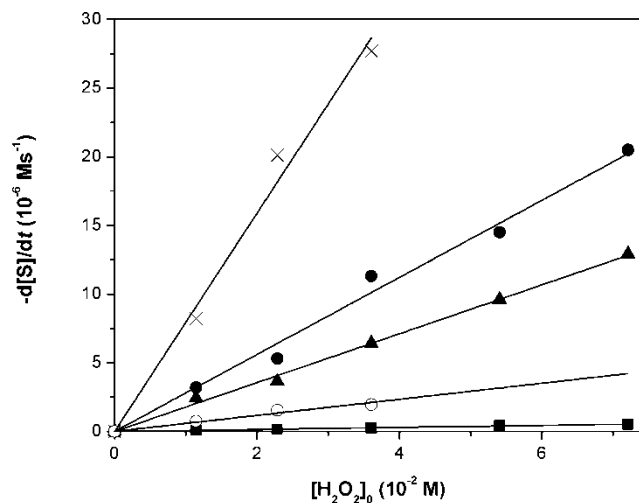
Figure 5. Hydrogen peroxide dependence of amino acid oxidation reactions in DMF/H_2O (3 : 1) at 35 °C for acyclic substrates. $[S]_0 = 3.6 \times 10^{-2}$ M, $[Fe^{III}(SALEN)Cl]_0 = 7.2 \times 10^{-6}$ M, $[NH_4OH]_0 = 3.6 \times 10^{-2}$ M. ■ ALAH, o *N*-Me-AIB, ▲ NORH, ● ABH, x AIBH.

30
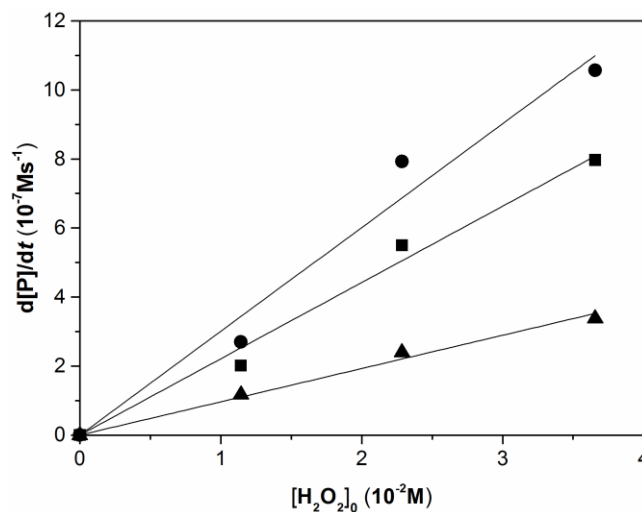
Figure 6. Hydrogen peroxide dependence of amino acid oxidation reactions in DMF/H_2O (3 : 1) at 35 °C. $[ACBCH]_0 = 3.6 \times 10^{-2}$ M, $[Fe^{III}(SALEN)Cl]_0 = 7.2 \times 10^{-6}$ M, $[NH_4OH]_0 = 3.6 \times 10^{-2}$ M. ● n-butyronitrile, ■ cyclobutanone, ▲ dehydroproline
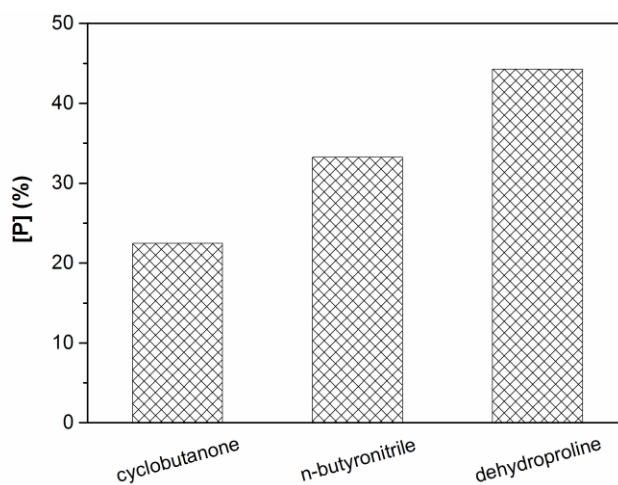

Figure 7. Proportion of the products formed in the reaction of ACBCH in DMF/H_2O (3:1) at 35 °C. $[ACBCH]_0 = 3.6 \times 10^{-2}$ M, $[Fe^{III}(SALEN)Cl]_0 = 7.2 \times 10^{-6}$ M, $[NH_4OH]_0 = 3.6 \times 10^{-2}$ M.

Linear correlation was determined by plotting the rate of the reaction versus catalyst concentration. Results are shown in Figures 8 and 9 for acyclic and for cyclic substrates, respectively.
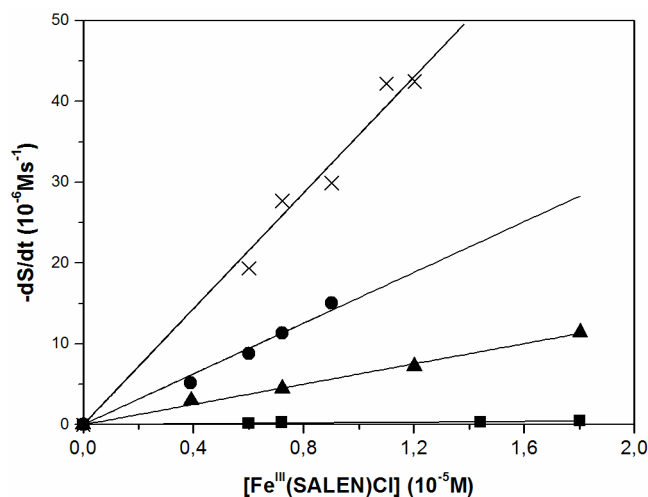
Figure 8. Correlation between catalyst concentration and the rate of the reaction of amino acid oxidation in DMF/H$_2$O (3 : 1) at 35 °C. [S]$_0$ = 3.6×10^{-2} M, [H$_2$O$_2$]$_0$ = 3.6×10^{-2} M, [NH$_4$OH]$_0$ = 3.6×10^{-2} M., x AIBH, ● ABH, ▲ NORH, ■ ALAH.
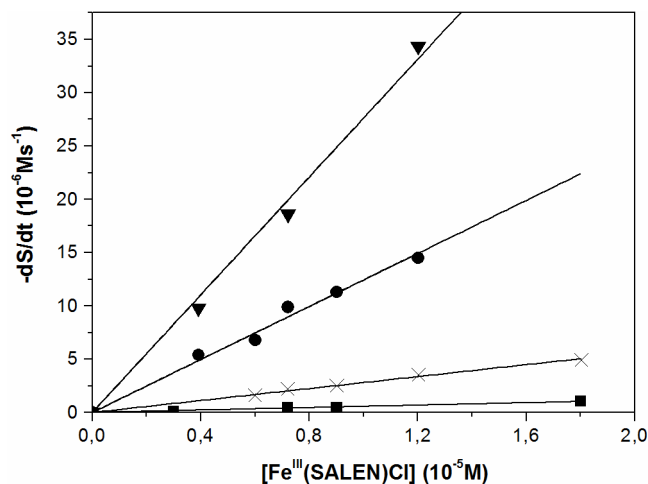
Figure 9. Correlation between catalyst concentration and the rate of the reaction of amino acid oxidation in DMF/H$_2$O (3 : 1) at 35 °C. [S]$_0$ = 3.6×10^{-2} M, [H$_2$O$_2$]$_0$ = 3.6×10^{-2} M, [NH$_4$OH]$_0$ = 3.6×10^{-2} M. ▼ACHCH, ● ACPCH, x ACBCH, ■ ACCH.

The nature of possible active intermediate was also investigated. [Fe^{IV}O(SALEN)]$^{•+}$ was generated in CH$_3$CN at 5 °C as previously reported by Rajagopal and coworkers [86, 87] and its reaction with ACC was followed with UV-Vis spectroscopy (Figure 10) by monitoring the peak – assigned to iron-oxo species – and it's

decrease at 470 nm. Paralell to the above described procedure, ethylene was detected as product by gas chromatography.
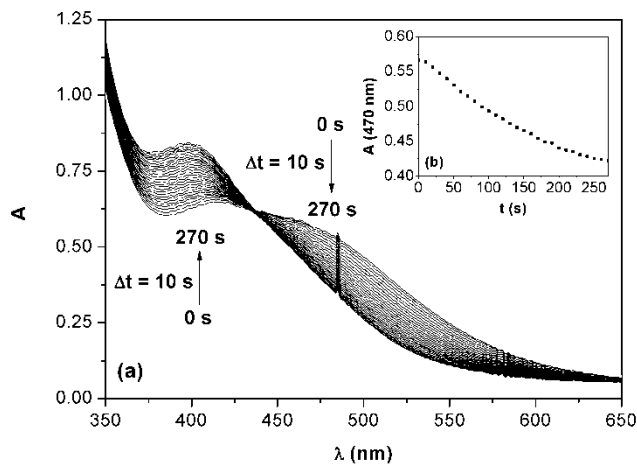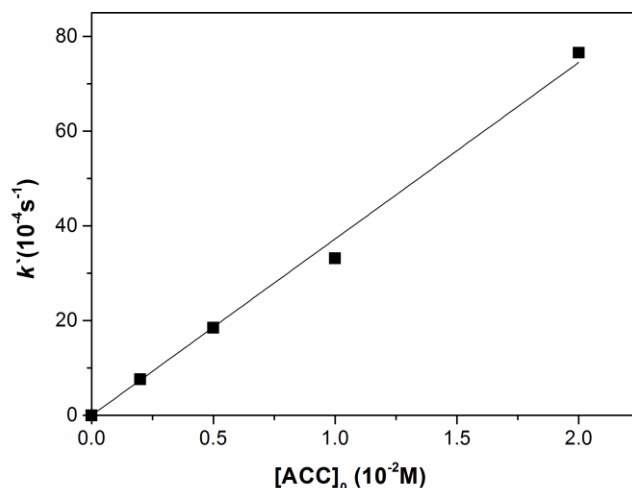

Figure 10. Oxidation of ACC in CH_3CN at 5 °C in the presence of $Fe^{IV}O$ species (a) $[ACC]_0 = 2 \times 10^{-3}$ M, $[Fe^{IV}O(SALEN)Cl]_0 = 2 \times 10^{-4}$ M and the decay of $Fe^{IV}O$ species (b).

Results of SIE measurements (5 % H_2O/D_2O) indicate ET-PT mechanism for this elemental step. Calculated k_H/k_D was found to be 2.45.

Correlation between the amount of catalyst and the reaction rate (Figure 11) and concentration of the substrate and the reaction rate (Figure 12) show first order dependence in the reaction of ACC and $[Fe^{IV}O(SALEN)]^{\bullet+}$ in CH_3CN. Measurements were carried out under pseudo first order conditions.
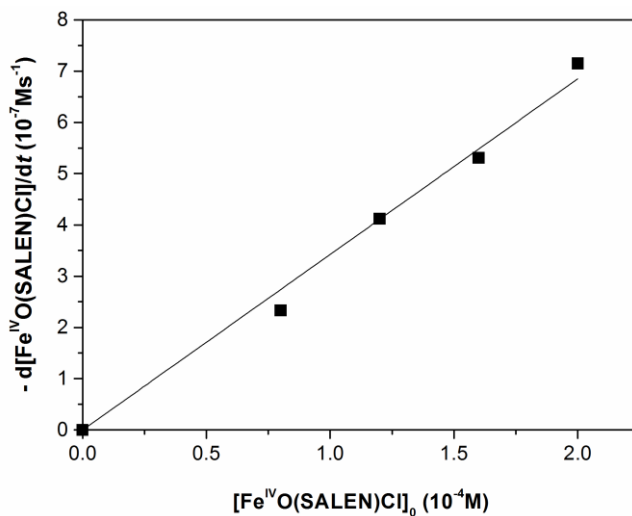
Figure 11. Catalyst concentration dependence in the oxidation of ACC in CH_3CN at 5 °C. $[ACC]_0 = 1 \times 10^{-2}$ M.

Figure 12. Substrate concentration dependence in the oxidation of ACC in CH$_3$CN at 5 °C. [Fe^{IV}O(SALEN)Cl]$_0$ = 2×10^{-4} M.

Activation parameters ($\Delta S^{\neq}$ = − 116 ± 7 J mol^{-1} K^{-1}, $\Delta H^{\neq}$ = 38 ± 2 kJ mol^{-1}) were determined using the Arrhenius and *Eyring-Polányi* correlations (Figure 13). The considerably high value of $\Delta S^{\neq}$ suggests an associative way of activation in the rate limiting step.
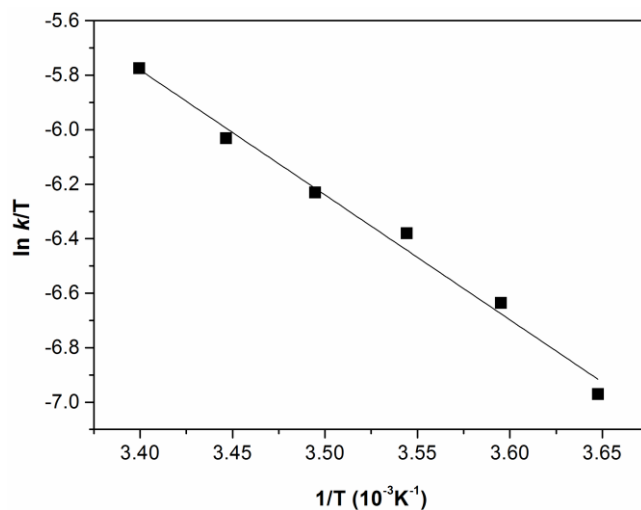

Figure 13. *Eyring* plot for the oxidation reaction of ACC in CH$_3$CN. [ACC]$_0$ = 2×10^{-3} M, [Fe^{IV}O(SALEN)Cl]$_0$ = 2×10^{-4} M.

The influence of substituents in position 5 on the SALEN ligand were also investigated for ACCH in DMF/H$_2$O (3 : 1) at 35 °C. The applied concentrations were: [ACCH]$_0$ = 3.6×10^{-2} M, [catalyst]$_0$ = 7.2×10^{-6} M, [H$_2$O$_2$]$_0$ = 3.6×10^{-2} M, [NH$_4$OH]$_0$ =

3.6×10^{-2} M). Studies unveiled increased reactivity for catalyst with electron withdrawing substituent (k(NO$_2$-SALEN) = 21.81 M^{-1} s^{-1}) and decreased reactivity for electron releasing group (k(MeO-SALEN) = 5.22×10^{-4} M^{-1} s^{-1}.

On the basis of the measurements, a *Michaelis – Menten* type kinetics is suggested. An intermediate complex formation can be implied between substrate and catalyst in a fast pre-equilibrium. The formation of a substrate radical follows in ET-PT reaction (relying on the SIE data obtained) between the coordinated substrate and the oxo-iron centre in RDS. The formation of the products may occur either via decarboxylation (Path C) or direct ring opening (Path E) depending on the ring strain of specific substrate as shown in Scheme 26.
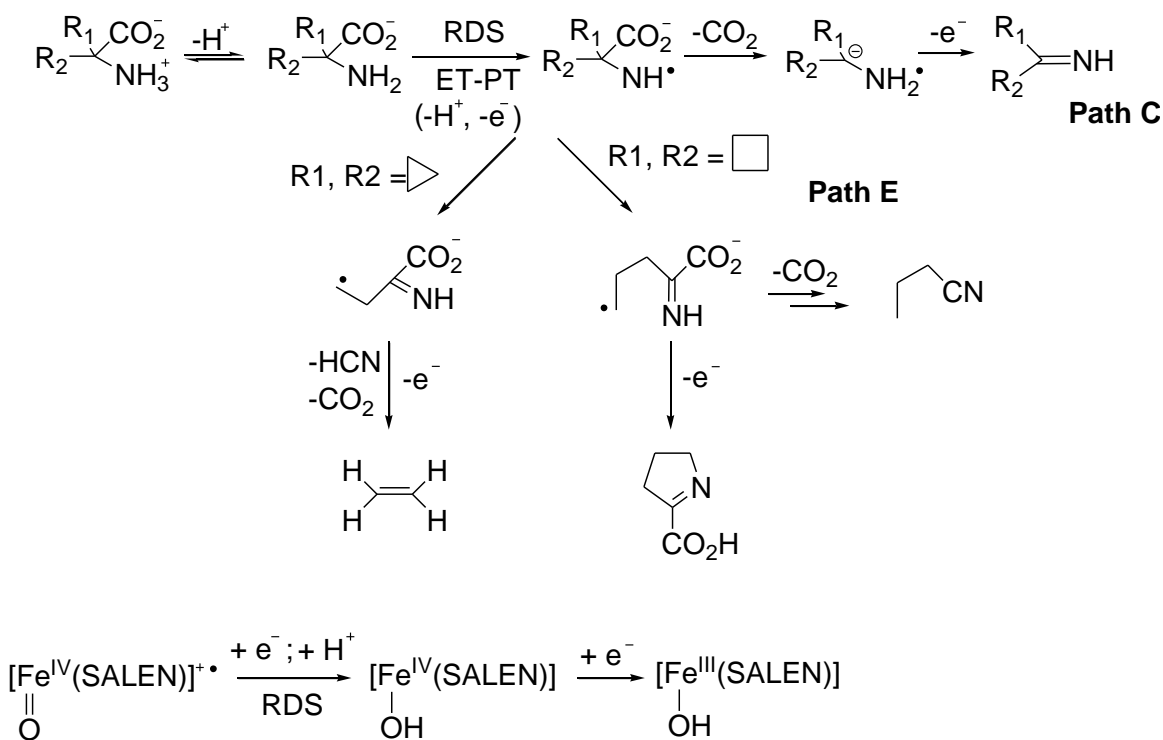
Scheme 26. Proposed mechanism for the oxidation of amino acids in the reaction of [Fe^{III}(SALEN)Cl] in the presence of H$_2$O$_2$ and NH$_4$OH

[Fe^{III}(SALEN)Cl] appeared to be active and selective in the oxidation of AAs. The oxidation of ACCH and AIBH – performed in the presence of various oxidants (H$_2$O$_2$,

PhIO, TBHP, MCPBA, PMS) – gave ethylene and acetone, respectively. The highest TOF values were obtained with H_2O_2.

The investigations revealed MM type behavior concerning the change of substrate concentration and first order dependence in the catalyst and the oxidant in the reaction of various cyclic and acyclic amino acids. Calculated SIE values suggest ET-PT mechanism in the RDS. Suspected active intermediate, $[Fe^{IV}O(SALEN)]^{\bullet+}$ - as a model for high-valent oxo centre - was generated following literature results and it's reaction was observed in CH_3CN at 5 °C. Spectral changes were monitored simultanously with GC analysis for product determination. The calculated activation parameters indicate an associative mechanism.
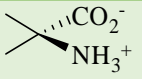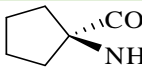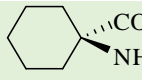
The following mechanism was proposed on the basis of results. The formation of an intermediate complex between the substrate and the catalyst can be implied in a fast pre-equilibrium. The formation of a substrate radical follows in ET-PT reaction between the coordinated substrate and the oxo-iron centre in RDS. Products can be formed either via decarboxylation or direct ring opening depending on the ring strain of the particular substrate.

4.2 Cu-containing amino acid models

### 4.2.1 Study of Cu^{II}(AA) complexes

Cu-containing amino acid complexes (see Table 4) were synthesized in CH_3OH. The procedure is going to be described in Section 5. Complexes were characterized with IR spectroscopy (for data, see Section 5) and with X-ray crystallography for ACBCH and ACHCH.

Table 4. The applied amino acids and their Cu^{II} complexes

Amino Acid		Complex
	AIBH	$[Cu^{II}(AIB)_2]$
	ALAH	$[Cu^{II}(ALA)_2].H_2O$
	ACBCH	$[Cu^{II}(ACBC)_2]$
	ACPCH	$[Cu^{II}(ACPC)_2].H_2O$
	ACHCH	$[Cu^{II}_2(ACHC)_4(H_2O)].H_2O$

The X-ray structure of the isolated $[Cu^{II}(ACBC)_2]$ and $[Cu^{II}_2(ACHC)_4(H_2O)].H_2O$ are shown in Figure 14. Crystal structure details are collected in Table A11. Selected bond lengths and angles are presented in Tables 5 and 6. For $[Cu^{II}(ACBC)_2]$ square planar geometry can be observed with very slight distortion. Amino acid ligands are arranged in *trans*-position towards each other. The O2 – Cu1 distance was found to be 2.83 Å, although it can not be considered as a metal-ligand interaction. Square pyramidal geometry is formed around both Cu centres for $[Cu^{II}_2(ACHC)_4(H_2O)].H_2O$. Cu1 is surrounded with two ACHC ligands in *trans*-position while for Cu2 ligands are arranged *cis* to each other. O1 plays a bridging role between Cu1 and Cu2 and coordinated to the latter as axial ligand, while a H_2O molecule occupies the axial position for Cu1. The complex is rich in H-bonds. Distortion can be observed

for both Cu centres, which can be characterized with τ value (Table 5) as a measure of trigonality for a five-coordinate system. τ equals zero in a perfect square pyramidal geometry and one for a perfect trigonal bipyramidal geometry as described by Reedijk and co-workers. [88]
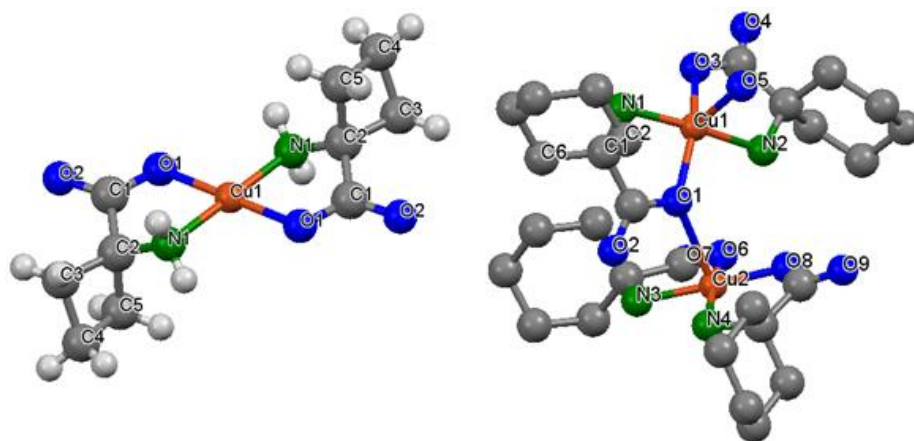
Figure 14. X-ray structure of $[Cu^{II}(ACBC)_2]$ (left side) and $[Cu^{II}_2(ACHC)_4(H_2O)].H_2O$ (right side). Hydrogen atoms are omitted for clarity for $[Cu^{II}_2(ACHC)_4(H_2O)].H_2O$.

Table 5. Selected bond lengths (Å) for $[Cu^{II}(ACBC)_2]$ and $[Cu^{II}_2(ACHC)_4(H_2O)].H_2O$

$[Cu^{II}(ACBC)_2]$			
Cu1–N1	1.987(6)	Cu1–O1	1.968(5)

$[Cu^{II}_2(ACHC)_4(H_2O)].H_2O$			
Cu1–N1	1.984(3)	Cu2–N3	1.978(2)
Cu1–N2	1.988(3)	Cu2–N4	1.977(3)
Cu1–O1	1.959(2)	Cu2–O1	2.537(2)
Cu1–O3	1.942(3)	Cu2–O6	1.944(2)
Cu1–O5	2.349(2)	Cu2–O8	1.927(2)
τ(Cu1)	0.34	τ(Cu1)	0.11

Table 6. Selected bond angles (°) for $[Cu^{II}(ACBC)_2]$ and $[Cu^{II}_2(ACHC)_4(H_2O)].H_2O$

$[Cu^{II}(ACBC)_2]$

N1–Cu1–O1	83.7(2)	N1–Cu1–O1	96.3(2)
N1–Cu1–N1	180.0(3)	C3–C2–C5	87.1(6)

$[Cu^{II}_2(ACHC)_4(H_2O)].H_2O$

|			
N1–Cu1–N2	175.2(1)	N3–Cu2–O1	88.42(9)
N1–Cu1–O1	83.4(1)	N3–Cu2–O6	85.0(1)
N1–Cu1–O5	91.8(1)	N3–Cu2–O8	178.2(1)
N2–Cu1–O3	83.8(1)	N4–Cu2–O1	87.3(1)
O1–Cu1–O3	154.7(1)	N4–Cu2–O6	171.9(1)
O1–Cu1–O5	103.88(9)	N4–Cu2–O8	85.3(1)
C2–C1–C6	110.4(3)[a]		

[a] average of the four corresponding angles is 110.4(6)

The IR spectra are informative regarding coordination through carboxylate groups for amino acids. The measured stretching frequencies are collected in Table 7, and show significant differences. Data correspond well with the bridging function of carboxylate O unveiled from X-ray measurements. For AIB, ALA and ACHC, two symmetric stretches are observed indicating some ambiguity. Still the lowest difference of $v_{as} - v_s$ does not exceed 200 cm^{-1}. For more data regarding IR spectra, see section 5.

Table 7. List of measured $v(CO_2)_{as}$ and $v(CO_2)_s$ stretching frequencies for solid Cu^{II}-containing amino acid complexes

	$v(CO_2)_s$ (cm^{-1})	$v(CO_2)_{as}$ (cm^{-1})
$[Cu^{II}(AIB)_2]$	1390, 1363	1627
$[Cu^{II}(ALA)_2].H_2O$	1394, 1354	1626
$[Cu^{II}(ACBC)_2]$	1391	1619
$[Cu^{II}(ACPC)_2].H_2O$	1374	1625
$[Cu^{II}_2(ACHC)_4(H_2O)].H_2O$	1369, 1343	1612

Cyclic voltammetry was used to determine redox properties of isolated amino acid complexes. Measurements were performed to the cathodic direction, and were carried out in DMF at room temperature under Ar. For detailed description, see Section 5. Voltammograms are shown in Figure 15, which exhibit one irreversible cathodic reduction peak. A slight pre-peak shoulder was detected for $[Cu^{II}(ALA)_2].H_2O$. Irreversibility can be explained with possible geometric change from square planar Cu^{II} to tetrahedral Cu^{I} as supported by DFT calculations for other Cu-containing amino acid complexes investigated by Simaan and co-workers [66]. Electrochemical data are collected in Table 8.
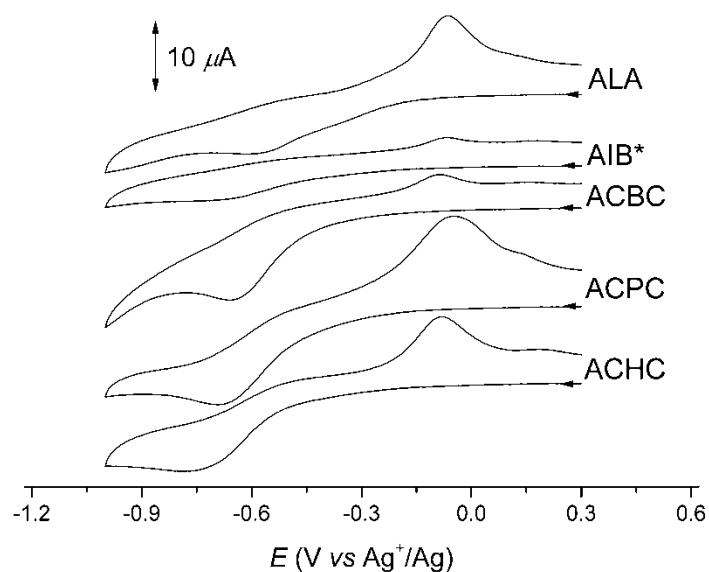
Figure 15. Cyclic voltammograms of Cu^{II} complexes in DMF shown at 100 mV/s scan rate. $[Cu^{II}(AA)]_0 = 1x10^{-3}$ M, $[TBAP]_0 = 0.1$ M

*solubility of the complex was limited

Table 8. Determined peak potentials for $Cu^{II}(AA)_2$ complexes in DMF
at 100 mV/s scan rate.

|	$E°'pc$	$E°'pa$
$[Cu^{II}(AIB)_2]$*	−735	−80
$[Cu^{II}(ALA)_2].H_2O$	−620	−63
$[Cu^{II}(ACBC)_2]$	−659	−84
$[Cu^{II}(ACPC)_2].H_2O$	−692	−55
$[Cu^{II}_2(ACHC)_4(H_2O)].H_2O$	−754	−80

*solubility of complex was limited

Catalytic activity of the synthesized amino acid complexes was studied in DMF/H_2O solvent mixture at 35 °C using a molar ratio of 1 : 5000 : 5000 : 5000 for [catalyst] : [S] : [H_2O_2] : [NH_4OH] respectively. In parallel with these, measurements using simple $CuCl_2$ as catalyst were carried out under the same conditions. In addition to the previously mentioned substrates, reactivity of a methylated amino acid (*N*-Me-AIB) was also investigated. Reactions were performed in a 20 cm^3 sealed tube as it was described earlier. Samples were taken from the head-space and analyzed by GC. Products were determined. Reactions were selective and gave corresponding carbonyls except for ACBCH, which resulted in three products: cyclobutanone as major product, Δ^1-pyrroline-2-carboxylic acid (dehydroproline) and *n*-butyronitrile. The degradation path of ACBCH forming cyclobutanone can be described as decarboxylation and the latter two as direct ring opening processes as it was shown earlier in Scheme 15. [61] The progress of the reaction and the proportion of the products in the oxidation of ACBCH are shown in Figures 16-19.
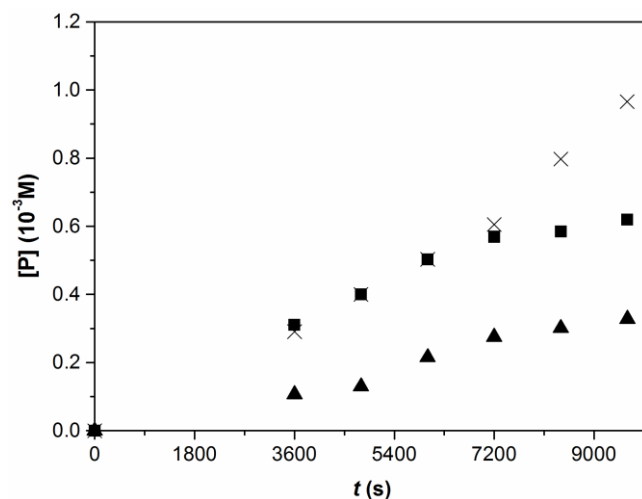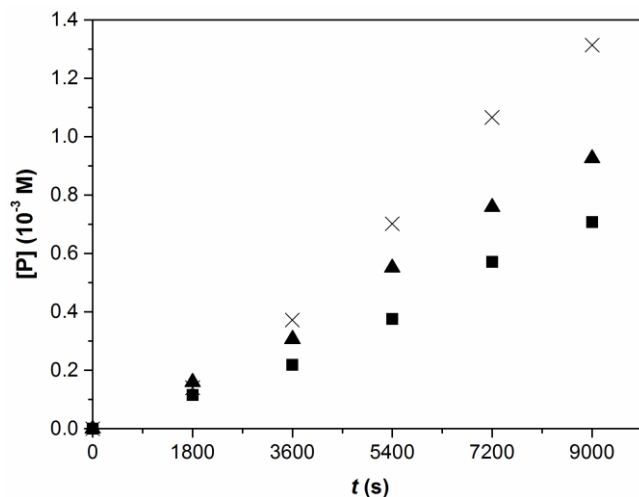
**Figure 16.** Progress of the oxidation reaction of ACBCH in DMF/H_2O (3:1) at 35 °C. [ACBCH]$_0$ = 3.6×10^{-2} M, [CuCl$_2$]$_0$ = 7.2×10^{-6} M, [H$_2O_2$]$_0$ = 3.6×10^{-2} M, [NH$_4$OH]$_0$ = 3.6×10^{-2} M. Cyclobutanone (×), dehydroproline (■), *n*-butyronitrile (▲).
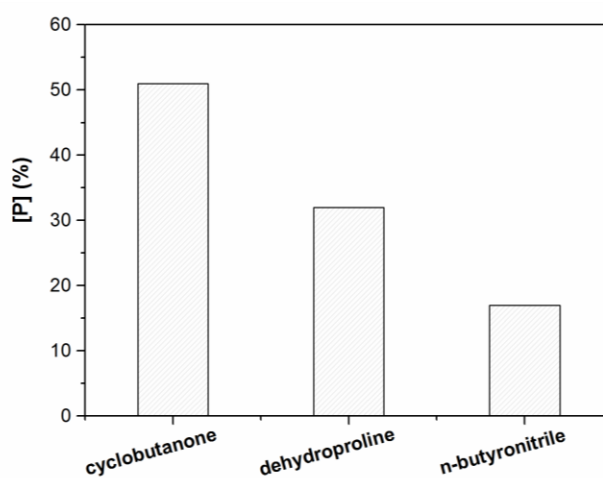
Figure 17. Proportion of products in the reaction of ACBCH in DMF/H_2O (3:1) at 35 °C . [ACBCH]$_0$ = 3.6×10^{-2} M, [CuCl$_2$]$_0$ = 7.2×10^{-6} M, [NH$_4$OH]$_0$ = 3.6×10^{-2} M.

42
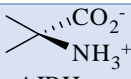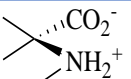
Figure 18. Progress of the oxidation reaction of $Cu^{II}(ACBC)_2$ in DMF/H_2O (3:1) at 35 °C. $[ACBCH]_0 = 3.6 \times 10^{-2}$ M, $[Cu^{II}(ACBC)_2]_0 = 7.2 \times 10^{-6}$ M, $[H_2O_2]_0 = 3.6 \times 10^{-2}$ M, $[NH_4OH]_0 = 3.6 \times 10^{-2}$ M. Cyclobutanone (×), dehydroproline (■), *n*-butyronitrile (▲)
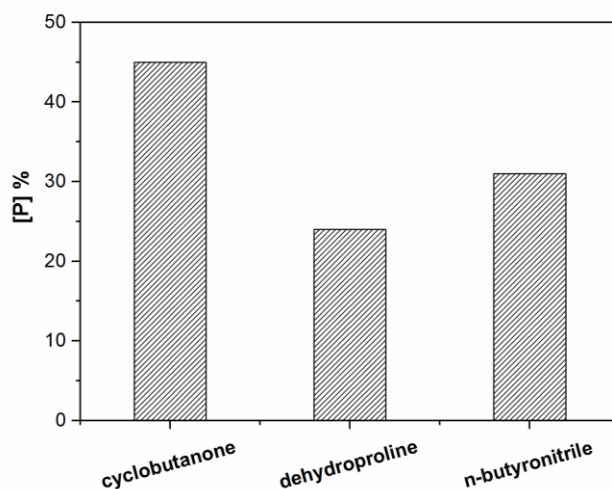
Figure 19. Proportion of the products in the reaction of $Cu^{II}(ACBC)_2$ in DMF/H_2O (3:1) at 35 °C. $[ACBCH]_0 = 3.6 \times 10^{-2}$ M, $[Cu^{II}(ACBC)_2]_0 = 7.2 \times 10^{-6}$ M, $[H_2O_2]_0 = 3.6 \times 10^{-2}$ M, $[NH_4OH]_0 = 3.6 \times 10^{-2}$ M.

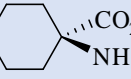Measured initial rate and calculated TOF values are collected in Table 9. The highest values were obtained with ACHCH for cyclic and with AIBH for acyclic substrates. *N*-methyl group in AIBH had a high impact yielding significant decrease in reaction rate and TOF. Calculated BDE values for N–H bond (determined with DFT calculations) [47] do not correlate with measured reactivity data.

43

Table 9. Kinetic data for the oxidation of amino acids.

Substrate	[CuCl$_2$]		[Cu(AA)$_2$]	
	-d[S]/dt (10^{-7} Ms^{-1})	TOF (h^{-1})	TOF (h^{-1})	BDE$_{N-H}$ (kJ/mol)
ACCH	0.04	2	-	407.79
ACBCH	2.40	103	166	-
ACPCH	4.52	150	175	-
ACHCH	16.85	809	-	-
ALAH	2.20	9	14	413.65
AIBH	19.60	853	860	418.68
N-Me-AIBH	1.26	98	-	-

In DMF/H$_2$O (3:1) at 35 °C. [CuCl$_2$]$_0$ = 7.2×10^{-6} M, [S]$_0$ = 3.6×10^{-2} M, [H$_2$O$_2$]$_0$ = 3.6×10^{-2} M, [NH$_4$OH]$_0$ = 3.6×10^{-2} M.

Reactions were performed in DMF/D$_2$O solvent mixture as well in order to determine possible isotope effects for AIBH and ACCH using CuCl$_2$ as catalyst. The progress of the reactions are shown in Figures 20 and 21. Calculated SIE values are quite low (3.14 and 1.44 for the reactions with AIBH and ACCH, respectively) indicating ET-PT mechanism in the rate determining step.
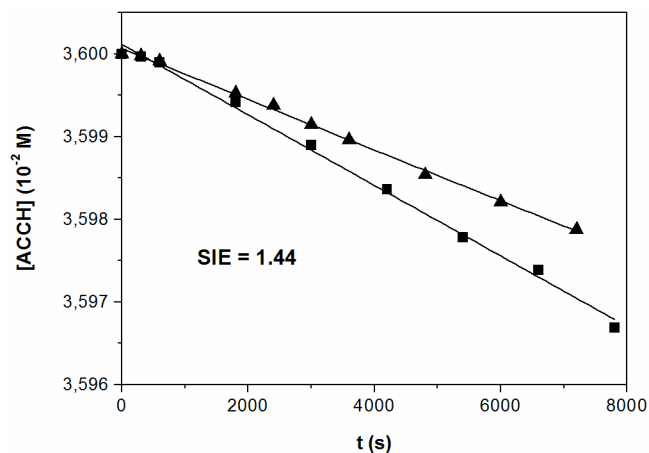
Figure 20. The progress of the oxidation reaction of ACCH in DMF/H$_2$O (■) and DMF/D$_2$O (▲) (3:1) at 35 °C. [ACCH]$_0$ = 3.6×10^{-2} M, [CuCl$_2$]$_0$ = 7.2×10^{-6} M, [NH$_4$OH]$_0$ = 3.6×10^{-2} M.
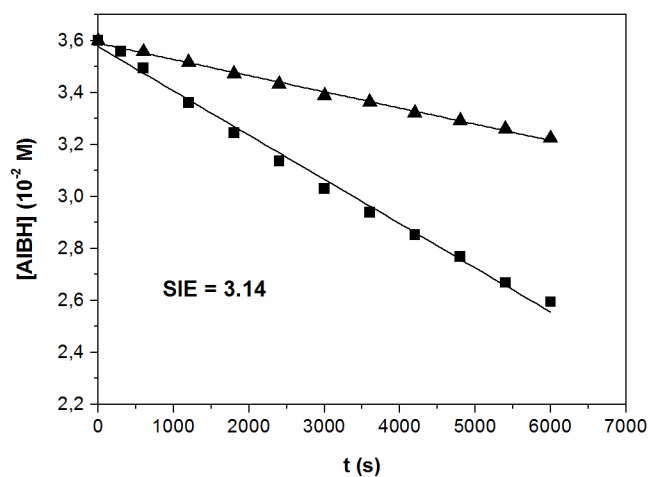
Figure 21. The progress of the oxidation reaction of AIBH in DMF/H$_2$O (■) and DMF/D$_2$O (▲) (3:1) at 35 °C. [AIBH]$_0$ = 3.6×10^{-2} M, [CuCl$_2$]$_0$ = 7.2×10^{-6} M, [NH$_4$OH]$_0$ = 3.6×10^{-2} M.

If the logarithm of the measured initial rate is plotted vs. $E°'$pc linear correlation is found with a negative slope (Figure 22) indicating amino acid complexes being stronger reducing agents as [Cu^I(AA)$_2$], can be oxidized easier by hydrogen peroxide.

Comparing the calculated TOF values (Figure 23) for reactions performed with CuCl$_2$ to those carried out using [Cu^{II}(AA)$_2$] complexes slight difference can be detected. As a result an identical active form of catalyst is assumed for the two systems studied.

45
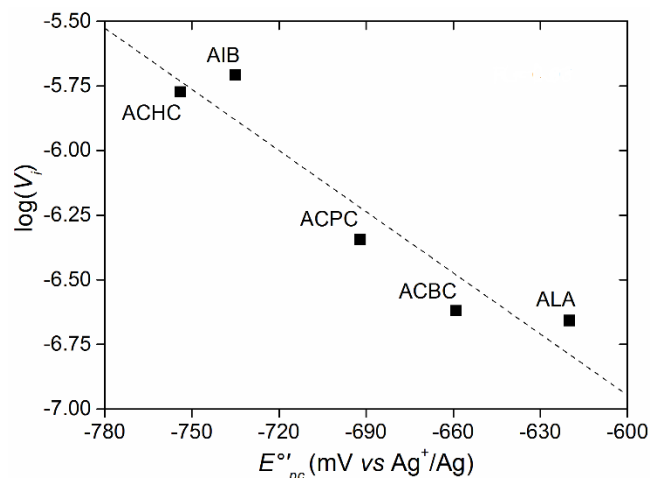
Figure 22. The $\log(V_i)$ values as a function of $E^{\circ\prime}_{pc}$ of the corresponding $Cu(AA)_2$ complexes.
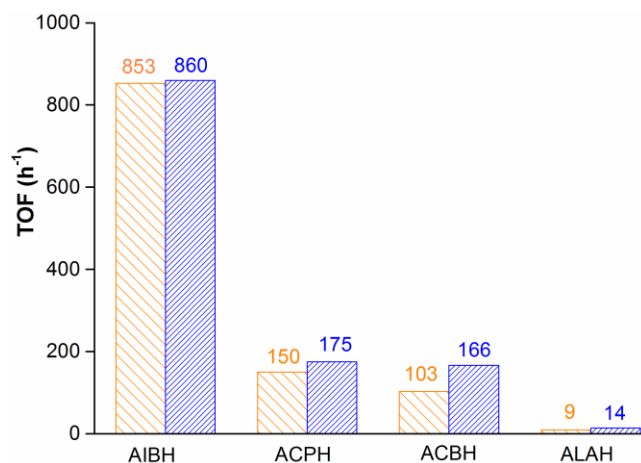
Figure 23. TOF values with $[CuCl_2]$ (blue) or $[Cu(AA)_2]$ (orange) as catalyst under identical conditions.

Reactions were carried out with different substrate concentrations for ACCH (data shown in Figure 24) and AIBH (data shown in Figure 26) using $CuCl_2$ as catalyst in DMF/H_2O with H_2O_2. Measurements suggest a *Michaelis-Menten* type kinetics for both cases. The obtained *Lineweaver-Burk* plots are presented in Figures 25 and 27. Calculated k_{cat} values are 1.25 s^{-1} and 0.0007 s^{-1} K_M was 110 mM and 4.5 mM for AIBH and ACCH respectively.
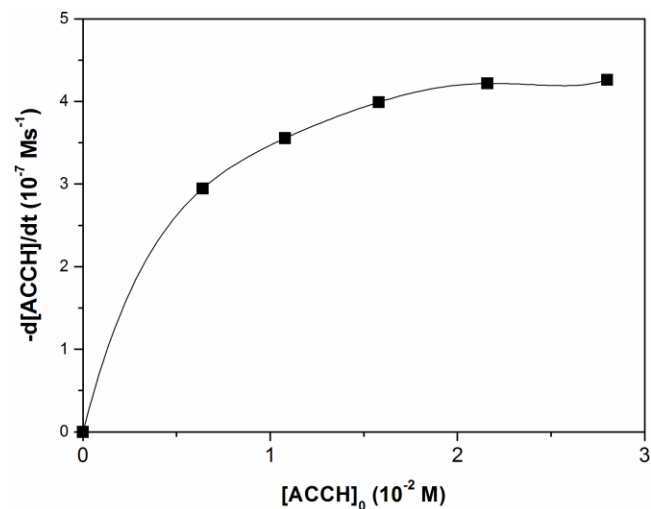
Figure 24. The rate of the reaction of ACCH as a function of the initial substrate concentration in DMF/H$_2$O (3:1) at 35 °C. $[CuCl_2]_0 = 7.2 \times 10^{-6}$ M, $[H_2O_2]_0 = 3.6 \times 10^{-2}$ M, $[NH_4OH]_0 = 3.6 \times 10^{-2}$ M
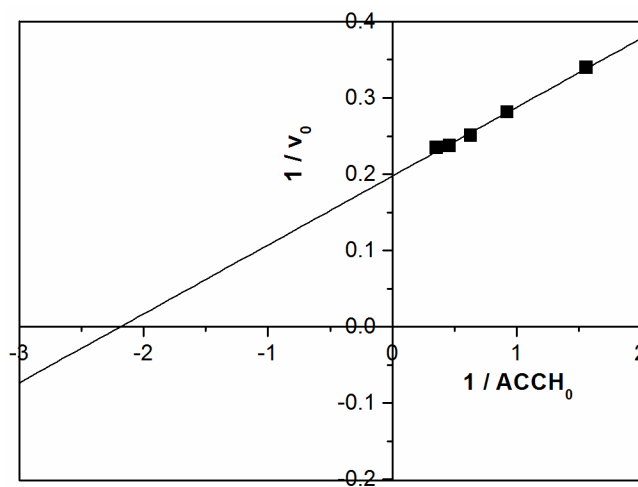
Figure 25. *Lineweaver-Burk* plot for the reaction of ACC in DMF/H$_2$O (3:1) at 35 °C. $[CuCl_2]_0 = 7.2 \times 10^{-6}$ M, $[H_2O_2]_0 = 3.6 \times 10^{-2}$ M, $[NH_4OH]_0 = 3.6 \times 10^{-2}$ M

47
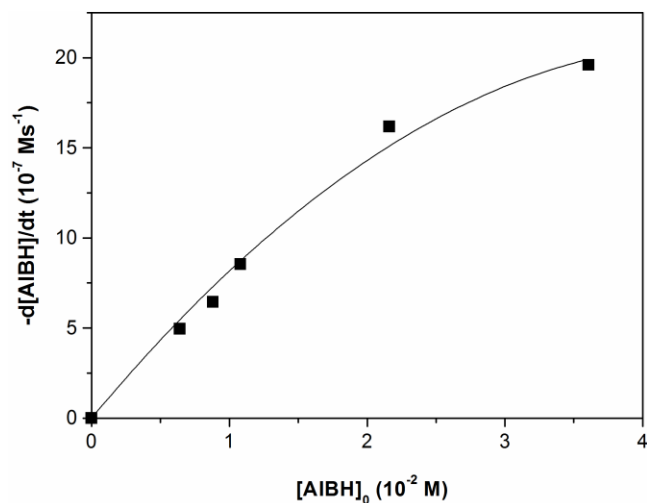
Figure 26. Correlation between the substrate concentration and the rate of the reaction of AIBH in DMF/H$_2$O (3 : 1) at 35 °C. [CuCl$_2$]$_0$ = 7.2×10^{-6} M, [H$_2$O$_2$]$_0$ = 3.6×10^{-2} M, [NH$_4$OH]$_0$ = 3.6×10^{-2} M
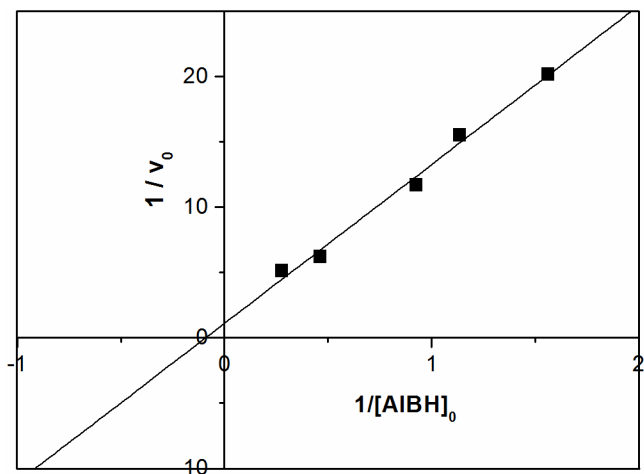
Figure 27. *Lineweaver-Burk* plot for the reaction of AIBH in DMF/H$_2$O at 35 °C. [CuCl$_2$]$_0$ = 7.2×10^{-6} M, [H$_2$O$_2$]$_0$ = 3.6×10^{-2} M, [NH$_4$OH]$_0$ = 3.6×10^{-2} M

Inhibition studies were performed by investigating the oxidation of AIBH in the presence of certain phosphonate, AMEPH in DMF/H$_2$O with CuCl$_2$ and H$_2$O$_2$. Results depict a strong inhibition as shown in Figure 28 as no product could be detected in the presence of AMEPH.
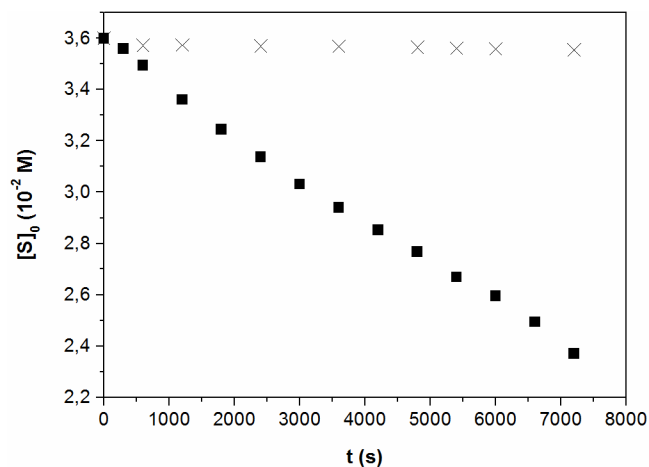
Figure 28. The reaction of AIBH (■) and AIBH in the presence of AMEP (×) in DMF/H$_2$O (3:1) at 35 °C. [CuCl$_2$]$_0$ = 7.2 × 10^{-6} M, [AIBH]$_0$ = 3.6 × 10^{-2} M, [AMEPH]$_0$ = 0 or 3.6 × 10^{-3} M, [H$_2$O$_2$]$_0$ = 3.6 × 10^{-2} M, [NH$_4$OH]$_0$ = 3.6 × 10^{-2} M.

The formation of acetone is detectable even in case of the reaction of AMEPH in the absence of AIBH with the molar ratio of 250 : 5000 : 5000 for [CuCl$_2$] : [S] : [H$_2$O$_2$] respectively. The results are shown in Figure 29 and Table 10.
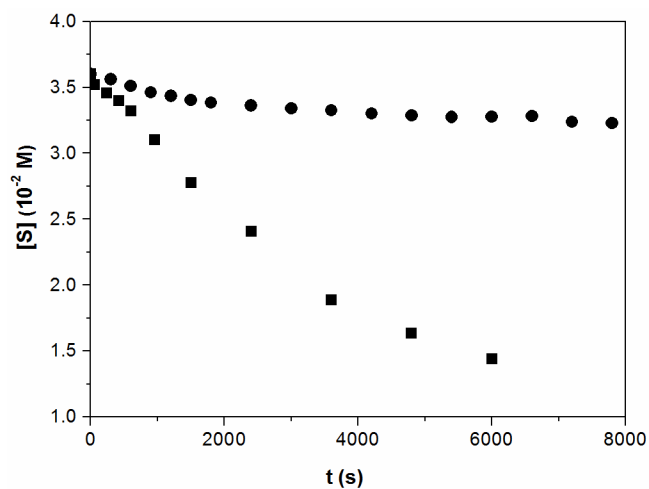
Figure 29. The reaction of AIBH (■) or AMEPH (●) in DMF/H$_2$O (3:1) at 35 °C. [CuCl$_2$]$_0$ = 1.8×10^{-3} M, [AIBH]$_0$ (or [AMEPH]$_0$) = 3.6×10^{-2} M, [H$_2$O$_2$]$_0$ = 3.6×10^{-2} M, [NH$_4$OH]$_0$ = 3.6×10^{-2} M.

Table 10. Kinetic data for the oxidation of AIBH and AMEPH

	AIBH	AMEPH
TON	12	2.4
conversion (%)	60	12
k' (10^{-4} s^{-1})	1.60 ± 0.05	0.35 ± 0.02

Comparison of the calculated pseudo first order rate constants gave a $k_{rel} = 4.6$, which correlates well with the observed inhibition.

$[Cu^{II}(AA)_2]$ complexes are efficient catalysts. Square planar geometry was observed for ACBCH with a slight distortion while the ACHCH-containing complex showed distorted square pyramidal geometry for both Cu centres arranged in trans-position to each other attested by the X-ray data obtained.

Redox properties of the isolated complexes were determined using cyclic voltammetry. Voltammograms exhibit one irreversible cathodic peak. Irreversibility can be explained with a possible geometric change from square planar Cu^{II} to tetrahedral Cu^{I} as supported by DFT calculations for other Cu-containing AA complexes.

Comparing the calculated TOF values for the reactions performed with $[CuCl_2]$ to those carried out using $[Cu^{II}(AA)_2]$ complexes, slight difference could be detected. As a result, an identical active form of catalyst is assumed for the two systems studied. The calculated SIE values indicate ET-PT mechanism.

Kinetic measurement for AA oxidation using $[CuCl_2]$ and $[Cu^{II}(AA)_2]$ complexes revailed Michaelis-Menten type behavior for both models.

Inhibition studies were performed with AIBH and AMEPH in the presence of $CuCl_2$. The comparison of pseudo first order rate constants gave $k_{rel} = 4.6$.

4.2.2 Cu^{II}-bipyridine-containing amino acid complexes

In order to unveil the effect of ligands and the possible enhancement in reactivity, Cu^{II}-containing amino acid complexes were synthesized with bipyridine ligand. For ACBCH, ACPCH, ACHCH and AMEP slow evaporation of CH$_3$OH from the reaction mixture gave single crystals suitable for X-ray measurements. Crystal structure details are given in Tables A12 and A13. Single crystal structures are presented in Figures 30 and 31. Amino acid complexes show distorted square pyramidal geometry as indicated by the calculated τ values (shown in Table 12). Besides *N* and *O* atoms of the amino acids, N atoms of bipyridine ligand occupy equatorial positions. This coordination is characteristic for amino acid complexes [89], and is also proposed for the enzyme–substrate complex [42] [43]. The '*O*' donor atom of a second carboxyl group from a neighboring carboxylate occupies the axial position. Each carboxylate serves as a bridging ligand forming a coordination polymer like the other amino acid complexes reported in earlier studies [66]. Cu^{II} complex containing AMEP as ligand was synthesized in CH$_3$OH/H$_2$O solvent mixture. Slow evaporation of the reaction mixture gave crystals suitable for X-ray measurements. The obtained structure (see Figure 32) shows two Cu^{II} ions bridged by a phosphonate. τ value indicates a slight distortion and square pyramidal geometry. Similarly to amino acids, AMEP is coordinated as bidentate to Cu1 through its N and O atoms. The measured bond lengths are in good agreement with common equatorial Cu-O distances (1.896 – 1.989 Å) in amino-phosphonate complexes found in the Cambridge Structural Database. The surrounding equatorial plane of Cu2 consists of 2N atoms of bipyridine, O of H$_2$O molecule and O of phosphonate group. Axial position is occupied by another H$_2$O molecule.
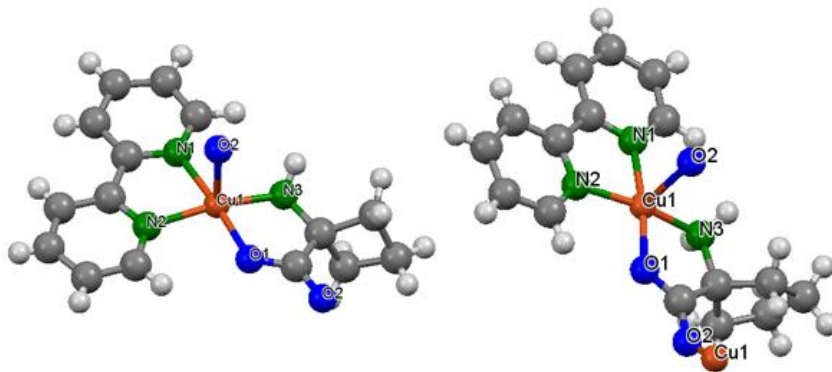
Figure 30. X-ray structure of $[Cu^{II}(bpy)(ACBC)]ClO_4.H_2O$ and $[Cu^{II}(bpy)(ACPC)]ClO_4.H_2O$. Anions and solvent molecules are omitted for clarity.
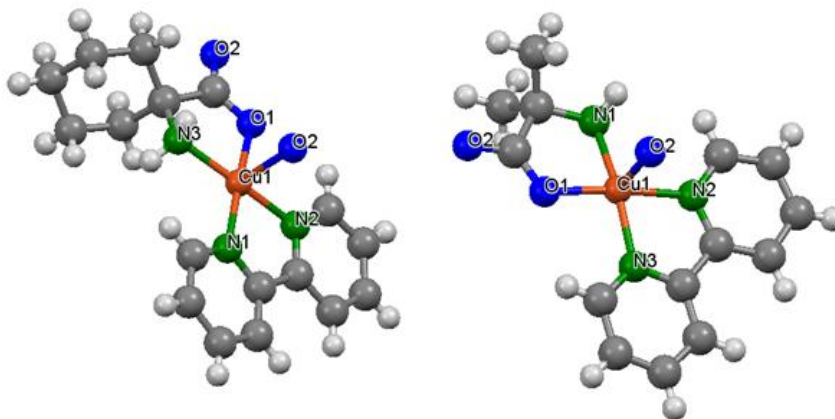
Figure 31. X-ray structure of $[Cu^{II}(bpy)(ACHC)]ClO_4.H_2O$ and $[Cu^{II}(bpy)(AIB)(H_2O)]ClO_4$. Anions and solvent molecules are omitted for clarity.
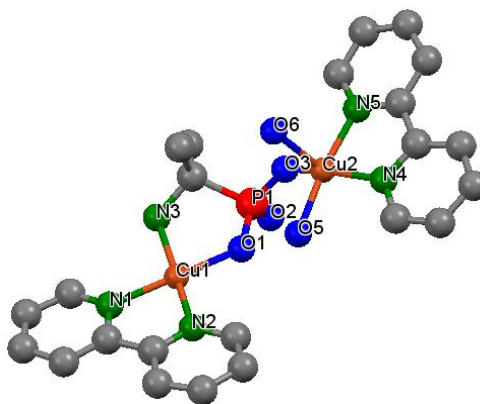
Figure 32. X-ray structure of $[Cu^{II}_2(bpy)_2(AMEP)(H_2O)_3](ClO_4)_2.3H_2O$. Hydrogen atoms, anions and solvent molecules are omitted for clarity.

Table 11. Selected bond lengths (Å) for the bpy-containing complexes with amino acids.

[Cu^{II}(bpy)(ACBC)]ClO$_4$.H$_2$O

Cu1–N1	2.010(3)	Cu1–O1	1.943(2)
Cu1–N2	1.991(3)	Cu1–O2	2.325(2)
Cu1–N3	1.962(3)		

[Cu^{II}(bpy)(ACPC)]ClO$_4$.H$_2$O

Cu1–N1	2.008(2)	Cu1–O1	1.934(2)
Cu1–N2	1.945(2)	Cu1–O2	2.454(3)
Cu1–N3	1.932(3)		

[Cu^{II}(bpy)(ACHC)]ClO$_4$.H$_2$O

Cu1–N1	1.980(6)	Cu1–O1	1.971(5)
Cu1–N2	1.984(5)	Cu1–O2	2.347(5)
Cu1–N3	1.977(6)		

[Cu^{II}(bpy)(AIB)(H$_2$O)]ClO$_4$

Cu1–N1	1.956(5)	Cu1–O1	1.927(3)
Cu1–N2	2.017(4)	Cu1–O2	2.290(4)
Cu1–N3	1.983(4)		

[Cu^{II}$_2$(bpy)$_2$(AMEP)(H$_2$O)$_3$](ClO$_4$)$_2$.3H$_2$O

Cu1–N1	2.019(7)	Cu1–O1	1.949(6)
Cu1–N2	2.007(8)	Cu1–O4	2.380(7)
Cu1–N3	2.026(7)	Cu2–O3	1.938(6)
Cu2–N4	2.029(8)	Cu2–O5	1.962(6)
Cu2–N5	2.000(7)	Cu2–O6	2.200(7)

Table 12. Selected bond angles (°) for the bpy-containing amino acid complexes.

[Cu^{II}(bpy)(ACBC)]ClO$_4$.H$_2$O

N1–Cu1–N2	81.50(12)	N1–Cu1–O2	89.39(10)
N1–Cu1–O1	174.99(11)	N3–Cu1–O1	84.22(10)
N2–Cu1–N3	167.53(13)	N3–Cu1–O2	102.79(12)
C13–C12–C15	87.3(3)	τ	0.12

[Cu^{II}(bpy)(ACPC)]ClO$_4$.H$_2$O

N1–Cu1–N2	81.73(10)	N1–Cu1–O2	93.85(10)
N1–Cu1–O1	174.03(9)	N3–Cu1–O1	85.01(9)
N2–Cu1–N3	168.27(12)	N3–Cu1–O2	98.20(10)
C13–C12–C16	105.2(3)	τ	0.10

[Cu^{II}(bpy)(ACHC)]ClO$_4$.H$_2$O

N1–Cu1–N2	81.70(2)	N1–Cu1–O2	91.6(2)
N1–Cu1–O1	172.9(2)	N3–Cu1–O1	82.3(2)
N2–Cu1–N3	171.6(3)	N3–Cu1–O2	94.0(2)
C13–C12–C16	108.8(5)	τ	0.02

[Cu^{II}(bpy)(AIB)(H$_2$O)]ClO$_4$

N2–Cu1–N3	81.11(18)	N1–Cu1–O2	97.2(2)
N2–Cu1–O1	174.26(17)	N1–Cu1–O1	84.62(16)
N1–Cu1–N3	167.6(2)	N2–Cu1–O2	92.33(16)
C3–C2–C4	111.3(5)	τ	0.11

[Cu^{II}$_2$(bpy)$_2$(AMEP)(H$_2$O)$_3$](ClO$_4$)$_2$.3H$_2$O

N1–Cu1–O1	171.5(3)	N4–Cu2–N5	81.2(3)
N2–Cu1–N3	168.9(3)	N4–Cu2–O3	155.0(3)
N1–Cu1–N2	81.4(3)	N4–Cu2–O6	104.1(3)
N3–Cu1–O1	87.0(3)	N5–Cu2–O5	172.0(3)
N1–Cu1–O4	88.9(3)	O3–Cu2–O5	93.0(3)
N3–Cu1–O4	97.6(3)	O5–Cu2–O6	93.8(3)
C12–C11–C13	110.0(9)		
τ(Cu1)	0.04	τ(Cu2)	0.28

EPR spectra of ACBC-, ACPC- and ACHC-containing complexes (see Figure A19-22) were recorded in frozen CH_3OH at -153 °C. Spectra are axial type and similar to those of the previously described amino acid complexes. Results support the square-pyramidal geometry of Cu^{II} ions, in agreement with the obtained X-ray data. Simulations support three superhyperfine nitrogen tensors, from which two are equivalent in accordance with measured data.

Single turnover oxidation of bound amino acids in the presence of H_2O_2 was performed. Products were determined with GC as described earlier. For the ACBC-containing complex, the proportion of the evolved products was different from those of previous experiments. Cyclobutanone was formed only in trace amounts while *n*-butyronitrile and dehydroproline were produced in 1 : 2 ratio. This result suggests a good functional model as product formation is more like the one in enzymatic system. Reaction with AIB-complex was carried out under Ar atmosphere as well, but the results did not show much difference. The reactivity of methylated AIB-containing complex appeared very similar to the others suggesting the same, bidentate coordination mode for amino acid. Possible isotop effect was investigated by changing H_2O to D_2O in solvent mixture. Rate constants from ln(P) vs. *t* plot and SIE values were determined (see Table 13). The presence and the relatively low value of SIE indicates ET-PT mechanism.

The investigation of oxidation reactions using amino phosphonate-containing complexes gave interesting results. Experimental conditions were the same as described above, except for the solvent. CH_3OH was applied instead of DMF/H_2O in order to prevent precipitation. Equimolar quantities (1 mM, 10 mM H_2O_2) were used. In the absence of NH_4OH, no ethylene was detected in the reaction of $[Cu^{II}(bpy)(ACC)(H_2O)]ClO_4$. Upon addition of NH_4OH, the same reaction took place as with $[Cu^{II}(ACC)_2(H_2O)]ClO_4$ giving ethylene as product, but at a rate three times higher. Conclusion of activity-enhancement by exogenous ligand can be drawn. Another interesting observation was the effect or better said absence of effect performed by additional phosphonate group in contrast to their inhibiting nature. [90] Consequently, the same mechanism can be implied for product formation for both amino acids as for amino phosphonates.

Table 13. Kinetic data for the oxidation of amino acids.[a]

Complex	k'_H[b] $(10^{-4}$ s$^{-1})$	k'_D $(10^{-4}$ s$^{-1})$	SIE (k'_H/ k'_D)	Yield $(\%)$[c]	BDE$_{N-H}$ (kJ/ mol)
[Cu^{II}(bpy)(ACC)(H$_2$O)]ClO$_4$	2.6	1.4	1.9	5	402.35
[Cu^{II}(bpy)(ACPC)(H$_2$O)]ClO$_4$	7.0	-	-	7.0	414.07
[Cu^{II}(bpy)(ACBC)]ClO$_4$.H$_2$O	5.5	2.3	2.4	20	375.14
[Cu^{II}(bpy)(ACPC)]ClO$_4$.H$_2$O	7.6	4.3	1.8	22	427.05
[Cu^{II}(bpy)(ACHC)]ClO$_4$.H$_2$O	9.6	3.9	2.5	38	-
[Cu^{II}(bpy)(AIB)(H$_2$O)]ClO$_4$	15.9	10.1	1.6	80	418.68
[Cu^{II}(bpy)(AIB)(H$_2$O)]ClO$_4$	17.4[e]			77[e]	-
[Cu^{II}(bpy)(MAIB)]ClO$_4$.H$_2$O	7.5	-	-	47	-
[Cu$^{II}_2$(bpy)$_2$(AMEP)(H$_2$O)$_3$](ClO$_4$)$_2$.3H$_2$O	41.1	-	-	92	-

[a] In DMF/H$_2$O (3:1) at 35 °C. [complex]$_0$ = 1.2x10^{-2} M, [H$_2$O$_2$]$_0$ = 3.6x10^{-2} M, [NH$_4$OH]$_0$ = 6x10^{-2} M

[b] $k'_{H(D)}$ was calculated from the ln[product] *vs t* plots

[c] rounded to integer, relative to the initial concentration of AA bound in the complex

[d] C–(α-C)–C endocyclic bond angle in the solid state, from crystallography

[e] under argon

Redox properties were investigated as well. Voltammograms (see Figure 33) show one reversible peak, which is most likely due to a geometric change form square pyramidal to tetrahedral accompanied by a one-electron change from Cu^{II} to Cu^{I}. Results are supported by DFT calculations and ESI-MS measurements according to literature. [66] Electrochemical data are listed in Table 14.
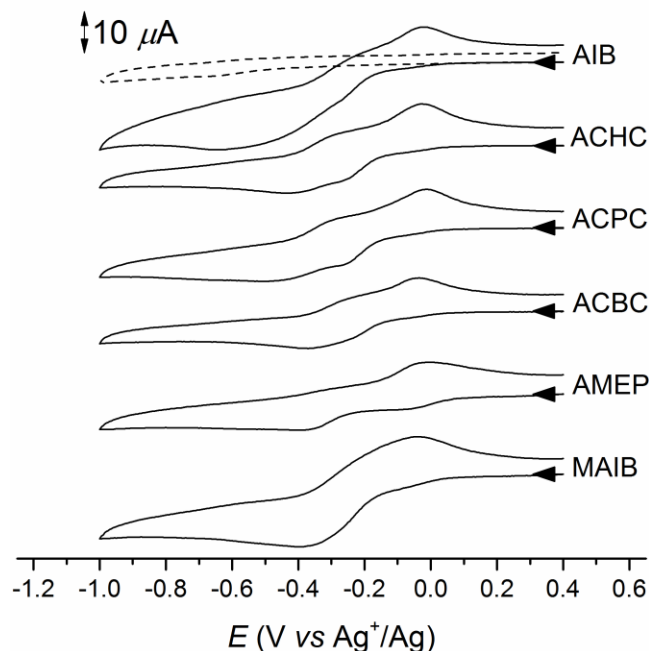
Figure 33. Cyclic voltammograms of bpy-containing complexes
(in CH_3OH, [complex] = 1×10^{-3} M, [TBAP] = 1×10^{-1} M, at 100 mV/s scan rate, neat
electrolyte under argon: dashed voltammogram)

Table 14. Electrochemical data for Cu^{II} bipyridine-containing amino acid complexes

	E_{pc} [mV]	E_{pa} [mV]
$[Cu^{II}(bpy)(ACC)(H_2O)]ClO_4$	−377	+95
$[Cu^{II}(bpy)(ACBC)]ClO_4 \cdot H_2O$	−380	+105
$[Cu^{II}(bpy)(ACPC)]ClO_4 \cdot H_2O$	−365	+90
$[Cu^{II}(bpy)(ACHC)]ClO_4 \cdot H_2O$	−355	+20
$[Cu^{II}(bpy)(AIB)(H_2O)]ClO_4$	−366	+55

The Cu^I-intermediate was investigated at -10 °C in the presence of H_2O_2. The intense blue color of the solved complex turned to brown-yellow after addition of H_2O_2, and remained stable for a few seconds. The process was monitored spectrophotometrically using UV-Vis instrument. An intense peak was observed with a maximum at around 440 nm. For the spectra, see Figure 34. Barely any difference was detected among the complexes applied, which can be due to MLCT process. Upon

addition of ascorbate in the absence of H_2O_2, the same spectral changes were recorded as with H_2O_2, interestingly.
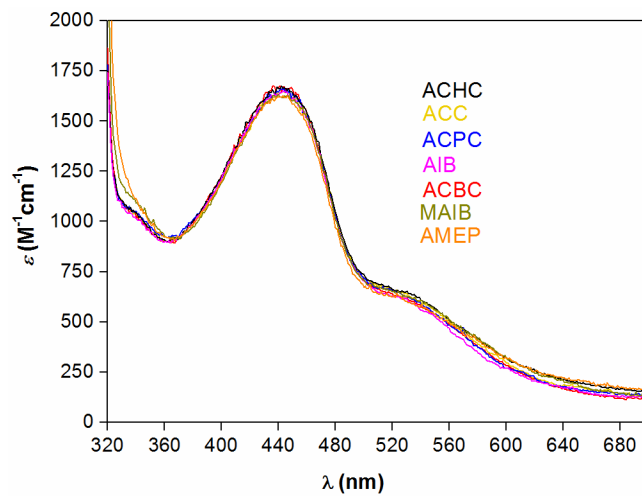
Figure 34. UV-Vis spectra of the bpy-containing complexes (1×10^{-3} M) instantly after addition of 1 equivalent ascorbate in methanol, at -10 °C.

On the basis of these results, the following mechanism can be suggested (Scheme 27). Formation of the reactive Cu^I-intermediate gives Cu^I-hydroperoxide adduct and – depending on the nature of the substrate – ring opening or decarboxylation process gives the corresponding product.
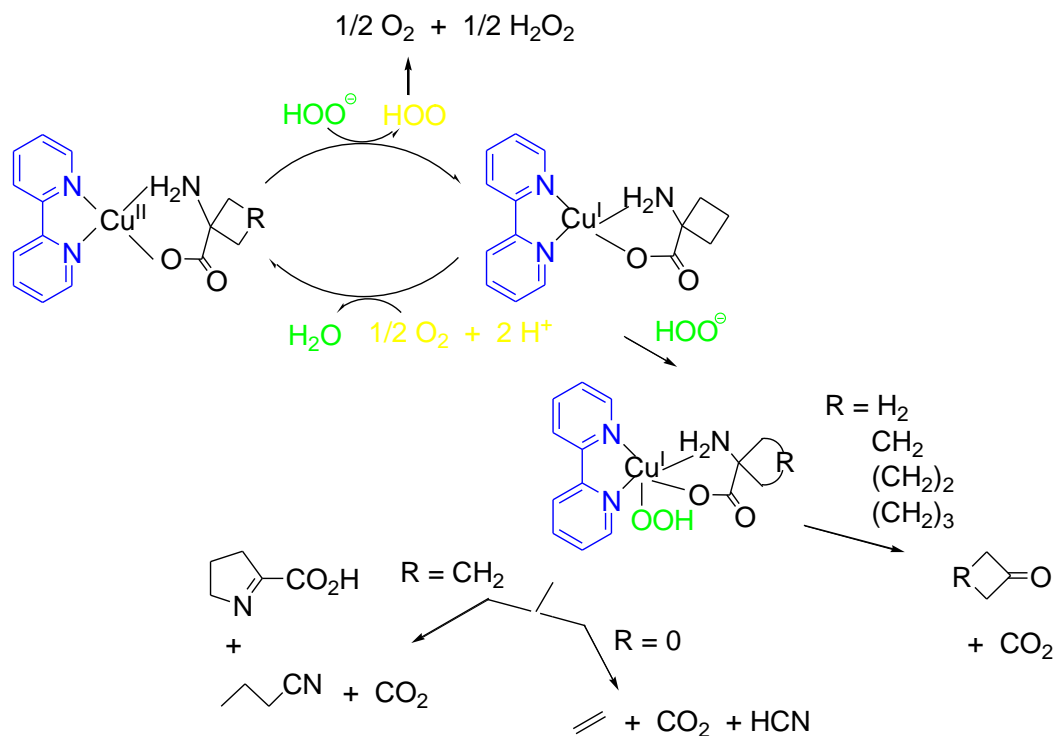
Scheme 27. The proposed mechanism for the investigated [Cu^{II}(bpy)] complexes.

AA complexes of Cu^{II} with bpy ligand are good structural and functional models of the enzyme ACCO.

Amino acid complexes of Cu^{II} with bpy ligand show distorted square pyramidal geometry. The EPR spectra for ACBC-, ACPC- and ACHC-containing complexes support the X-ray data.

The results of single turnover oxidation reactions of bound AAs suggest a good functional model as the product formation is more like the one in enzymatic system. The presence and the relatively low value of SIE reveal ET-PT mechanism.

Inhibition studies imply the same mechanism for the product formation for both the AAs and for the amino phosphonates equally.

Voltammograms show one reversible peak, which is most likely due to a geometric change from square pyramidal to tetrahedral accompanied by an electron change from Cu^{II} to Cu^{I}.

The suggested active oxidant responsible for substrate activation is a Cu^{I}-OOH intermediate for the bpy-containing complex on the basis of UV-Vis measurements. The formation of a reactive Cu^{I}-intermediate gives Cu^{I}-OOH adduct, and - depending on the

nature of the substrate - ring opening or decarboxylation process gives the corresponding product.

5. SUMMARY

The application of enzymes in biotechnology has many drawbacks. Therefore the synthesis of a transition metal complex, which mimics the structure and the function of the native enzyme, is of high importance. The action of the enzyme 1-aminocyclopropane-1-carboxylic acid oxidase, which catalyses the last step of ethylene biosynthesis, is in the focus of this work. Ethylene – the simplest a phytohormone – regulates plant growth, development, senescence and fruit ripening.

The synthesized $[Fe^{III}(SALEN)Cl]$, $[Cu^{II}(AA)_2]$ and the bpy containing cyclic and acyclic amino acid complexes appeared to be active and selective catalysts in the oxidation reactions of various amino acids. The investigations revealed *Michaelis-Menten* type behavior concerning the change of substrate concentration. The reaction rate showed first order dependence on both the catalyst and the oxidant H_2O_2.

On the basis of results a possible mechanism was proposed for the $[Fe^{III}(SALEN)Cl]$ complex containing system. This mechanism implies a fast pre-equilibrium in an intermediate complex between the substrate and the catalyst. The following step is the formation of a substrate radical in ET-PT reaction between the coordinated substrate and the oxo-iron centre in the RDS. Based on literature results the suspected active intermediate, $[Fe^{IV}O(SALEN)]^{\bullet+}$ is suggested as a model for high-valent oxo centre. Products can be formed either via decarboxylation or direct ring opening reaction depending on the ring strain of the particular substrate.

Detailed structural information was obtained regarding the $[Cu^{II}(AA)_2]$ complexes using X-ray diffraction measurements. The data suggest a square planar geometry for all studied complexes. Redox properties of the isolated complexes were determined using cyclic voltammetry, which shows a geometric change from square planar Cu^{II} to tetrahedral Cu^{I} as supported also by DFT calculations for other Cu-containing AA complexes. The comparison of the calculated TOF values for the reactions performed with $[CuCl_2]$ and $[Cu^{II}(AA)_2]$ complexes indicate only a slight difference. As a result, an identical active form of catalyst is assumed for the two systems studied.

In case of the bpy ligand containing Cu^{II} amino acid complexes a distorted square pyramidal geometry was observed according to X-ray and EPR measurements. The results of cyclic voltammetry indicate a geometric change from square pyramidal to

tetrahedral accompanied by a change in the oxidation state from Cu^{II} to Cu^{I}. The suggested active oxidant is a Cu^{I}-OOH intermediate for the bpy-containing complex. The formed reactive Cu^{I}-intermediate transformes to a Cu^{I}-OOH adduct, and – depending on the nature of the substrate – ring opening or decarboxylation reaction gives the final product.

6. EXPERIMENTAL

Materials

Solvents used for the reactions were purified by literature methods [91] and stored under argon. $Cu(ClO_4)_2.6H_2O$, bpy, the amino acid substrates and AMEP were purchased from commercial sources and used as recieved without further purification. ACPC was synthesized following a previously described procedure. [92] Caution! Perchlorate salts are potentially explosive. A small amount of material should only be prepared and handled with caution. $[Fe^{III}(SALEN)Cl]$ was prepared following a literature method. [93] Complexes $[Cu^{II}(ACC)(bpy)]ClO_4 \cdot H_2O$ and $[Cu^{II}(bpy)(AIB).(H_2O)]ClO_4$ have already been described. [66]

The following instruments were used for analytical measurements:

Avatar 330 FT-IR Thermo Nicolet instrument was used to record infrared spectra with mulled KBr pellets.

UV-Vis spectra were recorded on an Agilent 8453 diode–array spectrophotometer using quartz cells.

A Hewlett Packard 5890 gas chromatograph was used to perform GC analysis. The instrument was equipped with a flame ionization detector and a 30 m Supelcowax column.

Cyclic voltammograms were taken on a Voltalab 10 potentiostat with VoltaMaster 4 software for data processing. The electrodes were as follows: glassy carbon (working), Pt (auxiliary), and Ag/AgCl in 3 M KCl (reference). The potentials were referenced vs. the ferrocenium ferrocene redox couple (+416 mV in methanol in our setup).

Crystal evaluation and data collection were completed on a Bruker Nonius-Kappa CCD single-crystal diffractometer using Mo-Kα radiation ($\lambda = 0.71070$ Å) at 296, 293 and 203 K.

A Bruker ELEXSYS 500-X-band CW-EPR spectrometer equipped with a Dewar tube-holder filled with liquid N_2 was used for EPR measurements. Spectra were recorded in frozen CH_3OH at - 153 °C.

Automathic parameter fitting was carried out by a published simulation software. [94] Microanalyses were done by the Microanalytical Service of the University of Pannonia.

Synthesis of [Cu^{II}(ACBC)$_2$]

5 cm^3 aqueous solution of ACBCH (0.69 g, 6 mmol) was mixed with CuCl$_2$.2H$_2$O (0.51 g, 3 mmol) in 15 cm^3 CH$_3$OH, and triethyl-amine (0.84 cm^3, 6 mmol) was added dropwise to the mixture. Formation of a purple-blue crystalline precipitate was observed following the disappearance of a transient lilac color. Yield: 0.56 g (64 %), Anal. Calc. for C$_{10}$H$_{16}$CuN$_2$O$_4$: C, 41.16; H, 5.53; N, 9.60. Found: C, 41.4; H, 5.6; N, 9.8%. FT-IR bands (KBr pellet, cm^{-1}) 3285, 3238, 3126, 2974, 2950, 2868, 1619, 1391, 1272, 1158, 1070, 751, 690, 571. UV-Vis (CH$_3$OH/H$_2$O) [λ_{max}, nm (logε)] 243 (4.00), 611 (2.06). Crystals suitable for X-ray structural determination were obtained from CH$_3$OH-H$_2$O solvent mixture.

Synthesis of [Cu^{II}(ACPC)$_2$].H$_2$O

The complex was synthesized analogously to [Cu^{II}(ACBC)$_2$]. Yield: 0.71 g (74%). Anal. Calc. for C$_{12}$H$_{22}$CuN$_2$O$_5$: C, 42.66; H, 6.56; N, 8.29. Found: C, 42.7; H, 6.6; N, 8.4. FT–IR bands (KBr pellet, cm^{-1}) 3446, 3284, 3248, 2959, 2870, 1625, 1583, 1374, 1326, 1186, 1148, 821, 645, 596. UV-Vis (CH$_3$OH) [λ_{max}, nm (logε)] 245 (3.89), 594 (1.94).

Synthesis of [Cu$_2$^{II}(ACHC)$_4$(H$_2$O)].H$_2$O

The complex was synthesized analogously to [Cu^{II}(ACBC)$_2$]. Yield: 0.65 g (62%). Anal. Calc. for C$_{14}$H$_{26}$CuN$_2$O$_5$: C, 45.95; H, 7.16; N, 7.66. Found: C, 46.3; H, 7.2; N, 7.8. FT–IR bands (KBr pellet, cm^{-1}) 3441, 3320, 3250, 3147, 2929, 2859, 1612, 1603, 1453, 1369, 1343, 1175, 1098, 983, 814, 757, 670, 561. UV-Vis (CH$_3$OH) [λ_{max}, nm (logε)] 245 (3.84), 595 (1.85). Crystals suitable for X-ray structural determination were obtained from CH$_3$OH-H$_2$O solvent mixture.

Synthesis of [Cu^{II}(AIB)$_2$]

The complex was synthesized analogously to [Cu^{II}(ACBC)$_2$]. Yield: 0.59 g (73%). Anal. Calc. for $C_8H_{16}CuN_2O_4$: C, 35.88; H, 6.02; N, 10.46. Found: C, 35.4; H, 6.1; N, 10.2. FT–IR bands (KBr pellet, cm^{-1}) 3273, 3240, 3142, 2974, 2933, 1627, 1588, 1474, 1390, 1363, 1221, 1097, 1087, 893, 817, 782, 691, 576. UV-Vis (CH$_3$OH) [λ_{max}, nm (logε)] 244 (3.84), 600 (1.88).

Synthesis of [Cu^{II}(D,L-ALA)$_2$)].H$_2$O

The complex was synthesized analogously to [Cu^{II}(ACBC)$_2$]. Yield: 0.58 g (81%). Anal. Calc. for $C_6H_{14}CuN_2O_3$: C, 27.96; H, 5.48; N, 10.87. Found: C, 28.2; H, 5.5; N, 11.0. FT–IR bands (KBr pellet, cm^{-1}) 3395, 3267, 3158, 2970, 2935, 2877, 1626, 1591, 1451, 1394, 1354, 1301, 1160, 1120, 1062, 857, 789, 672, 566. UV-Vis (CH$_3$OH/H$_2$O) [λ_{max}, nm (logε)] 239 (3.86), 610 (1.81).

Synthesis of [Cu^{II}(bpy)(ACBC)]ClO$_4 \cdot$H$_2$O

2,2'-bipyridine (0.156 g, 1 mmol) and ACBCH (0.115 g, 1 mmol) were added to a stirred solution of Cu^{II}(ClO$_4$)$_2 \cdot$6H$_2$O (0.372 g, 1 mmol) in methanol (20 cm^3). Dropwise addition of triethylamine (140 μl, ca. 1 mmol, freshly distilled and stored under argon) resulted in a dark blue solution. After stirring for 1 hour at room temperature the solution was filtered and left to evaporate slowly to ~3 cm^3. Crystalline product was formed, which was filtered, washed with a minimal amount of cold methanol and dried. Yield: 0.34 g (75%). Anal. Calc. for $C_{15}H_{18}N_3CuClO_7$: C, 39.92; H, 4.02; N, 9.31. Found: C, 40.1; H, 4.0; N, 9.4. FT-IR bands (KBr pellet, cm^{-1}) 3469, 3409, 3195, 3071, 2989, 2950, 1630, 1600, 1474, 1442, 1372, 1315, 1252, 1142, 1113, 1088, 1029, 779, 731, 636, 626, 597. UV-Vis (CH$_3$OH) [λ_{max}, nm (logε)] 302 (4.20), 313 (4.19), 376 (2.29), 598 (2.02). Crystals suitable for X-ray structural determination were obtained from CH$_3$OH.

Synthesis of [Cu^{II}(bpy)(ACPC)]ClO$_4$·H$_2$O

   The complex was synthesized analogously to [Cu^{II}(bpy)(ACBC)]ClO$_4$·H$_2$O**.** Yield: 0.32 g (73%). Anal. Calc. for C$_{16}$H$_{20}$N$_3$CuClO$_7$: C, 41.30; H, 4.33; N, 9.03. Found: C, 41.4; H, 4.4; N, 8.9. FT-IR bands (KBr pellet, cm^{-1}) 3486, 3207, 3122, 3073, 2938, 2864, 1648, 1604, 1474, 1442, 1389, 1314, 1247, 1147, 1119, 1077, 1030, 766, 730, 636, 625, 500. UV-Vis (CH$_3$OH) [λ_{max}, nm (logε)] 302 (4.18), 302 (4.17), 372 (2.12), 588 (1.86). Crystals suitable for X-ray structural determination were obtained from CH$_3$OH.

Synthesis of [Cu^{II}(bpy)(ACHC)]ClO$_4$·H$_2$O

   The complex was synthesized analogously to [Cu^{II}(bpy)(ACBC)]ClO$_4$·H$_2$O**.** Yield: 0.40 g (83%). Anal. Calc. for C$_{17}$H$_{22}$N$_3$CuClO$_7$: C, 42.59; H, 4.63; N, 8.77. Found: C, 42.7; H, 4.7; N, 8.8. FT-IR bands (KBr pellet, cm^{-1}) 3461, 3304, 3247, 3112, 3026, 2929, 2868, 1642, 1602, 1478, 1447, 1381, 1146, 1117, 1089, 1033, 772, 732, 624, 570. UV-Vis (CH$_3$OH) [λ_{max}, nm (logε)] 302 (4.16), 313 (4.15), 368 (2.13), 590 (1.71). Crystals suitable for X-ray structural determination were obtained from CH$_3$OH.

Synthesis of [Cu^{II}(bpy)(MAIB)]ClO$_4$·H$_2$O

   The complex was synthesized analogously to [Cu^{II}(bpy)(ACBC)]ClO$_4$·H$_2$O**.** Yield: 0.35 g (77%). Anal. Calc. for C$_{15}$H$_{20}$N$_3$CuClO$_7$: C, 39.74; H, 4.45; N, 9.27. Found: C, 39.5; H, 4.3; N, 9.4. FT-IR bands (KBr pellet, cm^{-1}) 3446, 3308, 2974, 2925, 2872, 1660, 1604, 1475, 1445, 1388, 1318, 1219, 1111, 1087, 1033, 903, 768, 732, 624, 587. UV-Vis (CH$_3$OH) [λ_{max}, nm (logε)] 301 (4.04), 311 (4.04), 360sh (1.71), 592 (1.68).

Synthesis of [Cu^{II}$_2$(bpy)$_2$(AMEP)(H$_2$O)$_3$](ClO$_4$)$_2$·3H$_2$O

The complex was synthesized similarly to $[Cu^{II}(bpy)(ACBC)]ClO_4 \cdot H_2O$. The synthesis was performed with 0.5 mmol quantities and the product was isolated as blue microcrystalline solid. Yield: 0.12 g (48%). Anal. Calc. for $C_{23}H_{36}Cl_2Cu_2N_5O_{17}P$: C, 31.27; H, 4.11; N, 7.93. Found: C, 31.7; H, 4.0; N, 8.2. FT-IR bands (KBr pellet, cm^{-1}) 3435, 3153, 2929, 2853, 1605, 1543, 1473, 1448, 1303, 1185, 1160, 1082, 1054, 1030, 902, 772, 624. UV-Vis (CH_3OH) [λ_{max}, nm ($\log\varepsilon$)] 300 (4.22), 311 (4.21), 371 (1.80), 611 (1.73). Crystals suitable for X-ray structural determination were obtained from CH_3OH.

Analysis of the products and kinetic measurements

In a 20 cm^3 screw-cap vial 10 cm^3 of DMF/H_2O mixture (3/1) was used to dissolve the amino acid (ABH, ACCH, ACBCH, ACHCH, ACPCH, AIBH, *N*-Me-AIBH, ALAH, NORH). CH_3CN (10 µl) as inner standard, NH_4OH and the catalyst were then added to the mixture. Hydrogen peroxide was added through a septum with a syringe and the evolved acetone, acetaldehyde, methyl-ethylketone, cyclobutanone, cyclopentanone, cyclohexanone or ethylene were measured by removing 250 µl of the head-space with a gastight syringe. The sample was analyzed with a gas chromatograph. GC setup was: Supelcowax 30 m capillary column, 100 °C to 170 °C heating with 20 °C/min rate. Concentration of the corresponding product in the headspace is linearly proportional to the concentration of product in the reaction mixture. For ACBCH, two other peaks were observed in the chromatogram in addition to the peak of cyclobutanone. In order to investigate the nature of these species, ACBCH was also oxidized with $KMnO_4$ and the products were analyzed. [62] Concentrated NH_4OH (0.540 cm^3; 25%) and 89.7 mg of $KMnO_4$ were added to an aqueous solution (10 cm^3) of ACBCH (41.5 mg) in a sealable tube of 20 cm^3. The reaction was monitored first with a gas chromatograph. The observed peak was identical with one of the products in the oxidation reaction of ACBCH using $[Fe^{III}(SALEN)Cl]$ as catalyst and H_2O_2 as oxidant in the presence of base (RT= 0.935). TLC analysis was performed using *n*-butanol:glacial acetic acid:H_2O (4:1:1) as a solvent system and ninhydrin as a staining reagent. TLC displayed a brown spot below the starting material ACBCH, which was a pink spot. The brown spot corresponded to Δ^1-

pyrroline-2-carboxylic acid when compared to authentic TLC data. The liberated CO_2 was identified by the conventional limewater test. Ammonia - formed in the reaction - was determined by the micro *Kjeldahl* procedure.

Kinetic study on the oxidation of amino acids by [Fe^{III}(SALEN)Cl] in acetonitrile is performed under pseudo first order conditions. The progress of reaction is measured following the decay of absorbance of [Fe^{IV}O(SALEN)]$^{\bullet+}$ intermediate with time at appropriate wavelength [88]. The concentration of [Fe^{III}(SALEN)Cl], amino acid tetrabutyl-ammonium salt and hydrogen peroxide are 2×10^{-4} M, 2×10^{-3} M and 5×10^{-3} M, respectively. The temperature is 25 °C, unless otherwise stated. [Fe^{IV}O(SALEN)]$^{\bullet+}$ was generated with the addition of H_2O_2. The substrate was then added to the mixture. Spectral changes were recorded.

Stoichiometric oxidation of the mixed-ligand [Cu(bpy)(AA)]$ClO_4^.H_2O$ complexes was investigated in 3:1 DMF-H_2O (or D_2O) mixture at 35 °C. The complex was dissolved in a standard 20 cm^3 screw-cap vial 8.76×10^{-4} mol in 5.5 cm^3 DMF and 1.8 cm^3 H_2O (or D_2O). Acetonitrile was used as internal standard (7.3 μl). As base cc. NH_4OH was used (5 eqs. to the complex, 31 μl). Rubber septum was used to close the vial and concentrated H_2O_2 was injected (30 eqs. to the complex, 235 μl) through that. Solution was stirred at 35 °C. Samples were taken from the headspace with appropriate time intervals (250 μl, gas-tight syringe) depending on the rate of the corresponding reaction. GC setup was as follows: Supelcowax 30 m capillary column, 100 °C to 170 °C heating with 20 °C/min rate. Products of the reactions were identified as it has been described above.

The kinetic studies on the catalytic oxidation of amino acids by $CuCl_2$ or Cu(AA)$_2$ complexes were performed in a 3:1 DMF-H_2O mixture at 35 °C. The respective amino acid (3.6×10^{-4} mol) was dissolved in 10 cm^3 of the solvent in a screw-cap vial of 20 cm^3, which was sealed with a septum. CH_3CN (10 μl) as internal standard, the catalyst (7.2×10^{-8} mol) and NH_4OH (3.6×10^{-4} mol) were then added to the mixture. Hydrogen peroxide (32 μl, 3.6×10^{-4} mol) was injected through the septum with a syringe. In order to determine the evolved products 250 μl was removed from the headspace using a gas-tight syringe and analyzed with GC as described before.

7. REFERENCES

[1] I. B. Wilson, M. A. Harrison, *J. Biol. Chem.,* **236** (1961) 2292-2295.

[2] D. Voet, J. G. Voet, *Biochemistry 4th Edition* (2011) ISBN 978-0470-57095-1

[3] E. Kolker, E. N. Trifonov, *Pac. Symp. Biocomput.*, (1996) 461-471.

[4] R. W. Hay, *Bio-Inorganic Chemistry*, Ellis Harwood Ltd., Chiester (1984) ISBN 0-85312-200-8

[5] A. Gibello, E. Ferrer, M. Martin, A. Garridopertierra, *Biochem. J.*, **301**, (1994) 145-150.

[6] L. Que, *Bioinorganic Catalysis*, Second ed., Marcel Dekker, Inc, New York, (1999)

[7] Y. R. Boldt, M. J. Sadowsky, L. B. M. Ellis, L. Que, Jr., L. P. Wackett, *J. Bacteriol.,* **177** (1995) 1225-1232.

[8] M. M. Abu-Omar, A. Loaiza, N. Hontzeas, *Chem. Rev.*, **105** (2005) 2227-2252.

[9] A. Siegl, H. Sigel, R. K. O. Sigel, *Sustaining Life on Planet Earth: Metalloenzymes Mastering Dioxygen and Other Chewy Gases* (2015) ISBN 978-3-.319-12414-8

[10] I. G. Denisov, T. M. Makris, S. G. Sligar, I. Schlichting, *Chem. Rev.,* **105** (2005) 2253-2277.

[11] P. C. A. Bruijnincx, G. van Koten, R. J. M. Klein Gebbink, *Chem. Soc. Rev.,* **37** (2008) 2716–2744.

[12] K. D. Koehntop, Ć Joseph, J. P. Emerson, L. Que Jr, *J. Biol. Inorg. Chem.,* **10** (2005) 87–93.

[13] C. J. Schofield, Z. Zhang, *Curr. Opin. Struct. Biol.*, **9** (1999) 722–731.

[14] L. M. Hoffart, E. W. Barr, R. B. Guyer, J. M. Bollinger, C. Krebs, *Proc. Nat. Acad. Sci.,* **103** (2006) 14738-14743.

[15] J.C. Price, E.W. Barr, B. Tirupati, J. M. Bollinger Jr., C. Krebs, *Biochemistry,* **42** (2003) 7497–7508.

[16] J. M. Bollinger, J. C. Price, L. M. Hoffart, E. W. Barr, C. Krebs, *Eur. J. Inorg. Chem.*, (2005) 4245-4254.

[17] D. A. Proshlyakow, T. F. Henshow, G. R. Monterosso, M. J. Ryle, R. P. Hausinger, *J. Am. Chem. Soc.,* **126** (2004) 1022-1023.

[18] P. J. Riggs – Gelasco, J. C. Price, R. B. Guyer, J. H. Brehm, E. W. Barr, J. M. Bollinger Jr., C. Krebs, *J. Am. Chem. Soc.,* **126** (2004) 8108-8109.

[19] F. H. Vaillancourt, J. T. Bolin, L. D. Eltis, *Crit. Rev. Biochem. Mol. Biol*., **41** (2006) 241-267.

[20] M .Costas, M. P. Mehn, M. P. Jehnsen, L. Que Jr., *Chem. Rev*., **104** (2004) 939-986.

[21] M. J. Ryle, R. Padamkumar, R. P. Hausinger, *Biochemistry*, **38** (1999) 15278-15286.

[22] C.-K. Liu, C.-A. Hsu, M. T. Abbott, *Arch. Biochem. Biophys.,* **159** (1973) 180.

[23] K. I. Kirivikko, T. Pihlajaniemi, *Adv. Enzymol. Relat. Areas Mol. Biol.*, D. L. Purich, Ed., Wiley Interscience **72** (1998) 325.

[24] E. G. Pavel, J. Zhou, R. W. Busby, M. Gunsior, C. A. Townsend, E. I. Solomon, *J. Am. Chem. Soc.,* **120** (1998) 743-753.

[25] T. Urich, C. M. Gomes, A. Kletzin, C. Frazao, *Science,* **311** (2016) 996.

[26] N. J. Kerschaw, M. E. C. Caines, M. C. Sleeman, C. J. Schofield, *Chem. Commun*., (2006) 4251-4263.

[27] L. M. Mirica, X. Ottenwalder, T. D. P. Stock, *Chem. Rev*., **104** (2004) 1013-1045.

[28] J. P. Klinman, *Chem. Rev*., **96** (1996) 2541-2561.

[29] H. T. Nguyan, S. J. Elliott, J. H. Yip, S. J. Chan, *J. Biol. Chem.,* **273** (1998) 7957-7966.

[30] R. A. Steiner, K. H. Kalk, B. W. Dijkstra, *Proc. Nat. Acad. Sci. USA,* **99** (2002) 16625-16630.

[31] K. D. Karlin, S. Itoh, Copper-Oxygen Chemistry, ISBN 978-0-470-52835-8

[32] B. A. Eipper, D. A. Stoffers, R. E. Mains, *Annu. Rev. Neurosci*., **15** (1992) 57-85.

[33] B. A. Eipper, S. R. Milgram, E. I. Husten, H-Y. Yun, R. E. Mains, *Protein Sci*., **2** (1993) 489-497.

[34] A. B. Blecker, H. Kende, *Annu. Rev. Cell Dev. Biol*., **16** (2000) 1–18.

[35] H. Kende, *Plant Physiol*., **91** (1989) 1–4.

[36] P. John, *Physiol. Plant*., **100** (1997) 583–592.

[37] D. J. McGarvey, R. E. Christoffersen, *J. Biol. Chem*., **267** (1992) 5964–5967.

[38] A. J. Hamilton, G. W. Lycett, D. Grierson, *Nature,* **346** (1990) 284–287.

[39] A. J. Hamilton, M. Bouzayen, D. Grierson, *Proc. Natl. Acad. Sci. USA*., **88** (1991) 7434–7437.

[40] J. C. Fernández-Maculet, S. F. Yang, *Plant Physiol*., **99** (1992) 751–754.

[41] Y. S. Seo, A. Yoo, J. Jung, S.-K. Sung, D. R. Yang, W. T. Kim, W. Lee, *Biochem. J.*, **380** (2004) 339–346.

[42] A. M. Rocklin, D. L. Tierney, V. Kofman, N. M. W. Brunhuber, B. M. Hoffman, R. E. Cristoffersen, N. O. Reich, I. D. Lipscomb, L. Que J.r, *Proc. Nat. Acad. Sci. USA*, **96** (1999) 7905-7909.

[43] D. L. Tierney, A. M. Rocklin, J. D. Lipscomb, L. Que Jr., B. M. Hoffman, *J. Am. Chem. Soc.,* **127** (2005) 7005-7013.

[44] D. G. Mcrae, J. A. Coker, R. L. Legge, J. E. Thompson, *Plant Physiol.,* **73** (1983) 784-790.

[45] J. J. Smith, P. John, *Phytochemistry*, **32** (1993) 1381-1386.

[46] J. C. Fernandez-Maculet, J. G. Dong, S. F. Yang, *Biochem. Biophys. Res. Commun.,* **193** (1993) 1168-1173.

[47] J. Thrower, L. M. Mirica, K. P. McCusker, J. P. Klinman, *Biochemistry,* **45** (2006) 13108–13117.

[48] J. C. Price, E.W. Barr, T. E. Glass, C. Krebs, J. M. Bollinger Jr., *J. Am. Chem. Soc.*, **125** (2003) 13008–13009.

[49] W. Nam, *Acc. Chem. Res.*, **40** (2007) 522–531.

[50] L. Que Jr., *Acc. Chem. Res.*, **40** (2007) 493–500.

[51] J. U. Rohde, J. H. In, M. H. Lim, W. W. Brennessel, M. R. Bukowski, A. Stubna, E. Münck, W. Nam, L. Que Jr., *Science,* **299** (2003) 1037–1039.

[52] M. R. Bukowski, K. D. Koehntop, A. Stubna, E. L. Bominaar, J. A. Halfen, E. Münck, W. Nam, L. Que Jr., *Science,* **310** (2005) 1000–1002.

[53] J. Kaizer, E. J. Klinker, N. Y. Oh, J. U. Rohde, W. J. Song, A. Stubna, J. Kim, E. Münck, W. Nam, L. Que Jr., *J. Am. Chem. Soc.*, **126** (2004) 472–473.

[54] J. U. Rohde, S. Torelli, X. Shan, M. H. Lim, E. J. Klinker, J. Kaizer, K. Chen, W. Nam, L. Que Jr., *J. Am. Chem. Soc.*, **126** (2004) 16750–16761.

[55] E. J. Klinker, J. Kaizer, W. W. Brennessel, N. L. Woodrum, C. J. Cramer, L. Que Jr., *Angew. Chem. Int. Ed.,* **117** (2005) 3756–3760.

[56] M. P. Jensen, M. Costas, R. Y. N. Ho, J. Kaizer, I. Payeras, A. Mairata, E. Münck, L. Que Jr., J. U. Rohde, A. Stubna, *J. Am. Chem. Soc.*, **127** (2005) 10512–10525.

[57] T. K. Paine, M. Costas, J. Kaizer, L. Que Jr., *J. Biol. Inorg. Chem*., **11** (2006) 272–276.

[58] Z. Zhang, J.-S. Ren, I. J. Clifton, C. Schofield, *Chem. Biol*., **11** (2004) 1383–1394.

[59] J. Zhou, A. M. Rocklin, J. D. Lipscomb, L. Que Jr., E. I. Solomon, *J. Am. Chem. Soc*., **124** (2002) 4602-4609.

[60] J. S. Thrower, R. Blalock, J. P. Klinman, *Biochemistry,* **40** (2001) 9717-9724.

[61] M. C. Pirrung, J. Cao, J. Chen, *Chem. Biol*., **5** (1998) 49-57.

[62] M. Ito, H. Tokiwa, *Bull. Chem. Soc. Jpn*., **80** (2007) 1731-1739.

[63] Y. Nishida, T. Akamatsu, T. Ishii, Y. Oda, *Chem. Commun*., (1992) 496-497.

[64] T. Kobayashi, Y. Sasaki, T. Akamatsu, T. Ishii, Y. Oda, H. Masuda, H. Einaga, Y. Nishida, *Z. Naturforsch*., **54c** (1999) 534-541.

[65] W. Ghattas, C. Gaudin, M. Giorgi, A. Rockenbauer, A. J. Simaan, M. Réglier, *Chem. Commun*., (2006) 1027-1029.

[66] W. Ghattas, M. Giorgi, Y. Mekmouche, T. Tanaka, A. Rockenbauer, M. Réglier, Y. Hitomi, A. J. Simaan, *Inorg. Chem*., **47** (2008) 4627-4638.

[67] W. Ghattas, Z. Serhan, N. El Bakkali-Taheri, M. Réglier, M. Kodera, Y. Hitomi, A. J. Simaan, *Inorg. Chem*., **48** (2009) 3910-3912.

[68] S. Hong, S. M. Huber, L. Gagliardi, C. C. Cramer, W. B. Tolman, *J. Am. Chem. Soc*., **129** (2007) 14190-14192.

[69] G. Baráth, J. Kaizer, J. S. Pap, G. Speier, N. El Bakkali-Taheri, A. J. Simaan, *Chem. Commun*., **46** (2010) 7391-7393.

[70] M. L. Trehy, R. A. Yost, C. J. Miles, *Environ. Sci. Technol*., **20** (1986) 1117-1122.

[71] L. Padhye, U. Tezel, W. A. Mitch, S. Pavlostathis, C. H. Huang*, Environ. Sci. Technol*., **43** (2009) 3087-3093.

[72] E. R. Stadtman, R. L. Levine, *Amino Acids,* **25** (2003) 207-218.

[73] K. C. Brown, S.-H. Yang, T. Kodadek, *Biochemistry,* **34** (1995) 4733-4739.

[74] B. S. Berlett, E. R. Stadtman*, J. Biol. Chem*., **272** (1997) 20313-20316.

[75] B. Cuenoud, T. M. Tarasow, A. Schepartz, *Tetrahedron Lett*., **33** (1992) 895-898.

[76] N. Noorhasan, B. Patel, V. K. Sharma, *Water Res*., **44** (2010) 927-935.

[77] P. A. Parasantha, N. C. Ssandhya, B. K. Kempegowda, D. G. Bhadregowda, K. Mantelingu, S. Ananda, K. K. S. Rangappa, M. N. Kumara, *J. Mol. Catal. A. Chem*., **111** (2012) 353-354.

[78] P. A. Prashanth, B. K. Kempegowda, S. Ananda, K. S. Rangappa, M. N. Kumara, *J. Mol. Catal. A. Chem*., **383-384** (2014) 203-208.

[79] K. S. Rangappa, K. Mantjunathaswamy, M. P. Raghavendra, N. M. Made Gowda, *Int. J. Chem. Kinet*., **34** (2002) 49-55.

[80] P. G. Cozzi, *Chem. Soc. Rev*., **33** (2004) 410-421.

[81] K. C. Gupta, A. K. Sutar, *Coord. Chem. Rev*., **252** (2008) 1420-1450.

[82] B. Fan, H. Li, W. Fan, C. Jin, R. Li, *Appl. Catal. A*., **340** (2008) 67-75.

[83] L. M. Mirica, J. P. Klinman, *Proc. Nat. Acad. Sci*., **105** (2008) 1814-1819.

[84] K. Nehru, M. S. Seo, J. Kim, W. Nam, *Inorg. Chem*., **46** (2007) 293-298.

[85] J. P. Kirby, J. A. Roberts, D. G. Nocera, *J. Am. Chem. Soc*., **119** (1997) 9230-9236.

[86] A. M. I. Jayaseeli, S. Rajagopal, *J. Mol. Catal. A. Chem*., **309** (2009) 103-110.

[87] N. S. Venkataramanan, G. Kuppuraj, S. Rajagopal, *Coord. Chem. Rev*., **249** (2005) 1249-1268.

[88] A. W. Adison, T. N. Rao, J. Reedijk, J. van Rijn, G. C. Verschoor, *J. Chem. Soc. Dalton Trans.,* (1984) 1349-1356.

[89] F. H. Allen, *Acta Crystallogr. Sect. B*., **58** (2002) 380-388.

[90] L. Brisson, N. El Bakkali-Taheri, M. Giorgi, A. Fadel, J. Kaizer, M. Réglier, T. Tron, H. el Ajandouz, A. J. Simaan, *J. Biol. Inorg. Chem*., **17** (2012) 939-949.

[91] D. D. Perrin, W.L. Armarego, D. R. Perrin, *Purification of Laboratory Chemicals*, second ed., Pergamon Press, New York, 1990.

[92] A. Fadel, *J. Org. Chem*., **64** (1999) 4953-4955.

[93] V. K. Sivasubramanian, M. Ganesan, S. Rajagopal, R. Ramaraj, *J. Org. Chem*., **67** (2002) 1506–1514.

[94] A. Rockenbauer, L. Korecz, *Appl. Magn. Reson*., **10** (1996) 29-43.

Appendix

Table A1. Kinetic data for the oxidation of ACCH catalyzed by [Fe^{III}(SALEN)Cl] with H$_2$O$_2$ in DMF/H$_2$O (3 : 1) at 35 °C.

Run	Subs.	[S]$_0$ (10^{-2} M)	[H$_2$O$_2$]$_0$ (10^{-2} M)	[Fe]$_0$ (10^{-5} M)	-d[S]/dt (10^{-7} Ms^{-1})
1	ACCH	3.60	3.60	**0.30**	1.24
2	ACCH	3.60	3.60	**0.72**	4.35
3	ACCH	3.60	3.60	**0.90**	4.65
4	ACCH	3.60	3.60	**1.80**	1.04
5	ACCH	**0.50**	3.60	0.72	1.56
6	ACCH	**1.08**	3.60	0.72	2.74
7	ACCH	**2.16**	3.60	0.72	4.07
8	ACCH	3.60	**2.29**	0.72	2.69
9	ACCH	3.60	**2.97**	0.72	3.47
10	ACCH	3.60	**5.45**	0.72	5.44
11	ACCH	3.60	**7.20**	0.72	8.83
12	ACCD	3.60	3.60	0.72	3.16

Table A2. Kinetic data for the oxidation of ACHCH catalyzed by [Fe^{III}(SALEN)Cl] with H$_2$O$_2$ in DMF/H$_2$O (3 : 1) at 35 °C.

Run	Subs.	[S]$_0$ (10^{-2} M)	[H$_2$O$_2$]$_0$ (10^{-2} M)	[Fe]$_0$ (10^{-5} M)	-d[S]/dt (10^{-5} Ms^{-1})
41	ACHCH	3.60	3.60	**0.39**	0.98
42	ACHCH	3.60	3.60	**0.72**	1.86
43	ACHCH	3.60	3.60	**1.20**	3.43
44	ACHCH	**0.66**	3.60	0.72	0.48
45	ACHCH	**0.88**	3.60	0.72	0.59
46	ACHCH	**1.44**	3.60	0.72	0.83
47	ACHCH	**2.16**	3.60	0.72	1.11
48	ACHCH	**2.80**	3.60	0.72	1.12
49	ACHCH	3.60	**1.14**	0.72	0.76
50	ACHCH	3.60	**2.29**	0.72	1.31
51	ACHCD	3.60	3.60	0.72	1.03

Table A3. Kinetic data for the oxidation of ACPCH catalyzed by [Fe^{III}(SALEN)Cl] with H$_2$O$_2$ in DMF/H$_2$O (3 : 1) at 35 °C.

Run	Subs.	[S]$_0$ (10^{-2} M)	[H$_2$O$_2$]$_0$ (10^{-2} M)	[Fe]$_0$ (10^{-5} M)	-d[S]/dt (10^{-5} Ms^{-1})
13	ACPCH	3.60	3.60	**0.39**	0.54
14	ACPCH	3.60	3.60	**0.60**	0.68
15	ACPCH	3.60	3.60	**0.90**	1.13
16	ACPCH	3.60	3.60	**1.20**	1.45
17	ACPCH	**0.50**	3.60	0.72	0.32
18	ACPCH	**0.66**	3.60	0.72	0.40
19	ACPCH	**0.88**	3.60	0.72	0.50
20	ACPCH	**1.44**	3.60	0.72	0.71
21	ACPCH	**2.52**	3.60	0.72	0.93
22	ACPCH	3.60	**1.14**	0.72	0.38
23	ACPCH	3.60	**2.29**	0.72	0.70
24	ACPCH	3.60	**3.60**	0.72	0.99
25	ACPCH	3.60	**5.45**	0.72	1.48
26	ACPCH	3.60	**7.20**	0.72	2.19
27	ACPCD	3.60	3.60	0.72	0.75

Table A4. Kinetic data for the oxidation of ACBCH catalyzed by [Fe^{III}(SALEN)Cl] with H$_2$O$_2$ in DMF/H$_2$O (3 : 1) at 35 °C.

Run	Subs.	$[S]_0$ (10^{-2} M)	$[H_2O_2]_0$ (10^{-2} M)	$[Fe]_0$ (10^{-5} M)	$-d[S]/dt$ (10^{-6} Ms^{-1})
28	ACBCH	3.60	3.60	**0.60**	1.62
29	ACBCH	3.60	3.60	**0.72**	2.19
30	ACBCH	3.60	3.60	**0.90**	2.49
31	ACBCH	3.60	3.60	**1.20**	3.53
32	ACBCH	3.60	3.60	**1.80**	4.94
33	ACBCH	**1.08**	3.60	0.72	1.08
34	ACBCH	**1.80**	3.60	0.72	1.68
35	ACBCH	**2.16**	3.60	0.72	1.85
36	ACBCH	**2.88**	3.60	0.72	2.02
37	ACBCH	3.60	**1.14**	0.72	0.59
38	ACBCH	3.60	**2.29**	0.72	1.68
39	ACBCH	3.60	**7.20**	0.72	4.92
40	ACBCD	3.60	3.60	0.72	0.87

Table A5. Kinetic data for the oxidation of ALAH catalyzed by [Fe^{III}(SALEN)Cl] with H_2O_2 in DMF/H_2O (3 : 1) at 35 °C.

Run	Subs.	$[S]_0$ $(10^{-2}$ M$)$	$[H_2O_2]_0$ $(10^{-2}$ M$)$	$[Fe]_0$ $(10^{-5}$ M$)$	$-d[S]/dt$ $(10^{-7}$ M s$^{-1})$
52	ALAH	3.60	3.60	**0.60**	1.39
53	ALAH	3.60	3.60	**1.44**	2.81
54	ALAH	3.60	3.60	**1.80**	4.38
55	ALAH	**0.34**	3.60	0.72	0.95
56	ALAH	**0.72**	3.60	0.72	1.35
57	ALAH	**1.08**	3.60	0.72	1.96
58	ALAH	**1.80**	3.60	0.72	2.34
59	ALAH	**2.80**	3.60	0.72	2.40
60	ALAH	3.60	**1.14**	0.72	0.49
61	ALAH	3.60	**2.29**	0.72	1.31
62	ALAH	3.60	**3.60**	0.72	2.47
63	ALAH	3.60	**5.45**	0.72	4.37
64	ALAH	3.60	**7.20**	0.72	5.22
65	ALAD	3.60	3.60	0.72	1.17

Table A6. Kinetic data for the oxidation of NORH catalyzed by [Fe^{III}(SALEN)Cl] with H$_2$O$_2$ in DMF/H$_2$O (3 : 1) at 35 °C.

Run	Subs.	[S]$_0$ (10^{-2} M)	[H$_2$O$_2$]$_0$ (10^{-2} M)	[Fe]$_0$ (10^{-5} M)	-d[S]/dt (10^{-5} Ms^{-1})
66	NORH	3.60	3.60	**0.39**	0.30
67	NORH	3.60	3.60	**1.20**	0.72
68	NORH	3.60	3.60	**1.80**	1.14
69	NORH	**0.34**	3.60	0.72	0.19
70	NORH	**0.66**	3.60	0.72	0.26
71	NORH	**0.89**	3.60	0.72	0.38
72	NORH	**1.50**	3.60	0.72	0.58
73	NORH	**2.50**	3.60	0.72	0.60
74	NORH	3.60	**1.14**	0.72	0.24
75	NORH	3.60	**2.29**	0.72	0.37
76	NORH	3.60	**3.60**	0.72	0.64
77	NORH	3.60	**5.45**	0.72	0.96
78	NORH	3.60	**7.20**	0.72	1.29
79	NORD	3.60	3.60	0.72	0.30

Table A7. Kinetic data for the oxidation of ABH catalyzed by [Fe^{III}(SALEN)Cl] with H_2O_2 in DMF/H_2O (3 : 1) at 35 °C.

Run	Subs.	$[S]_0$ $(10^{-2}$ M)	$[H_2O_2]_0$ $(10^{-2}$ M)	$[Fe]_0$ $(10^{-5}$ M)	$-d[S]/dt$ $(10^{-5}$ Ms$^{-1})$
80	ABH	3.60	3.60	**0.39**	0.52
81	ABH	3.60	3.60	**0.60**	0.88
82	ABH	3.60	3.60	**0.90**	1.50
83	ABH	**0.29**	3.60	0.72	0.25
84	ABH	**0.73**	3.60	0.72	0.47
85	ABH	**1.08**	3.60	0.72	0.68
86	ABH	**2.16**	3.60	0.72	0.85
87	ABH	**2.60**	3.60	0.72	0.90
88	ABH	3.60	**1.14**	0.72	0.32
89	ABH	3.60	**2.29**	0.72	0.53
90	ABH	3.60	**3.60**	0.72	1.13
91	ABH	3.60	**4.80**	0.72	1.45
92	ABH	3.60	**7.20**	0.72	2.05
93	ABD	3.60	3.60	0.72	0.35

Table A8. Kinetic data for the oxidation of AIBH catalyzed by [Fe^{III}(SALEN)Cl] with H$_2$O$_2$ in DMF/H$_2$O (3 : 1) at 35 °C.

Run	Subs.	[S]$_0$ (10^{-2} M)	[H$_2$O$_2$]$_0$ (10^{-2} M)	[Fe]$_0$ (10^{-5} M)	-d[S]/dt (10^{-5} Ms^{-1})
94	AIBH	3.60	3.60	**0.60**	1.93
95	AIBH	3.60	3.60	**0.72**	2.77
96	AIBH	3.60	3.60	**0.90**	2.99
97	AIBH	3.60	3.60	**1.20**	4.25
98	AIBH	**0.16**	3.60	0.72	0.33
99	AIBH	**0.64**	3.60	0.72	1.05
100	AIBH	**1.58**	3.60	0.72	1.56
101	AIBH	**2.16**	3.60	0.72	1.84
102	AIBH	**2.88**	3.60	0.72	2.02
103	AIBH	3.60	**1.14**	0.72	0.82
104	AIBH	3.60	**2.29**	0.72	2.01
105	AIBD	3.60	3.60	0.72	2.24

Table A9. Kinetic data for the oxidation of N-Me-AIBH catalyzed by [Fe^{III}(SALEN)Cl] with H$_2$O$_2$ in DMF/H$_2$O (3 : 1) at 35 °C.

Run	Subs.	[S]$_0$ (10^{-2} M)	[H$_2$O$_2$]$_0$ (10^{-2} M)	[Fe]$_0$ (10^{-5} M)	-d[S]/dt (10^{-5} Ms^{-1})
106	N-Me-AIB	3.60	**1.14**	0.72	0.08
107	N-Me-AIB	3.60	**2.29**	0.72	0.15
108	N-Me-AIB	3.60	**3.60**	0.72	0.20

Table A10. Kinetic data for the oxidation of ACCH with $[Fe^{IV}O(SALEN)]^{\bullet+}$ in CH_3CN.

Run	Subs.	$[S]_0$ $(10^{-3}\ M)$	$[H_2O_2]_0$ $(10^{-3}\ M)$	$[Fe]_0$ $(10^{-4}\ M)$	k $(10^{-1}\ M^{-1}s^{-1})$	T (°C)	SIE
109	ACCH	2	5	2	2.58	1	-
110	ACCH	2	5	2	3.65	5	-
111	ACCH	2	5	2	4.78	9	-
112	ACCH	2	5	2	5.64	13	-
113	ACCH	2	5	2	6.97	17	-
114	ACCH	2	5	2	9.14	21	-
115	ACCH	0.2	5	2	3.80	5	-
116	ACCH	0.5	5	2	3.70	5	-
117	ACCH	1	5	2	3.32	5	-
118	ACCH	10	5	0.8	2.91	5	-
119	ACCH	10	5	1.2	3.43	5	-
120	ACCH	10	5	1.6	3.32	5	-
121	ACCH	10	5	2	3.57	5	-
122	ACCD	2	5	2	1.49	5	2.45
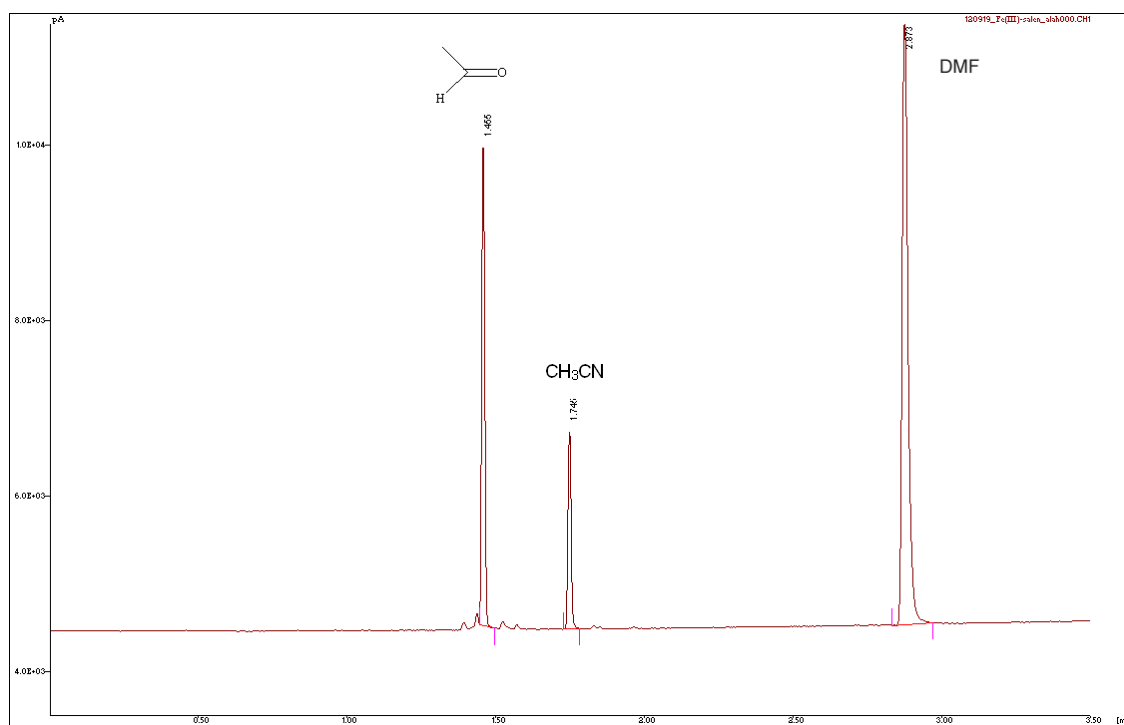
Figure A1. Chromatogram of a sample from the head-space. The oxidation reaction of ALAH in DMF/H$_2$O (3 : 1) at 35 °C.
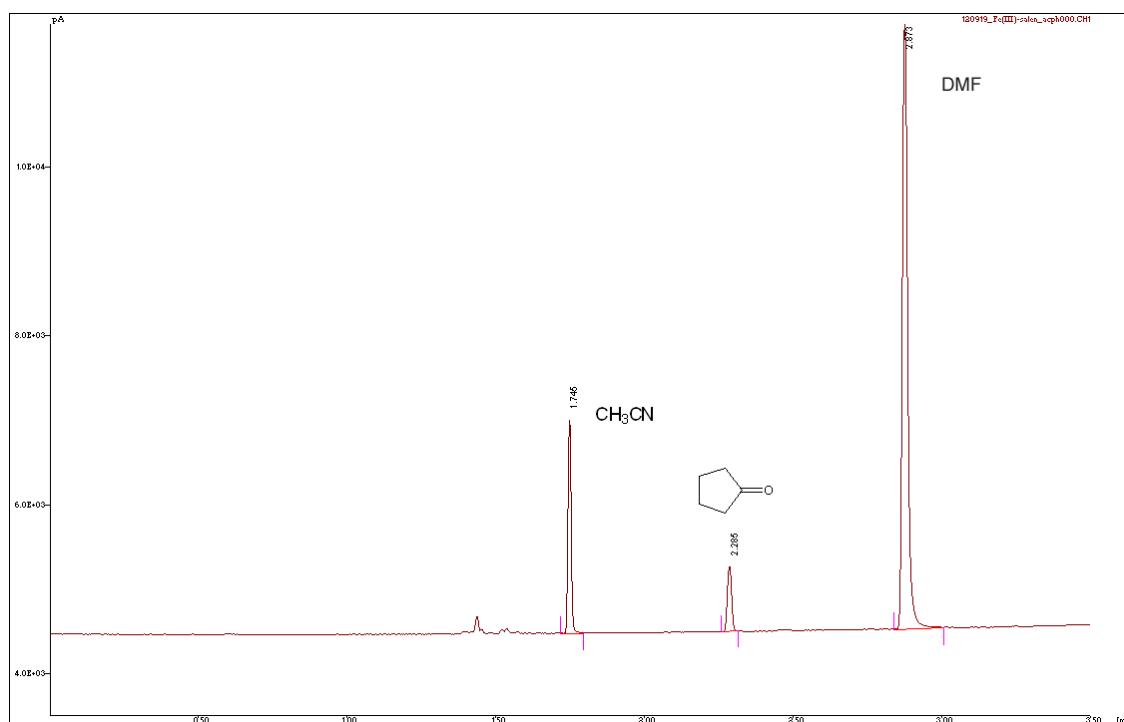
Figure A2. Chromatogram of a sample from the head-space. The oxidation reaction of ACPCH in DMF/H$_2$O (3 : 1) at 35 °C.
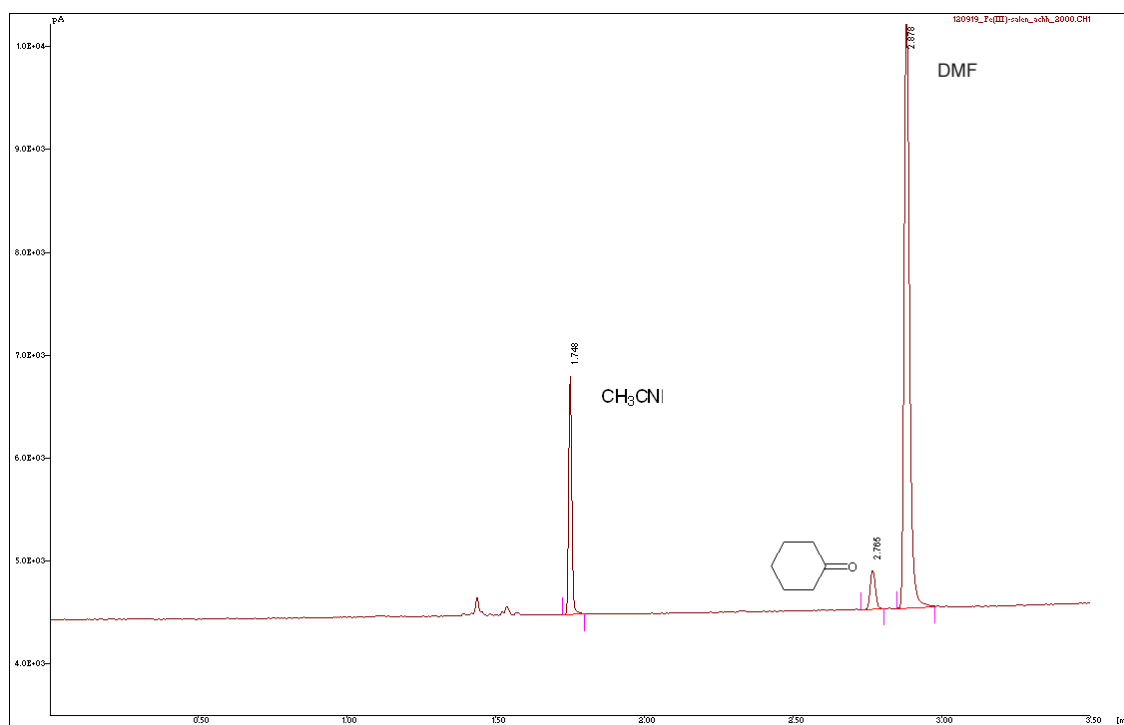
Figure A3. Chromatogram of a sample from the head-space. The oxidation reaction of ACHCH in DMF/H_2O (3 : 1) at 35 °C.
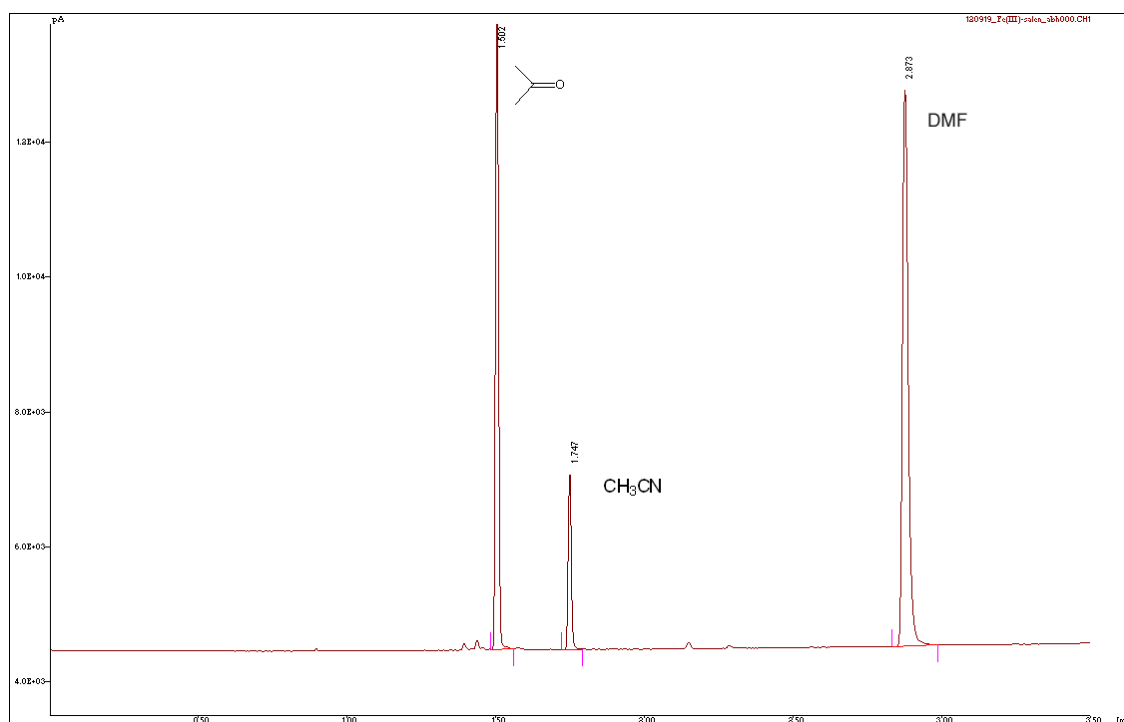
Figure A4. Chromatogram of a sample from the head-space. The oxidation reaction of ABH in DMF/H_2O (3 : 1) at 35 °C.
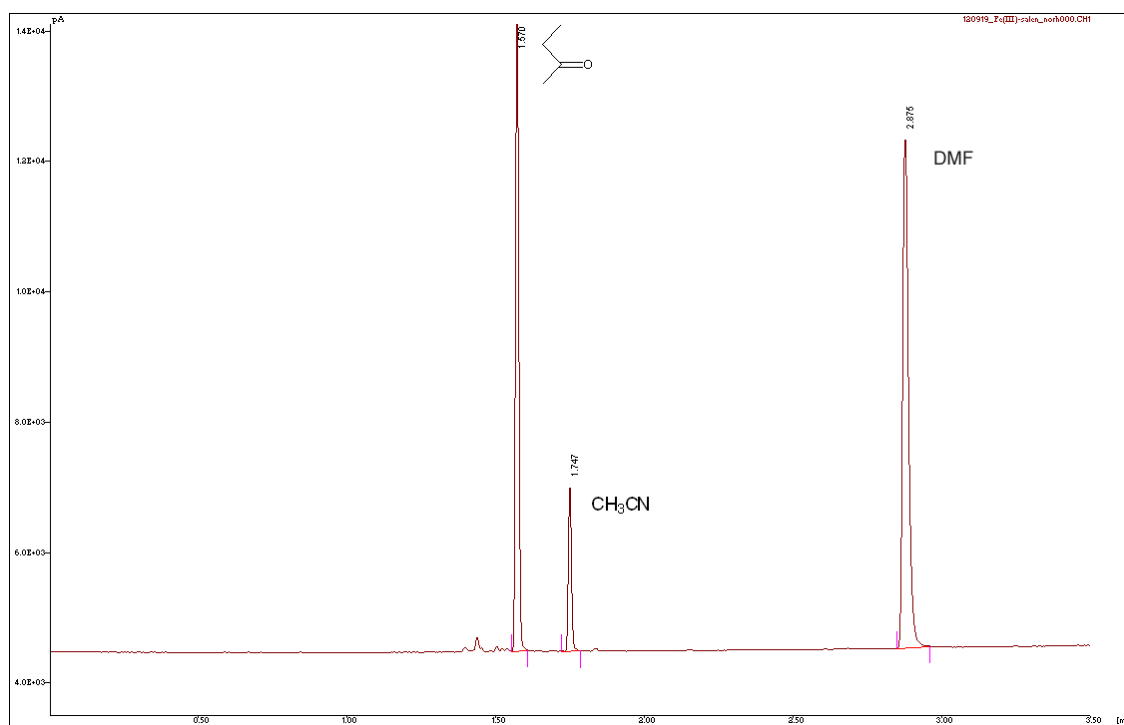
Figure A5. Chromatogram of a sample from the head-space. The oxidation reaction of NORH in DMF/H$_2$O (3 : 1) at 35 °C.
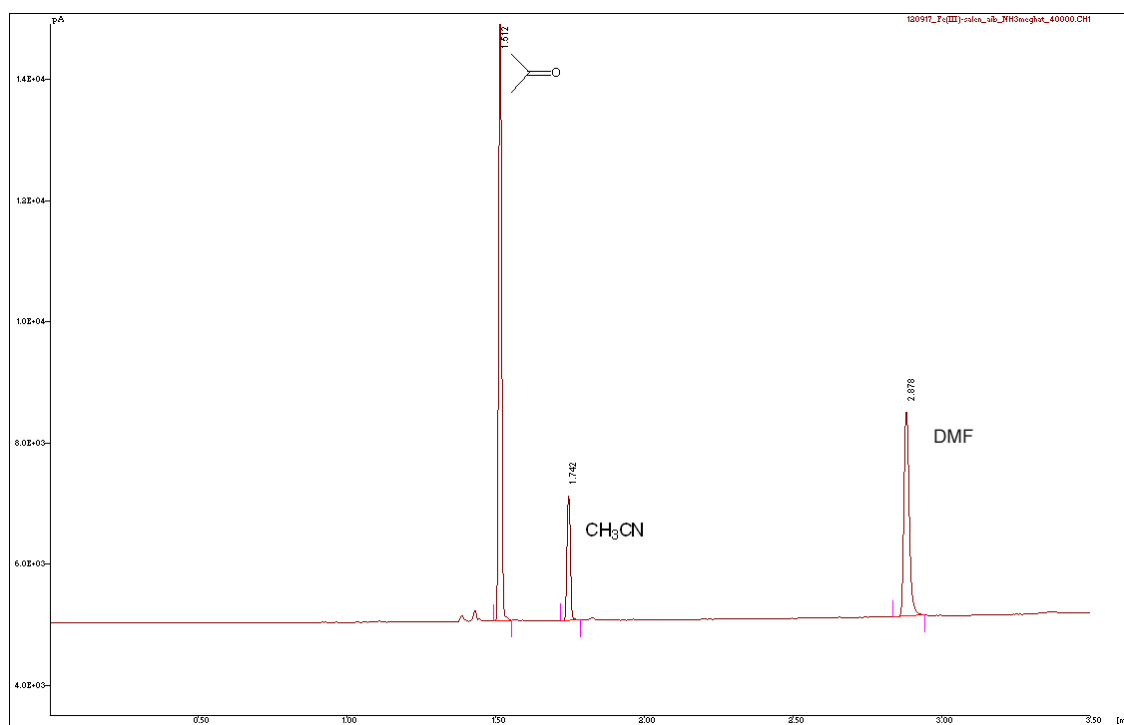
Figure A6. Chromatogram of a sample from the head-space. The oxidation reaction of AIBH in DMF/H$_2$O (3 : 1) at 35 °C.

84
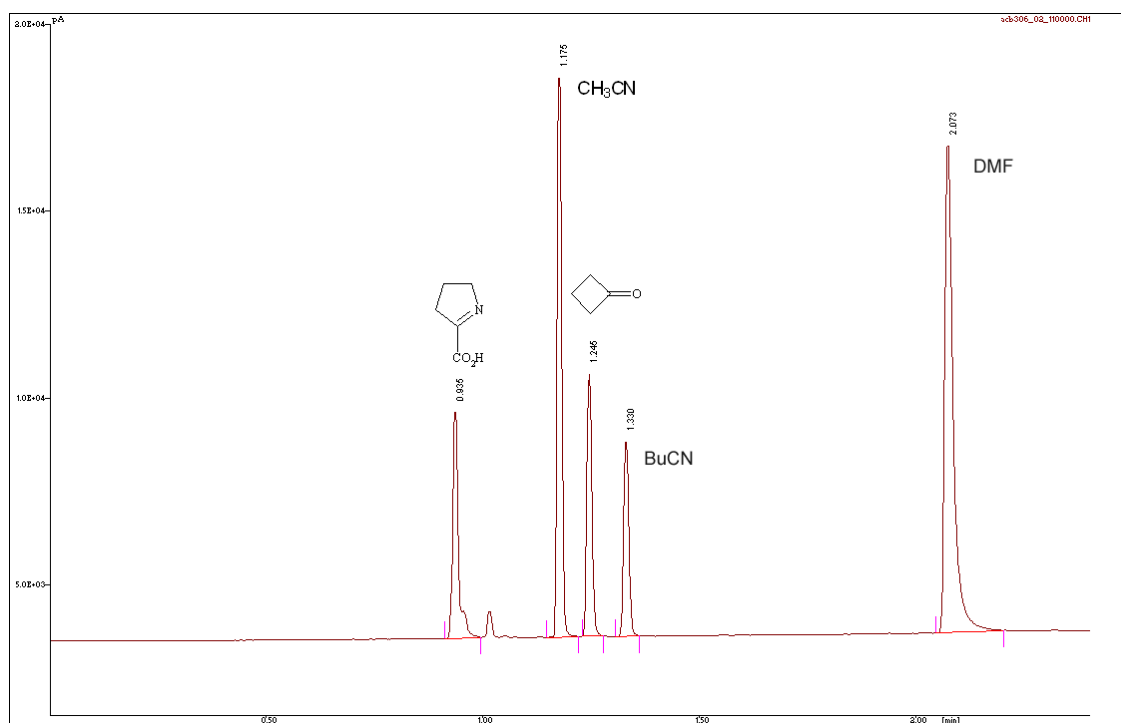
Figure A7. Chromatogram of a sample from the head-space. The oxidation reaction of ACBCH in DMF/H$_2$O (3 : 1) at 35 °C.
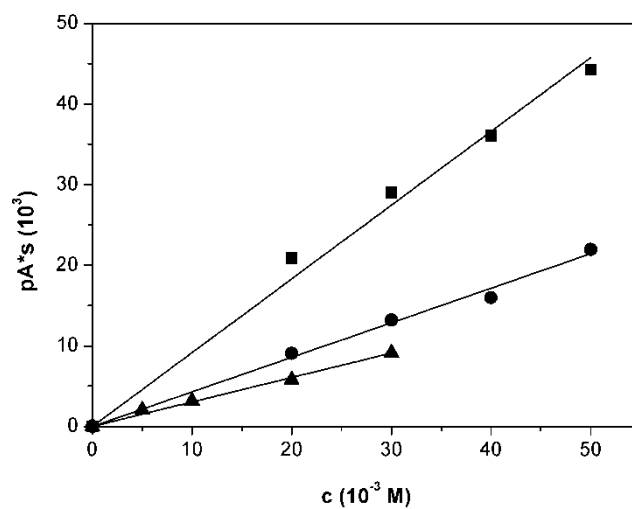
Figure A8. Calibration curves for ▲cyclobutanone, ●cyclopentanone and ■cyclohexanone.
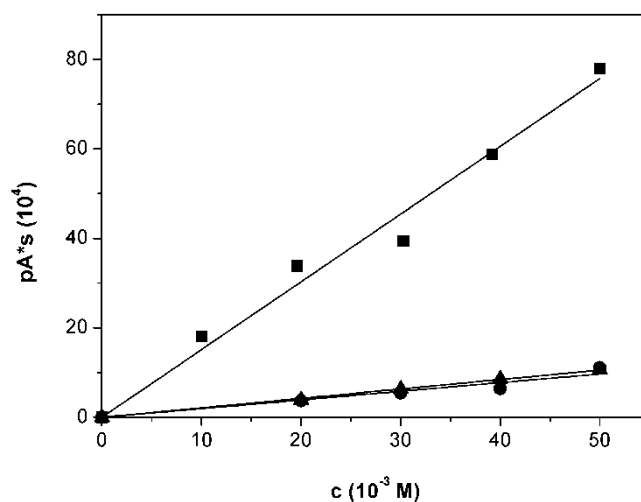
Figure A9. Calibration curves for ▲ethyl-methyl ketone, ●acetone and ■acetaldehide.
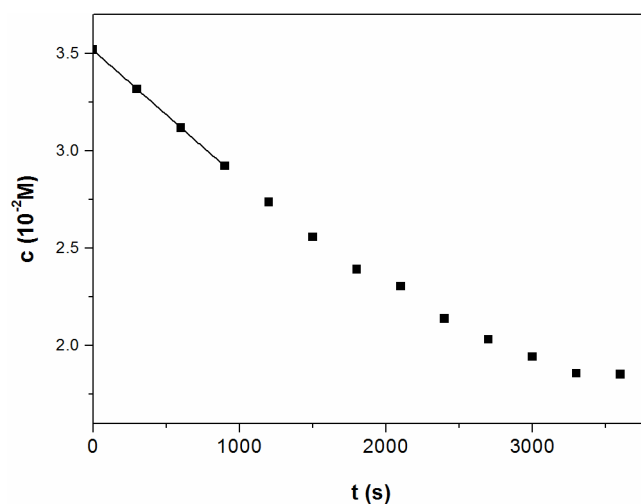
Figure A10. Determination of initial rate in the reaction of NORH in DMF/H_2O (3 : 1) at 35 °C. $[NORH]_0 = 3.6 \times 10^{-2}$ M, $[Fe^{III}(SALEN)Cl]_0 = 7.2 \times 10^{-6}$ M, $[H_2O_2]_0 = 3.6 \times 10^{-2}$ M, $[NH_4OH]_0 = 3.6 \times 10^{-2}$ M.
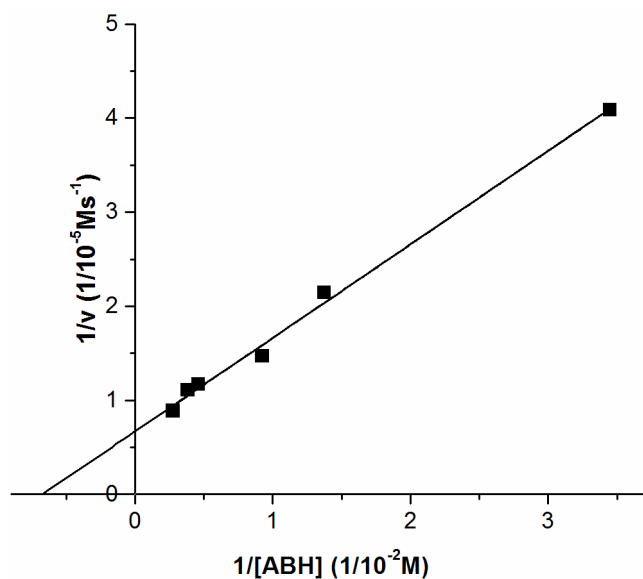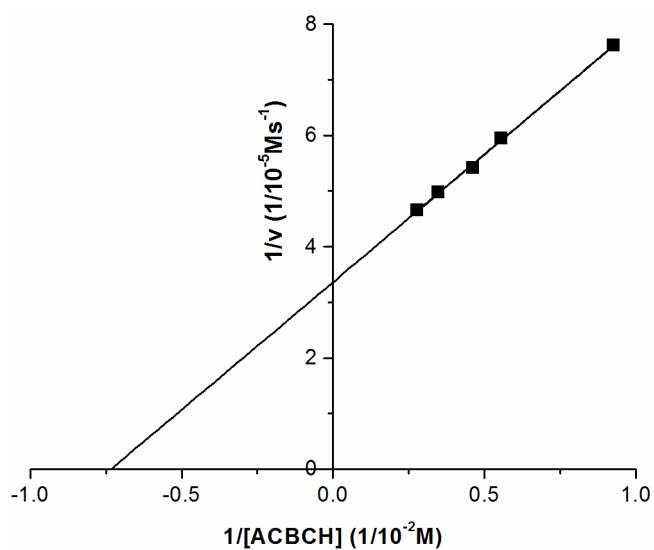
Figure A11. *Lineweaver-Burk* plot for ABH. Correlation between substrate concentration and the rate of the reaction of ABH in DMF/H_2O (3 : 1) at 35 °C. $[Fe^{III}(SALEN)Cl]_0 = 7.2 \times 10^{-6}$ M, $[H_2O_2]_0 = 3.6 \times 10^{-2}$ M, $[NH_4OH]_0 = 3.6 \times 10^{-2}$ M.
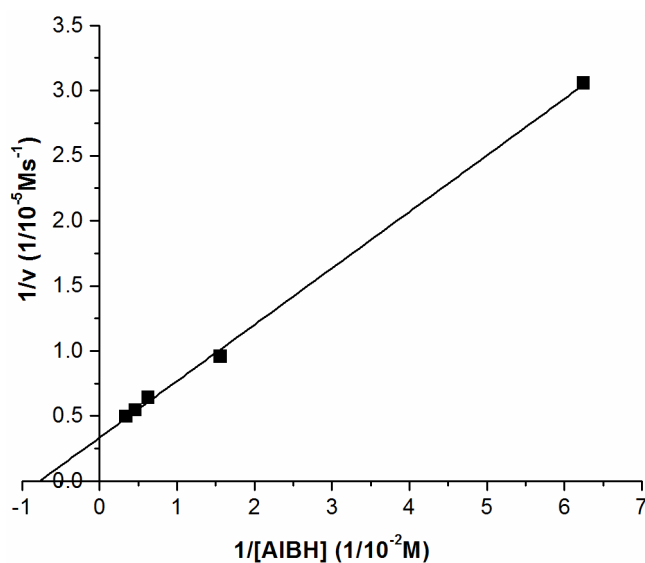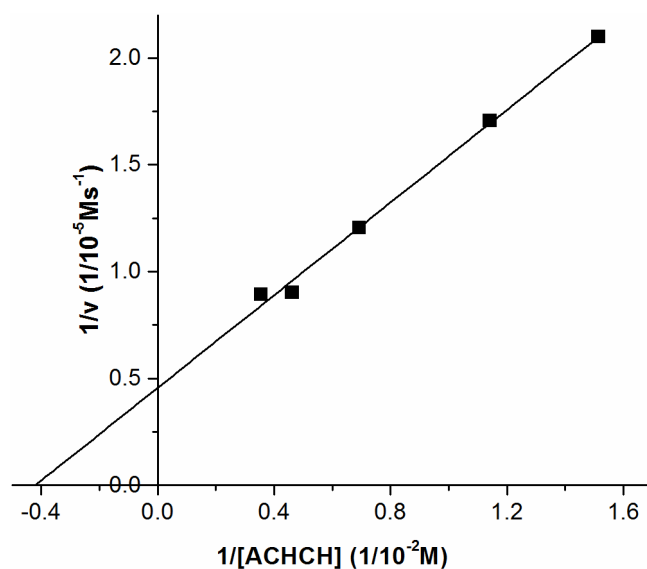

Figure A12. *Lineweaver-Burk* plot for AIBH. Correlation between substrate concentration and the rate of the reaction of AIBH in DMF/H_2O (3 : 1) at 35 °C. $[Fe^{III}(SALEN)Cl]_0 = 7.2 \times 10^{-6}$ M, $[H_2O_2]_0 = 3.6 \times 10^{-2}$ M, $[NH_4OH]_0 = 3.6 \times 10^{-2}$ M.
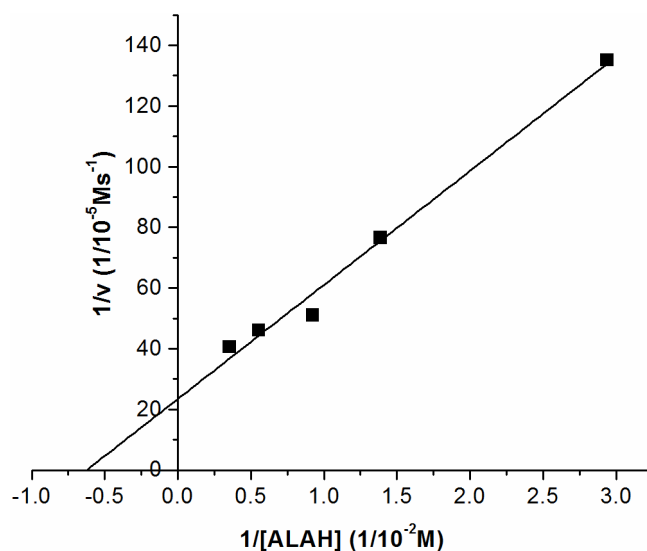
Figure A13. *Lineweaver-Burk* plot for ALAH. Correlation between substrate concentration and the rate of the reaction of ALAH in DMF/H_2O (3 : 1) at 35 °C. $[Fe^{III}(SALEN)Cl]_0 = 7.2 \times 10^{-6}$ M, $[H_2O_2]_0 = 3.6 \times 10^{-2}$ M, $[NH_4OH]_0 = 3.6 \times 10^{-2}$ M.
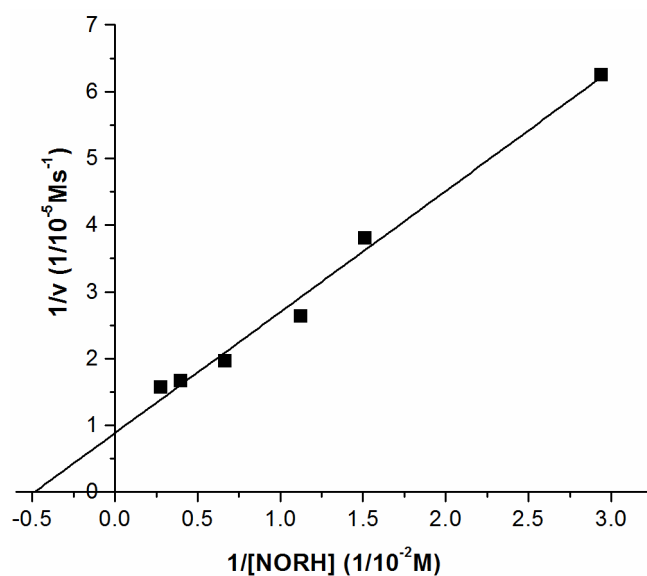
Figure A14. *Lineweaver-Burk* plot for NORH. Correlation between substrate concentration and the rate of the reaction of NORH in DMF/H_2O (3 : 1) at 35 °C. $[Fe^{III}(SALEN)Cl]_0 = 7.2 \times 10^{-6}$ M, $[H_2O_2]_0 = 3.6 \times 10^{-2}$ M, $[NH_4OH]_0 = 3.6 \times 10^{-2}$ M.
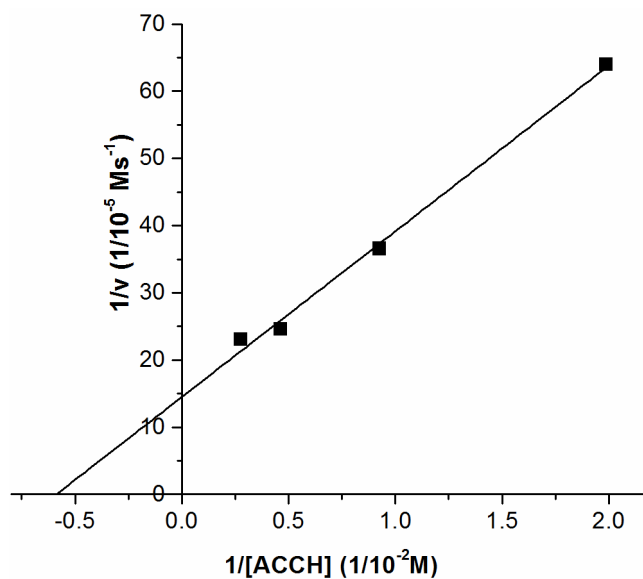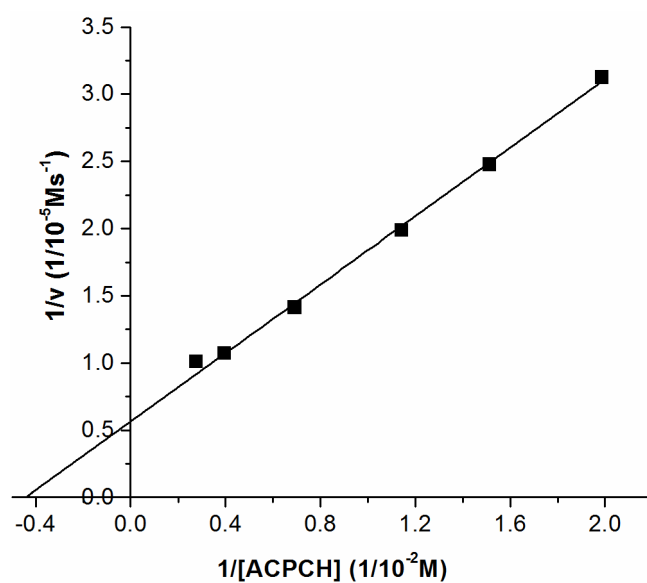
Figure A15. *Lineweaver-Burk* plot for ACCH. Correlation between substrate concentration and the rate of the reaction of ACCH in DMF/H_2O (3 : 1) at 35 °C. $[Fe^{III}(SALEN)Cl]_0 = 7.2 \times 10^{-6}$ M, $[H_2O_2]_0 = 3.6 \times 10^{-2}$ M, $[NH_4OH]_0 = 3.6 \times 10^{-2}$ M.

Figure A16. *Lineweaver-Burk* plot for ACBCH. Correlation between substrate concentration and the rate of the reaction of ACBCH in DMF/H_2O (3 : 1) at 35 °C. $[Fe^{III}(SALEN)Cl]_0 = 7.2 \times 10^{-6}$ M, $[H_2O_2]_0 = 3.6 \times 10^{-2}$ M, $[NH_4OH]_0 = 3.6 \times 10^{-2}$ M.

Figure A17. *Lineweaver-Burk* plot for ACHCH. Correlation between substrate concentration and the rate of the reaction of ACHCH in DMF/H_2O (3 : 1) at 35 °C. $[Fe^{III}(SALEN)Cl]_0 = 7.2 \times 10^{-6}$ M, $[H_2O_2]_0 = 3.6 \times 10^{-2}$ M, $[NH_4OH]_0 = 3.6 \times 10^{-2}$ M.

Figure A18. *Lineweaver-Burk* plot for ACPCH. Correlation between substrate concentration and the rate of the reaction of ACPCH in DMF/H_2O (3 : 1) at 35 °C. $[Fe^{III}(SALEN)Cl]_0 = 7.2 \times 10^{-6}$ M, $[H_2O_2]_0 = 3.6 \times 10^{-2}$ M, $[NH_4OH]_0 = 3.6 \times 10^{-2}$ M.

Table A11. Crystal structure details for [Cu^{II}(ACBC)$_2$] and [Cu$^{II}_2$(ACHC)$_4$(H$_2$O)].H$_2$O.

Compound reference	[Cu^{II}(ACBC)$_2$]	[Cu$^{II}_2$(ACHC)$_4$(H$_2$O)].H$_2$O
Chemical formula	C$_5$H$_8$Cu$_{0.5}$NO$_2$	C$_{28}$H$_{52}$Cu$_2$N$_4$O$_{10}$
Formula Mass	145.89	731.82
Crystal system	monoclinic	monoclinic
a/Å	10.381(1)	10.733(1)
b/Å	5.1906(5)	13.629(1)
c/Å	9.912(1)	22.776(3)
α/°	90	90
β/°	90.345	100.41(5)
γ/°	90	90
Unit cell volume/Å^3	534.08(9)	3276.8(6)
Temperature/K	293(2)	293(2)
Space group	P2$_1$/c	P2$_1$/c
Number of formula units per unit cell, Z	4	4
Radiation type	MoKα	MoKα
Absorption coefficient, μ/mm^{-1}		
No. of reflections measured	5465	38240
No. of independent reflections	1293	7987
R$_{int}$	0.1051	0.081
Final R1 values (I > 2σ(I))	0.0587	0.0524
Final wR values (I > 2σ(I))	0.1369	0.1291
Final R1 values (all data)	0.1379	0.1185
Goodness of fit	0.971	1.028
CCDC number		

Table A12. Crystal structure details for $[Cu^{II}(bpy)(ACBC)]ClO_4.H_2O$,
$[Cu^{II}(bpy)(ACPC)]ClO_4.H_2O$, $[Cu^{II}(bpy)(ACHC)]ClO_4.H_2O$

Compound reference	$[Cu^{II}(bpy)(ACBC)]ClO_4.H_2O$	$[Cu^{II}(bpy)(ACPC)]ClO_4.H_2O$	$[Cu^{II}(bpy)(ACHC)]ClO_4.H_2O$
Chemical formula	$C_{15}H_{18}Cu_1Cl_1N_3O_7$	$C_{16}H_{20}Cu_1Cl_1N_3O_7$	$C_{17}H_{22}Cu_1Cl_1N_3O_7$
Formula Mass	451.31	465.34	479.37
Crystal system	monoclinic	monoclinic	orthorhombic
a/Å	12.3898(2)	9.9783(2)	23.8007(8)
b/Å	8.0417(1)	8.1230(2)	10.3423(3)
c/Å	19.3665(4)	23.9669(5)	8.2427(3)
α/°	90	90	90
β/°	108.163(1)	105.705(1)	90
γ/°	90	90	90
Unit cell volume/Å³	1833.44(5)	1870.09(7)	2028.97(12)
Temperature/K	293(2)	293(2)	293(2)
Space group	$P2_1/c$	$P2_1/c$	$Pna2_1$
Number of formula units per unit cell, Z	4	4	4
Radiation type	MoKα	MoKα	MoKα
Absorption coefficient, μ/mm⁻¹	1.381	1.356	1.253
No. of reflections measured	17326	20554	13425
No. of independent reflections	4747	4235	2702
R_{int}	0.044	0.03	0.064
Final R1 values (I > 2σ(I))	0.049	0.047	0.0569
Final wR values (I > 2σ(I))	0.1248	0.1366	0.1437
Final R1 values (all data)	0.0735	0.0568	0.0803
Goodness of fit	1.05	1.043	1.043
CCDC number			

Table A13. Crystal structure details for [Cu^{II}(bpy)(AIB)(H$_2$O)]ClO$_4$, [Cu$^{II}_2$(bpy)$_2$(AMEP)(H$_2$O)$_3$](ClO$_4$)$_2$.3H$_2$O

Compound reference	[Cu^{II}(bpy)(AIB)(H$_2$O)]ClO$_4$	[Cu$^{II}_2$(bpy)$_2$(AMEP)(H$_2$O)$_3$](ClO$_4$)$_2$.3H$_2$O
Chemical formula	C$_{14}$H$_{16}$Cu$_1$Cl$_1$N$_3$O$_6$	C$_{23}$H$_{36}$Cl$_2$Cu$_2$N$_5$O$_{17}$
Formula Mass	426.29	883.52
Crystal system	monoclinic	triclinic
a/Å	12.3774(3)	7.8553(3)
b/Å	8.1484(2)	12.1483(4)
c/Å	18.8882(5)	19.4059(8)
α/°	90	81.629(1)
β/°	114.785(2)	87.324(2)
γ/°	90	75.527(4)
Unit cell volume/Å^3	1729.51(8)	1773.90(12)
Temperature/K		243(2)
Space group	P2$_1$/c	P$^-$1
Number of formula units per unit cell, Z	4	2
Radiation type	MoKα	MoKα
Absorption coefficient, μ/mm^{-1}	1.453	1.473
No. of reflections measured	16606	19622
No. of independent reflections	4426	8256
R$_{int}$	0.0532	0.1006
Final R1 values (I > 2σ(I))	0.0745	0.1073
Final wR values (I > 2σ(I))	0.2249	0.2639
Final R1 values (all data)	0.1269	0.1653
Goodness of fit	1.021	1.128
CCDC number		
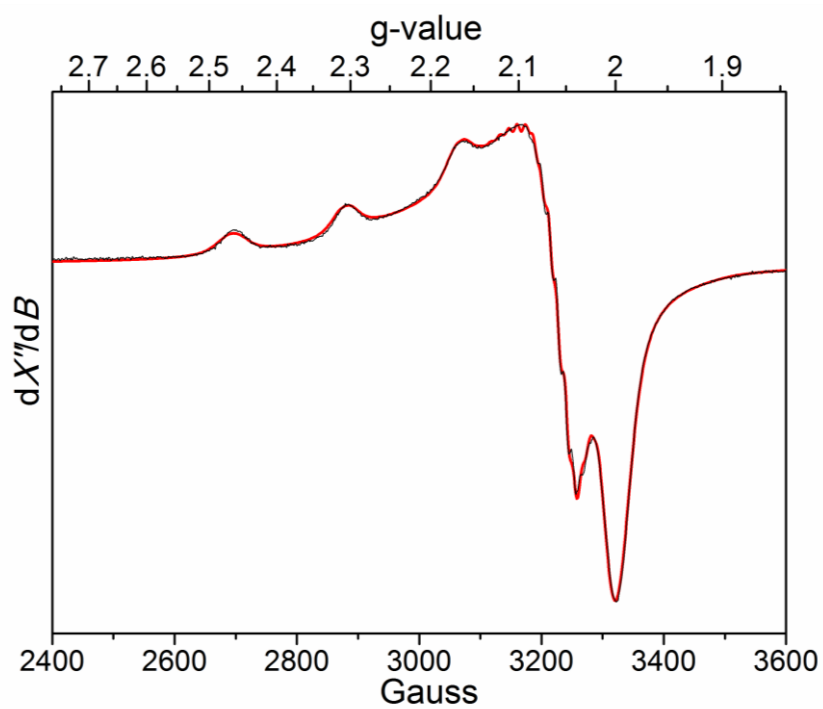
Figure A19. The EPR spectra of [Cu^{II}(bpy)(ACBC)]ClO$_4$.H$_2$O
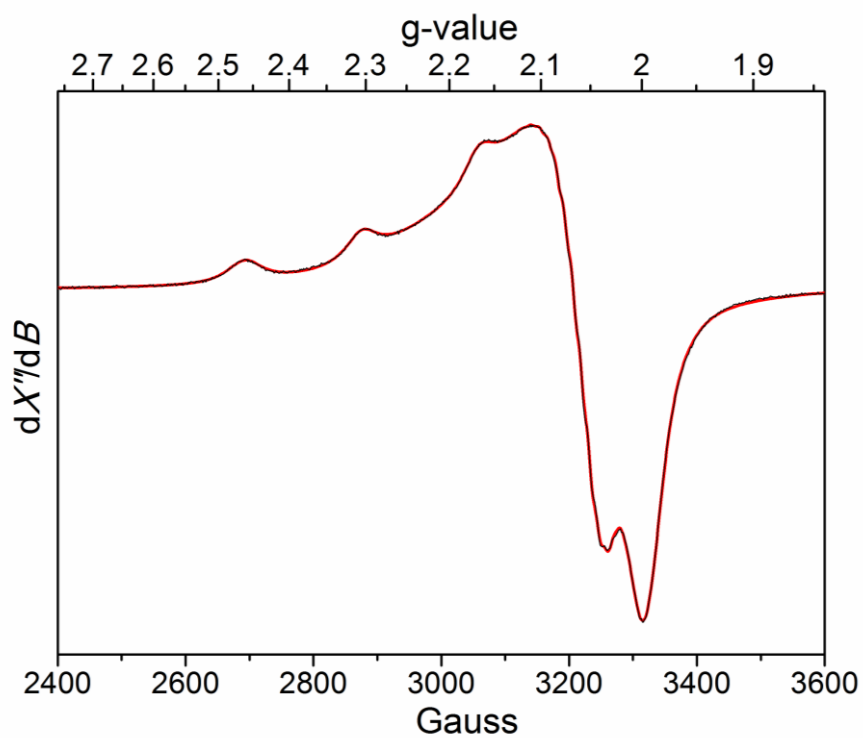
Figure A20. The EPR spectra of [Cu^{II}(bpy)(ACPC)]ClO$_4$.H$_2$O
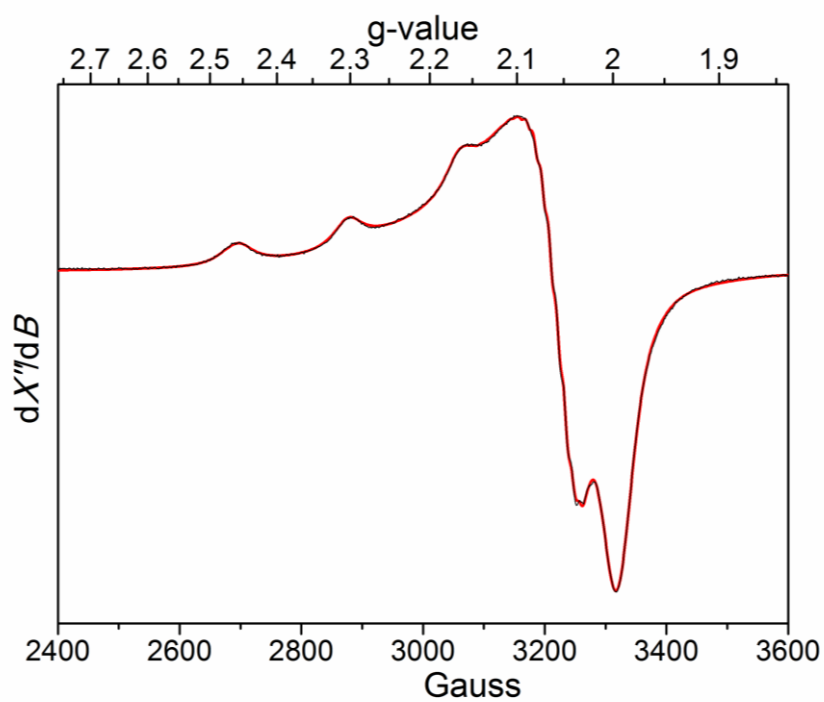
Figure A21. The EPR spectra of $[Cu^{II}(bpy)(ACHC)]$ $ClO_4.H_2O$
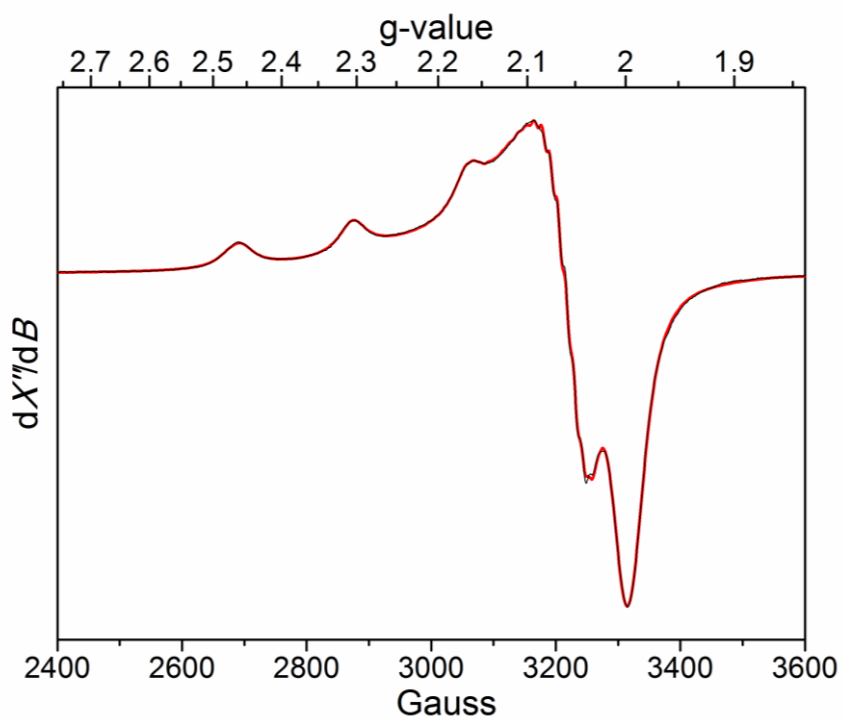
Figure A22. The EPR spectra of $[Cu^{II}(bpy(AIB)(H_2O)]ClO_4$